THE EFFECT OF A TRANSVERSE MAGNETIC FIELD ON A PROPAGATING PLANE GASEOUS DETONATION WAVE

by

John Peter Thomas

A Dissertation Submitted to the Faculty of the

DEPARTMENT OF AEROSPACE AND MECHANICAL ENGINEERING

In Partial Fulfillment of the Requirements
For the Degree of

DOCTOR OF PHILOSOPHY

WITH A MAJOR IN MECHANICAL ENGINEERING

In the Graduate College

THE UNIVERSITY OF ARIZONA

1 9 6 9

THE UNIVERSITY OF ARIZONA

GRADUATE COLLEGE

I hereby recommend that this dissertation prepared under my direction by John Peter Thomas

entitled The Effect of a Transverse Magnetic Field on a Propagating Plane Gaseous Detonation Wave

be accepted as fulfilling the dissertation requirement of the degree of Doctor of Philosophy

Russell E. Peterson — Dissertation Director — May 15, 1969 — Date

After inspection of the dissertation, the following members of the Final Examination Committee concur in its approval and recommend its acceptance:*

Russell E. Peterson	May 15, 1969
E K Parks	May 15 1969
Jay E. Treat	May 15, 1969
Roy M. Emrich	May 15, 1969
Lawrence B. Scott Jr	MAY 15, 1969

*This approval and acceptance is contingent on the candidate's adequate performance and defense of this dissertation at the final oral examination. The inclusion of this sheet bound into the library copy of the dissertation is evidence of satisfactory performance at the final examination.

STATEMENT BY AUTHOR

This dissertation has been submitted in partial fulfillment of requirements for an advanced degree at The University of Arizona and is deposited in the University Library to be made available to borrowers under rules of the Library.

Brief quotations from this dissertation are allowable without special permission, provided that accurate acknowledgment of source is made. Requests for permission for extended quotation from or reproduction of this manuscript in whole or in part may be granted by the copyright holder.

SIGNED: John Peter Thomas

DEDICATION AND ACKNOWLEDGEMENTS

This dissertation is dedicated to my wife, Marianne, whose encouragement has aided me in completing my graduate studies.

I wish to express my gratitude to Dr. R. E. Petersen for his assistance and supervision in the development and completion of this dissertation. Also, I wish to thank Professor W. Roos, of Sacramento State College, for his assistance in the design and fabrication of the electromagnet used in this study.

TABLE OF CONTENTS

TABLE OF CONTENTS--Continued

LIST OF ILLUSTRATIONS

ABSTRACT

This study involves the experimental investigation of the effect a transverse magnetic field has on certain characteristics of a propagating steady state* detonation wave. The wave characteristics measured were the propagation velocity and the variation in pressure behind the wave front. It also contains a theoretical calculation, based upon a simplified one dimensional model for the wave propagating through the magnetic field, which predicts that there should be no observable changes in these characteristics.

The detonation wave was generated in a 1" tube of square cross-section using oxyacetylene mixtures of varying mixture ratios and initial pressures. Its propagation velocity was measured using electronic counters whose stop and start circuits were actuated by means of piezo-electric gages, which were placed at measured intervals along the tube axis. The variation in pressure behind the wave front was measured by photographing the trace on an oscilloscope screen of the output from a Kistler gage-charge amplifier combination.

The transverse magnetic field was generated by means of a D.C. electromagnet and rectifier set combination. With the magnet on, a maximum field strength of approximately 12,000 gauss was generated during the tests.

The theoretical calculations use available information on wave propagation velocity and its electrical conductivity along with

*Steady state in the special sense of constant wave velocity.

the magnetic field strength mentioned in the preceding paragraph in order to predict the possible orders of magnitude for static pressure and propagation velocity variations due to the presence of the magnetic field. It was found from the magnitude of these calculated changes that they should not be observable using the instrumentation of this study.

For each mixture ratio, at a given initial pressure, two experimental runs were made for comparative purposes. One run was made with the magnet off and the other with it on. The measured propagation velocities and pressure profiles for these two runs were compared to observe any changes due to the presence of the transverse magnetic field.

There were no observed changes in the propagation velocities. This agrees with the results predicted by the theoretical calculations.

However, there are observed variations or changes in the pressure profiles. The variations show as increases in the static pressure of the gases in the rarefaction wave. This seems to indicate that the magnetic field slowed down the flowing gases, which follow the propagating wave, and as a result converted part of their velocity pressure into static pressure.

The observed variations in static pressure seem to correlate with the variation in the magnitude of the induced Lorentz force. That is, for the approximately constant magnitude of magnetic field strength of this study, they increase both with increasing electrical conductivity and propagation velocity.

The maximum observed local variation in pressure was for an equimolar mixture at an initial pressure of 15 psig. This variation was measured to be approximately 50 psi. Because of the magnitudes of these observed variations, the possibility exists that electrical conductivities far in excess of those reported to date were present in the detonation wave.

The measured values of propagation velocity and pressure at the rarefaction-detonation wave interface agree closely with those already reported by various investigators.

CHAPTER 1

INTRODUCTION

This chapter will give a general review of the detonation phenomenon in confined* gaseous combustible mixtures. Its most important observed characteristics will be discussed qualitatively and the limitations on the proposed quantitative theories for evaluating these characteristics will be given.

Also the possibility will be discussed of observing changes in some of these characteristics due to magnetogasdynamic effects when the detonation wave, which has a following flow of electrically conducting gas, passes through a transverse magnetic field. The purpose of this study is to experimentally observe these possible changes in the characteristics. The experimental method used to observe these changes will also be outlined.

Historical Notes

In 1881 during investigations into the cause of spontaneous explosions in French coal mines, the two French physicists, Berthelot and Vieille,[1] first identified the wave nature of detonative combustion. Mallard and Le Chatelier,[2] also physicists and countrymen of Berthelot and Vieille independently arrived at the same conclusion. These

*Confined in the sense that a container is provided to contain the combustible mixture before detonation is initiated. Unconfined will mean that no container has been provided.

investigators established that the apparent spontaneous explosion was actually a finite combustion wave-front moving at an extremely high velocity of the order of thousands of feet per second through the entrapped coal dust air mixture. This was in sharp contrast to the usual combustion process in gas mixtures where the flame front (deflagration wave) progresses at a relatively low velocity of the order of a few feet per second. About 1900 Chapman[3] and Jouguet[4] each independently advanced the theory that the detonative combustion process could be described if the wave were treated as a shock discontinuity followed by a rapid combustion zone. This model has been observed experimentally to adequately describe the gross character of the fully established detonation wave, however it did not describe either the structure and observed characteristics of the wave or its initiation process.

Since then there have been numerous experimental investigations of both the development or initiation of detonation and also of the fully developed wave in an attempt to better understand the mechanism of initiation and the observed characteristics of the fully developed wave. Until recently the greatest interest in understanding the detonation phenomenon was of course the fact that it could possibly lead to better methods for controlling and/or preventing explosions with their accompanying hazards. This goal is still being pursued.[5] With the advent of jet and rocket technology many new problems involving high speed aerodynamics and high temperature chemical reactions became of interest. The detonation phenomenon, which can be readily produced in the laboratory, proves an ideal model for the study of some of these

problems. Oppenheim[6] states that one of the more important problems being investigated using this technique is that of combustion instability in rocket thrust chambers.

General Discussion

Some excellent treatises on the investigation of and the characteristics of the detonation phenomenon are References 7 through 11. Other sources of reference on the detonation phenomenon are the various scientific journals, government research and combustion symposia publications. Some examples of these are References 12 through 23.

Experimental investigations have been conducted using both noncondensed (gaseous) and condensed (liquid and solid) phases of a combustible substance. They also have been conducted both when the combustible substance and its oxidizer were confined and unconfined. In all cases detonation could be initiated, within certain limits of oxidizer to fuel ratio and at suitable initial pressure and temperature conditions, by ignition of the combustible mixture using a source such as a shock wave, spark plug, glow plug, etc. Observation shows that upon ignition a deflagration wave propagates from the point of ignition into the unburned mixture and that after a certain distance of travel develops into a detonation wave. For a more detailed discussion of both the initiation and limits of detonation refer to References 7 through 11.

The greatest majority of the experimental investigations have been with respect to confined gaseous mixtures of oxidizer and fuel because the resulting final pressures, in the fully developed detonation wave, are much lower than those of detonation in condensed phase

mixtures. For safety reasons these relatively low pressures are desirable. Since this investigation involves detonation with respect to a confined noncondensed combustible mixture, all of the subsequent discussion in this dissertation will be with regard to this type of system. However, in general the properties and characteristics of the detonation phenomenon are the same for both the condensed and noncondensed combustible mixtures excepting for the much more intense pressures involved in detonation in the condensed phase.

These experimental investigations of detonation have been quite successful in obtaining data because in most cases they are readily reproducible. The data obtained have been used in attempts to both devise qualitative and quantitative explanations for the initiation of detonation and for the structure and characteristics of the fully developed wave.

It may be stated at this point that the development of a theoretical (or quantitative) model for the initiation of a fully developed wave has been of limited success. This is primarily due to both the extremely complex fluid flow patterns (turbulent flow) which are observed experimentally and which are not in general reproducible[24] and also due to the unknown coupling of these flow patterns with the unknown chemical reactions. In other words the initiation process is a non-equilibrium or nonsteady-state situation involving unknown chemical reaction rates and species,[15] within a flame front, which is coupled with the fluid flow ahead of the front.

Oppenheim and Urtiew[19] suggest a satisfactory semi-empirical quantitative theory for the initial stages of the transition from a

deflagration to a detonation wave. However, they also state that there is no available quantitative theory for the latter stages of this initiation process.

A purely theoretical analysis would require the simultaneous solution of the unsteady forms of the hydrodynamic equations of motion and chemi-kinetic governing equations for the system. Obtaining suitable mathematical forms for these equations is difficult both because of the fact that all stages of the initiation process are not completely understood[19] and because of the unsteady nature of the process.

During certain stages of the development of detonation the fluid flow is observed to be turbulent.[6,11] Even for non-reacting mixtures there is no adequate mathematical model which can be used to solve the turbulent flow situation because there is no completely satisfactory means for specifying a value for the hydrodynamic transport property of viscosity. For the case of reacting mixtures the attempts to devise a suitable mathematical model are further complicated by the necessity for knowing all of the chemical reactions involved as well as their rates. Even if these reactions and rates were known there would be a further difficulty because of the fact that thermodynamic equilibrium properties would be difficult to specify due to:

a) the probable difference between the rates of the various reactions.

b) the differences between the rates of the reactions and the rates at which the chemical energy released is redistributed amongst the various thermal modes (translational, vibrational and rotational) of the particles making up the system.

In summary, mathematical equations that lead to satisfactory solutions for fluid flow situations are limited to physical cases for which the use of thermodynamic or equilibrium properties are adequate for describing the behavior of the system and for which adequate values for the transport or non-equilibrium properties may be specified. Since this is not the case during the initiation of detonation then no suitable mathematical equations are available which completely describe this phenomenon.

Quantitative theories for certain of the observed characteristics of the fully developed detonation wave have been more successful than those for the initiation process. However, again development of a suitable general theoretical model for the fully developed wave has not been accomplished[11,14,25] due to essentially the same reasons as for the case of the initiation process. In this chapter a qualitative discussion of the more significant of the observed characteristics of the fully developed detonation wave and its structure will be given while a simplified quantitative theory will be deferred until Chapter 3.

Limits of Detonability

It has been observed experimentally that a steady state detonation wave can be generated in an oxidizer-fuel mixture only within certain limits of composition and only above a certain minimum initial pressure for the mixture. Examples of such limits of composition and pressure are given in References 8, 9 and 11.

There is no satisfactory quantitative theory[8] for these limits of detonation. However, a probable qualitative explanation is that, for mixtures outside the limits of detonation, the rate of chemical energy

release in the flame is not great enough to both provide for energy losses in the system (such as heat transfer through the tube wall) and also provide energy of expansion in order to cause the transition from the laminar to turbulent flame front. Transition from a laminar to a turbulent flame has always been observed during the initial stages of the initiation process and therefore it seems to be a necessary condition during the development of a detonation wave.

Characteristics and Structure of the Fully Developed or Steady State Detonation Wave

The fully developed or steady state detonation wave is made up of a shock wave plus a following chemical reaction zone which propagates as a complex at a uniform or constant velocity along the tube axis into the unreacted mixture. The chemical energy released by the reacting gases in the reaction zone sustains the constant velocity of the detonation wave. Since the detonation wave is not followed by a containing piston it is therefore followed by a rarefaction wave in which the products of the reaction expand. The gases in the rarefaction wave travel in the same direction as the detonation wave and decrease from a maximum velocity at the interface between the reaction zone and the rarefaction wave to a stagnant condition sufficiently far upstream from the detonation wave front. Because of this the terminology stationary and non-stationary are used in conjunction with, respectively, the detonation wave and the rarefaction wave.

Early photographic evidence[7,8] seemed to indicate that for rapidly reacting mixtures the detonation wave was planar or one dimensional

in nature. These photographs show a plane wave which was extremely thin because of the rapid chemical reaction in the reaction zone. Therefore the details in the reaction zone could not be resolved. More recent photographic evidence[6,11,12] seem to indicate that the normal mode of propagation for the detonation wave is as a multi-dimensional or turbulent fluid complex.

Detonation of mixtures which approach the limits of detonation results in a decrease in the reaction rate in the reaction zone and as a result of this the reaction zone is thickened thus allowing resolution of the detail in the zone. Near the limits of detonation spinning detonation is observed. Photographs[8] of the spinning detonation wave head-on show a single rotating luminous region in the reaction zone which occupies only a fraction of the tube cross-section. This indicates that the combustible mixture which is preconditioned by the shock wave at the detonation front is further compressed by a transverse wave causing it to react chemically. Experiment has shown that the rotating system is actually an acoustic wave behind which chemical reaction occurs and that the gas itself does not rotate.

As the mixture composition is varied such that it progresses away from the limits of detonation photographs[6] show that the number of transverse waves increase in number and occupy the entire tube cross-section. It is observed that these transverse waves move through the unreacted mixture causing it to react. Each wave eventually collides with another wave and they then are reflected and move off in opposite directions into unreacted gas. The reactions therefore appear to be periodic in nature. The frequency increases or the number of waves

increases monotonically as the mixture progresses away from the limits of detonation. Therefore the conclusion is drawn that the normal mode of propagation for detonation is as a turbulent or multi-headed spin complex. Spinning or single-headed spin is a special case for the lowest mode of the more general situation for wave propagation.

In general it is observed that the rate of propagation of the steady state wave increases with increasing reaction rates or increasing rates of energy deposition behind the wave front.

As was stated previously there is no satisfactory quantitative or theoretical means for determining the detonation wave structure. A solution to this problem would require the simultaneous solution of the hydrodynamic equations of motion along with the chemi-kinetic equations for the system. This of course is an insurmountable problem for the following reasons:

a) Difficulty in specifying a suitable coordinate system for the observed multi-dimensional flow field.

b) Because of the turbulent flow field, suitable values for the systems non-equilibrium or transport properties would be difficult to specify.

c) Difficulty in specifying equilibrium or thermodynamic properties because of the unknown reactions and their rates.

d) The strong coupling between the shock wave and the reaction zone is unresolved.[26]

e) The chemical kinetics for the system is not completely known.[25] Even in the case of a stationary deflagration wave the chemical kinetics is not fully understood.[27]

The most successful quantitative analysis with respect to the detonation phenomenon has been in predicting the stationary wave velocity. Using a simplified one dimensional laminar theoretical analysis, which will be outlined in Chapter 3, a theoretical velocity called the Chapman-Jouguet velocity can be computed. Comparison of this theoretical velocity with experimentally measured velocities gives close agreement for fast reacting mixtures in which the observed wave appears to approach one dimensionality. For mixtures approaching the limits of detonation there is some deviation between the theoretical and experimental values. The obvious reason for this discrepancy is the fact that, in the simplified treatment, one dimensionality as well as laminar flow is assumed; also no account is taken of viscosity, heat transfer, energy to excite the transverse acoustic modes in the reaction zone, and the diffusion of chemical species. In other words the simplified treatment treats the wave as a discontinuity in which case the details of the wave structure are not accounted for.

Attempts have been made to modify the simplified theory by accounting for some of the neglected items in order to try to explain the observed difference in velocity. Limited success has been attained by certain authors.[9,13,14,17] In general the authors are quick to point out the limitations of their treatments because of the lack of complete understanding of the wave structure and the chemical reactions within it.

The simplified theory also allows the calculation of temperature and pressure for the gas immediately behind the detonation wave or at the detonation-rarefaction wave interface. As for the case of wave velocity these computed values of temperature and pressure agree

closely with measured values when the wave appears to approach one dimensionality.

Ionization and Electrical Conductivity in Detonation Waves

The fact that the high temperature gases in both deflagration waves[27,28,29] and shock waves[30,31] are ionized and are electrically conducting has been known for a long time. At first it was believed that ionization in both the shock and deflagration waves was due solely to the thermal mechanism suggested by Saha.[32] Measured[31] values of ionization in shock waves in general agree with computed equilibrium values. Shuler and Weber[28] found that measured values of ionization in hydrogen-oxygen flames agreed closely with the equilibrium values computed using Saha's Equation. However for acetylene-oxygen flames they found disagreement between the measured and computed values. Measured values were from 10 to 100 times those of the computed equilibrium values. They attributed this difference primarily to the formation of free carbon atoms which were ionized by the thermal mechanism due to the high temperature of the gases.

Calcote[27] found this explanation inadequate because it did not explain the difference between measured and computed (equilibrium) ionization for lean mixtures in which the temperature was not sufficiently high to produce the ionization of free carbon. He suggested a non-equilibrium mechanism due to unknown chemical reactions involving primarily hydro-carbon radicals which are present in hydro-carbon-oxygen flames but not in hydrogen oxygen flames. That this mechanism of ionization is non-equilibrium was suggested by the fact

that the measured ionization fell off rapidly from a maximum in the reaction zone to an equilibrium value in the gases behind the reaction zone.

Ionization due to the thermal mechanism (electronic excitation due to the collision and transfer of thermal energy) is called either thermal or equilibrium ionization. Ionization due to the unknown chemical mechanism is called either chemi- or non-equilibrium ionization. There is some evidence that the thermal mechanism for ionization dominates at very high temperatures while the chemi-ionization mechanism dominates at moderate and low temperatures. However this conclusion which is drawn from experimental data may be erroneous due to suspected inadequacies in the measuring instrumentation[25].

Chemi-Ionization has been also observed[25,26,33,34] in acetylene-oxygen detonation waves. The general conclusions that may be drawn from these studies are as follows:

a) Ionization and electrical conductivities attained in detonation waves are much greater than those attained in shock waves at comparable temperatures.

b) At relatively low initial pressures electrical conductivity rapidly increases through the shock wave, at the detonation wave front, to a maximum value in the combustion zone and then falls off rapidly (almost exponentially), to an equilibrium value in the rarefaction wave.

c) The indicated maximum conductivity is up to 20 times greater than the equilibrium value attained in the rarefaction wave.

d) Electrical conductivity increases with increasing initial pressure for the detonable mixture.

e) Electrical conductivity in the acetylene-oxygen detonation wave is greater than that in the hydrogen-oxygen wave.

f) At low initial pressures, ion concentrations in the reaction zone of the hydrocarbon-oxygen detonation wave are the same as those measured in the reaction zone for comparable deflagration waves.

Kelly, Toong and Tung[25] found that at an initial pressure of one atmosphere the peaking of electrical conductivity in the reaction zone no longer occurred. They found that conductivity increased rapidly through the shock front to the equilibrium value in the reaction zone and then maintained this value into the rarefaction zone. This suggests that at the higher initial pressures and therefore correspondingly higher temperatures in the reaction zone the thermal mode of ionization dominates the chemical mode while at relatively low pressures the chemical mode dominates. However as is suggested by these authors this seeming disappearance of chemi-ionization may be due to the inadequacy of the measuring instrumentation. The conductivity is measured by means of an axially located D.C. probe. They point out that the spatial resolution of the probe is perfectly adequate at relatively low initial pressures where the reaction zone is relatively thick but at atmospheric pressure where the reaction zone thickness is approximately 0.1 mm the spatial resolution is poor. The authors also suggest that the measured values of conductivity in general may be erroneous due to the perturbation of the flow field by the physical presence of the probe and also due to sheathing and fringing effects.

The maximum conductivity measured by Kelly, Toong and Tung was approximately 10^{-3} mhos/cm for a stochiometric acetylene-oxygen mixture

at an initial pressure of 760 mm. For reasons explained in the preceding paragraph this may not be the value actually attained in the combustion zone. By direct comparison with their work at the lower initial pressures a possibility is suggested that conductivities of up to 20 times this measured value may exist in the reaction zone. Also since ion concentrations at low pressures were found to be the same, both in deflagration and detonation waves, then the work of Shuler and Weber, with deflagration waves in which ionization of up to 100 times the equilibrium values were measured, suggest the possibility of conductivities in the detonation wave even greater than 20 times the equilibrium value.

Other possible reasons for the values of conductivity observed by Kelly, Toong and Tung not being truly representative are as follows:

a) The measuring probe was located along the axis of the detonation tube and therefore was measuring a local rather than an average value of conductivity. Pressure increases across the transverse wave in single-headed spin of up to 160 times the initial pressure with accompanying temperatures of up to 3800°K have been observed[11] in $CO-O_2$ detonation. In acetylene-oxygen detonation temperatures up to 5000°K have been observed.[11] These high temperatures are also attributed to the presence of the transverse waves in the reaction zone. These temperatures and pressures indicate highly localized regions of intense or rapid chemical reaction with accompanying highly localized regions of high electrical conductivity. Therefore the reading from the single fixed probe may not be giving a truly representative reading for the number and intensity of these local regions of high conductivity.

b) The physical presence of the probe may interfere with the motion of the transverse waves and therefore disturb the mechanism for completion of the chemical reactions with its accompanying generation of ions.

Magnetogasdynamic Effects In Shock and Detonation Waves

Whenever an electrically conducting medium is moved through a transverse magnetic field a body force is induced in the conducting medium which opposes its motion. This body force is due to the influence of the transverse magnetic field on the motion of the electrically charged particles in the conducting medium. The interaction of the conducting medium and the magnetic field will result in energy conversion within and transfer between the two along with a resulting change in their properties. If the conducting medium is a partially ionized gas* then the interaction is called the Magnetogasdynamic Effect. Since the gases in both detonation and shock waves are electrically conducting, then a Magnetogasdynamic Effect should occur when they propagate through transverse magnetic fields. This Magnetogasdynamic Effect with respect to a propagating detonation wave is illustrated schematically in Figure 1.

At this point a brief qualitative description of the most significant characteristics of the Magnetogasdynamic Effect will be given

---

*Henceforth in this dissertation the terminologies plasma, ionized gases and electrically conducting gases will be used interchangeably.[35] This use of the term plasma does not conform to its definition, however, it is used here because of its convenience.

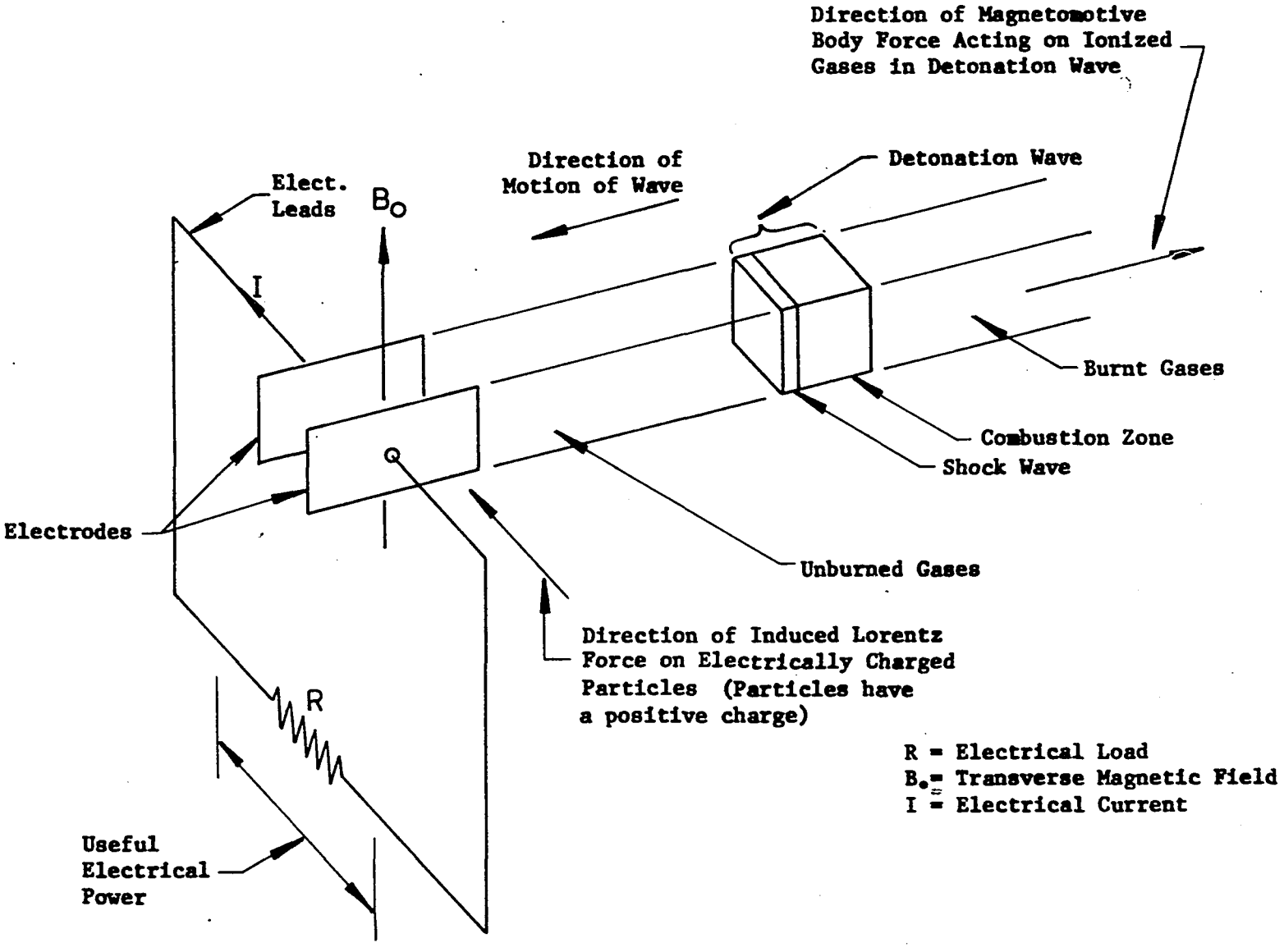

FIGURE 1. MGD EFFECT WITH RESPECT TO A PROPAGATING DETONATION WAVE

both from a microscopic and macroscopic standpoint. This will be followed by a brief review of some of the literature (both theoretical and experimental) on this effect with respect to shock and detonation waves.

Qualitative Explanation of the MGD* Effect

The model used for the discussion of the MGD Effect will be that of a laminar, homogeneous, isotropic continuous plasma which is at thermodynamic equilibrium. As has been stated previously, the flowing fluid which follows the detonation wave appears in general to be turbulent and to have discontinuities present in it (transverse waves in the reaction zone and also the shock at the wave front). Any observable MGD effects will be due to the transverse velocity component of this flowing fluid with respect to a magnetic field. The extension of the following discussion of the MGD effects in laminar, continuous flow to that of fluid flow in a detonation wave should become obvious upon completion of the discussion.

An electrically charged particle moving through magnetic and/or electric fields will have a force induced on it. This induced force is called the Lorentz force and is given by the following equation:

$$\vec{F}_L = q' (\vec{V} \times \vec{B} + \vec{E}) \qquad (1)$$

where: q' = the magnitude of the electrical charge on the particle

$\vec{V}$ = the velocity of the particle

$\vec{B}$ = the magnetic field strength

$\vec{E}$ = the electric field strength

---

*The abbreviation MGD for Magnetogasdynamic will be made henceforth in this dissertation.

In this study the applied electric field ($\vec{E}$) is zero and therefore equation (1) reduces to:

$$\vec{F}_L = q'(\vec{V} \times \vec{B}) \qquad (2)$$

Inspection of equation (2) indicates that the Lorentz force will be entirely due to the transverse component of $\vec{B}$ with respect to $\vec{V}$ and its direction will be perpendicular to both $\vec{B}$ and $\vec{V}$.

Because of the action of the Lorentz force charged particles will be accelerated in the direction of the force resulting in an electric current as is shown in Figure 1. Since this induced change in direction or motion for the charged particles is in a direction perpendicular to the magnetic lines of force then a second force will be induced which will be perpendicular to both the first induced force and to the magnetic field. Due to this second induced force component there will be an acceleration of the particles in the direction of this force with a resultant change in their momentums. Due to these induced components of momentum the interchange of momentum and energy between the particles themselves and other particles will be changed upon collision. The statistical average of the induced momentum of the charged particles and the resulting changes in the momentum and energy interchange upon collision result in the macroscopically observed characteristics of the MGD Effect.

Before entering the transverse magnetic field, the particles in the plasma may be thought of as having two motions which when superimposed upon one another give, their actual motion. The first motion may be thought as being microscopic in nature and would be the random thermal motion, which for a system in thermodynamic equilibrium, is

associated with the macroscopic thermodynamic properties of temperature and entropy. Because of the random or disordered nature of this motion, the interaction between the magnetic field and the charged particles should statistically average out to zero on a macroscopic scale. The second motion is an ordered motion (non random) and is that equal to the macroscopic velocity of the plasma. This motion is due to the fact that the particles are moving as a whole with a given velocity. Due to this ordered motion of the particles, there will be induced components of motion and force on the charged particles, as described in the preceding paragraph. The first induced component of force will produce a drift of the charged particles as a whole in a given direction resulting in a macroscopic electrical current flow (Refer Fig. 1). The magnitude and direction of the induced current is essentially determined by taking the cross product of the magnetic field vector and the product of the macroscopic velocity vector of the plasma with its scalar conductivity. Collisions and interchange of momentum and energy between particles due to this first induced component of motion result in the familiar joule heating or I^2R loss. The second induced component of force also produces a drift of charged particles as a whole in a given direction; however, this drift is canceled out due to collisions between the charged and neutral particles making up the plasma. The collisions result in a net momentum interchange between the charged and uncharged particles. It is this effect which produces the body force which opposes the motion of the plasma. The magnitude and direction of this body force is determined by taking the cross product of the magnetic field vector and the induced electrical current vector.

Possible Chemi-Kinetic Effects Due to the Presence of a Transverse Magnetic Field

As well as inducing a purely Lorentz type body force the magnetic field may also influence the chemical kinetics of the system[24] and thereby change its characteristics. As was pointed out previously it is the chemical energy released in the combustion zone which sustains the detonation wave at a constant velocity and which also influences some of the observable features of the wave. The chemical energy released provides for all of the inherent energy losses in the system, such as heat transfer, viscous effects, etc., as well as energy to sustain the observed transverse waves in the reaction zone. As the rate of the chemical reaction or the rate of the energy deposition in the combustion zone increases, both the wave velocity and the number of transverse waves also increases while the thickness of the reaction zone decreases. It is therefore obvious how these observable characteristics would be qualitatively affected if the presence of the transverse magnetic field either increased or decreased the reaction rate.

There are two possible ways in which the presence of the magnetic field may affect the chemical kinetics of the system.

The first would be during the initiation or preliminary stage for the reaction. Fong, Bollinger and Edse[24] point out that many of the chain carriers needed for self-sustaining combustion are electrically charged. Because of the presence of the magnetic field, changes in the velocity of these charged carriers should occur. How this will affect the reaction rate can be hypothesized as follows: It is assumed that

the change in particle velocity, will result in both a change in the rate or probability of collision and a change in the momentum transfer upon collision; thus, the rate at which the reaction goes to completion will also be changed.

The second possible chemi-kinetic effect due to the presence of the magnetic field would be that of changing the decay of ionization or recombination rate of the non-equilibrium charged particles in the reaction zone. Kelly, Toong and Tung[25] suggest two possible mechanisms for the decay. These two mechanisms are: (a) attachment of electrons to neutral particles; and (b) recombination of electrons with positive ions. The probability of collision between electrons and neutral particles is greater than that between electrons and positive ions due to the greater density of neutral particles; because of this they hypothesize that the attachment mechanism dominates. Another reason for their conclusion is that it can account for the experimentally observed exponential decay of the non-equilibrium charged particles. As was explained in the preceding paragraph the presence of the magnetic field should change the rate of collisions for the charged particles. This changed rate of collision should change the rate of decay of the non-equilibrium charged particles and therefore the rate of decay of the electrical conductivity.

This changed rate of decay of ionization should result in two ways in which the wave characteristics may be affected. First, a change in the average conductivity of the wave should result, causing a change in the average induced body force. Secondly, since both the recombination and reattachment mechanisms are exothermic reactions,

then the rate of conversion of chemical energy to thermal energy should change.

In summary the presence of the transverse magnetic field should produce the following effects on the characteristics of the detonation wave and its following rarefaction wave.

a) A body force will be induced which will oppose the motion of the waves and therefore slow them down. This reduction in propagation velocity of the wave will be due to the slowing down of its associated following fluid by the induced Lorentz body force. The two are coupled hydrodynamically through the conservation laws (mass, momentum, energy). The result of the induced Lorentz body force acting on the wave is therefore equivalent to a dissipation effect.

b) Unknown chemi-kinetic effects may be produced causing both a change in the rate of conversion of chemical to thermal energy and a change in the variation of electrical conductivity in the wave. The possible change in the rate of chemical energy conversion would case changes in the wave thickness, the number of transverse waves in the reaction zone, and in the wave propagation velocity. The possible change in electrical conductivity will result in a change in the induced body force. The effect of the induced body force was explained in the preceding paragraph.

Theoretical Studies of the MGD Effect in Shock and Detonation Waves

There have been many theoretical attempts to ascertain the effects that a transverse magnetic field will have on the propagation characteristics of both shock waves[36,37,38] and detonation waves[24,39,40,41,42]. These theoretical studies use exactly the same simplified one

dimensional (or planar), laminar, steady state or constant velocity of propagation model which was used to determine the Chapman-Jouguet detonation velocity mentioned previously. However because of the presence of the magnetic field and the resulting Magnetogasdynamic Effect, additional governing equations (Maxwell's Electromagnetic Eqs, Ohms Law) must be introduced into the analysis as well as additional terms in the conservation equations of momentum (magnetomotive body force term) and energy (I^2R loss term). Also, in all cases the additional simplifying assumption of uniform and infinite electrical conductivity through the wave is made. In general, the results of these analyses for detonation waves are to predict a steady state velocity of propagation for the wave which is equal to the Chapman-Jouguet velocity plus an additional term involving the effect or modification of this velocity due to the presence of the magnetic field. This treatment suffers from the same deficiencies as that which was used to obtain the Chapman-Jouguet condition with the additional inadequacy that no account is taken of the variation of conductivity through the wave and also its finite magnitude which was indicated by the work of Kelly, Toong and Tung.[25]

It is because of the insurmountable task of getting a realistic mathematical model for the MGD Effect with respect to the detonation wave that no attempt is made to account for the detonation wave structure in the preceding analyses. Even with the simplified model in which the wave is treated as a discontinuity, additional simplifying assumptions are made in order to obtain mathematical solutions.

Because of the inadequacies of the preceding analysis, its results are not used for the calculations in this study. However, the

same physical model is used in an attempt to predict whether the measured electrical conductivities[25] would produce a Lorentz body force of sufficient magnitude so that the instrumentation used in this study would record an observable effect. The recorded effects would be either or both wave velocity deficits and changes in the static pressure profile of the rarefaction wave. The method of study and instrumentation will be discussed later in this chapter. The calculations using the measured conductivities seem to indicate that there should be no observable static pressure profile variation. The calculations also seem to indicate that because of the small velocity variation of the following fluid there should be no observable velocity deficit as a result of hydrodynamic coupling with the shock front. If there is an observable variation in either or both the pressure profile and the velocity of propagation then this would seem to indicate that the measured values of conductivity are erroneous.

Following is a qualitative explanation of why there should be a variation in the static pressure profile. For the assumed one dimensional steady-state wave, which is propagating through a transverse magnetic field, the derived Lorentz body force is a product of the following fluid velocity and its conductivity to the first power and the magnetic field strength to the second power. Behind the detonation wave front, where the conductivity and absolute fluid velocity are finite, there may be appreciable slowing down of the fluid due to the induced Lorentz body force. If all of the gases had the same conductivity and the same velocity, the only observable effect should be a flow of electrical current and an overall slowing down of the system due to the

conversion of mechanical kinetic energy into electrical work. However, as has been pointed out previously, the conductivity of the gases in the rarefaction wave are in general much less than those in the reaction zone of the detonation wave. Also for the one dimensional model the velocity of the gases in the rarefaction wave progressively decrease in magnitude in a direction away from the detonation wave. Therefore the derived expression for the induced Lorentz body force indicates that it should progressively decrease through the rarefaction wave and in general should be much greater in the reaction zone of the detonation wave. Because of this greater braking force in the detonation wave the following gases in the rarefaction wave should be compressed resulting in a conversion of part of their dynamic pressure into static pressure. In other words there should be a choking effect which would be observable as a variation in the static pressure profile for the rarefaction wave. It is this variation or perturbation of the rarefaction wave that the present study has attempted to record. Perturbations to the flow within the detonation wave itself and therefore variations in static pressure should also occur however these should not be observable with the present instrumentation because of its inadequate spatial resolving powers.

As was mentioned previously, wave velocity deficits may also occur due to both the action of the induced magnetomotive force and the unknown chemi-kinetic effects. The recording of these possible velocity deficits has also been attempted in this study.

Experimental Studies of the MGD Effect in Shock and Detonation Waves

Some experimental studies of the MGD Effect with respect to both shock[37,43] and detonation[24] waves have already been conducted. A brief discussion of the significant features of these studies follow.

Dolder and Hide[43] studied the effect of a magnetic field on a strong shock wave propagating axially through argon in a tube of circular cross-section. Argon was used because of the large conductivities (up to 10^2mhos/cm) which can be produced in it.[37] The magnetic field was generated by discharging a capacitor bank through a circular coil which was mounted axially on a transparent section of the shock tube. The discharge of the capacitor bank was synchronized with the passage of the wave through the coil. Because of the method of generating the magnetic field it had both radial (transverse) and axial components and also had a non-uniform distribution across the tube cross-section. Therefore there were both radial and axial components of electrical current and Lorentz body force of non-uniform distribution. They observed the effect of the field on the wave by recording the intensity of the light pattern emitted by the wave on photographic film both with and without the presence of the field. Their results indicated that with the presence of a magnetic field of greater than 9000 gauss (measured at the center of the coil) the intensity of the light emitted increased.

They attribute this effect to two causes:

a) the I^2R heating of the gas

b) the heating of the gas due to pulsating hydrodynamic compression caused by the induced radial Lorentz body force. It is

suggested by this author and also in Reference 37 that another possible reason for this increased luminosity could be the increased rate of recombination of non-equilibrium ionized particles.

Patrick and Brogan[37] also conducted experiments in which interaction between a magnetic field and strong shocks propagating through argon were recorded. By a suitable adjustment of the flow passage geometry within the coil and also due to placement of the coil an essentially uniform transverse magnetic field was obtained, in contrast to that of Dolder and Hide. They obtained a photographic record using a mirror camera which showed the production of shock waves indicating a strong interaction between the propagating shock and the transverse magnetic field. The magnetic field strength and propagating shock strength speed were respectively approximately 6000 gauss and Mach 18.

Fong, Bollinger and Edse[24] studied experimentally the effect that a transverse magnetic field has on the initiation or generation of a fully developed detonation from a deflagration wave. Their studies involved use of both AC and DC generated magnetic fields with respect to initiation of detonation in a hydrogen-oxygen mixture which was confined in a tube of circular cross-section. They found the initiation process was inhibited by the presence of either AC or DC fields. It was also found that the presence of a 30 gauss AC field inhibited the generation process more than a 1000 gauss DC field. No satisfactory explanation for this phenomenon was suggested. This author suggests that the possible reason for the inhibiting effect(of either AC or DC fields) is that the presence of the magnetic field limits the motion of the ionized chain carriers which are involved in the chemi-kinetics of the deflagration process. The reaction process in

the deflagration wave influences its motion and therefore will also influence the rate at which detonation is initiated.

The preceding experimental results seem to indicate that a chemikinetic effect should be observed when the detonation wave propagates through the magnetic field.

Purpose and Scope of the Study

The purpose of this experimental study is to attempt to resolve the following questions:

a) Will there be an experimentally observable MGD Effect on the detonation wave upon propagation through the transverse magnetic field?

b) If there are observable results, do these indicate a chemikinetic effect (should be indicated by a change in the wave front propagation velocity) or do they indicate a hydrodynamic effect due to the induced Lorentz body force (should be indicated by changes in the rarefaction wave pressure profile and also wave propagation velocity)?

c) If there are observable results what are their order of magnitude?

The scope of the study is to experimentally observe the propagation velocity of a fully developed detonation wave and the static pressure profile of its accompanying rarefaction wave both in the presence of and in the absence of a strong transverse magnetic field in order to resolve the preceding questions. The detonation wave was generated in acetylene-oxygen mixtures of varying composition and at varying initial pressures. The selection of acetylene as the

combustible fuel is justified in Chapter 2. No attempt is made to correlate experimental information with a theoretical analysis because of the previously mentioned difficulties in generating a suitable analysis.

Method of Study

Acetylene and oxygen were mixed under controlled conditions so that a mixture of known composition was produced. The acetylene-oxygen mixture was then introduced into a tube of square cross-section and ignited by means of a glow plug at one end of the tube. A square wound wire coil placed inside the tube at the ignition end promoted turbulence and hence rapid transition from a deflagration to a fully developed detonation wave. With the mixtures and initial pressures used in this study the transition was expected to take place a short distance downstream from the point of ignition.

The velocity of the wave was determined by means of electronic counters whose start and stop circuits were actuated by voltage pulses produced by piezo-electric gages. The gages were placed at known intervals along the tube axis and so that their sensitive surfaces were flush with the inside surface of the tube. The detonation wave upon passing the gage produced a voltage pulse which actuated the counter circuits. The counters recorded the time interval for the wave to propagate the known distance between two gages, thereby allowing the wave velocity to be calculated. Six gages along with three counters were used to get three velocity readings for successive intervals along the tube axis.

The purpose of the multiple velocity readings is threefold. First, if successive readings are the same, this establishes the fact that the wave has reached steady state or a constant velocity of propagation. Second, the variation of velocity or velocity deficit for a particular run may be determined directly by a comparison of the readings upstream from the magnet to that across the magnet gap. Finally the readings may be averaged to get an average set of data for computing the propagation velocity.

The pressure variation within the wave was recorded by photographing the display on an oscilloscope screen of the voltage pulse produced by the piezo-electric gage as the wave passes its surface. The voltage produced by the gage is directly proportional to its mechanical deformation which in turn is directly proportional to the pressure acting on its surface. Only the voltage pulse produced by the last gage (or the gage furthest from the point of ignition) was recorded in this way.

The transverse magnetic field was produced by a D.C. magnet which was placed so that the detonation tube was within its gap and so that the last gage was immediately downstream of the gap.

For each combustible mixture at a given initial pressure two runs were made for comparative purposes. One run was made with the magnet on and the other with it off. In this way variations in both the wave front propagation velocity and its pressure profile upon passage through the gap of the magnet may be determined.

CHAPTER 2

APPARATUS AND INSTRUMENTATION

The overall experimental system is shown photographically in Figure 2 and schematically in Figure 3. It may be thought of as being made up of four subsystems as follows:

a) The mixing system and its associated instrumentation.

b) The tube, instrument bosses and ignition system.

c) The electromagnet and rectifier set.

d) The measuring instrumentation, probes and probe adapters.

A brief discussion of these subsystems and their components is given in the following paragraphs.

Before discussing the system components, a few general statements will be made about the overall system with respect to its design, fabrication and instrumentation.

The chief considerations in the design and fabrication of the hardware were: ease of assembly, durability of materials and safety. Ease in assembling the system also guaranteed ease in disassembling it for maintenance, which was necessary periodically during the tests. Whenever possible the materials which came in contact with the gases were selected to be stainless steel both in order to prevent possible corrosion and for safety reasons. As reported in Reference 44, pure acetylene is highly unstable at pressures above approximately 30 psig and also upon contact with certain materials such as copper, silver, etc., it forms highly unstable compounds. The selection of stainless

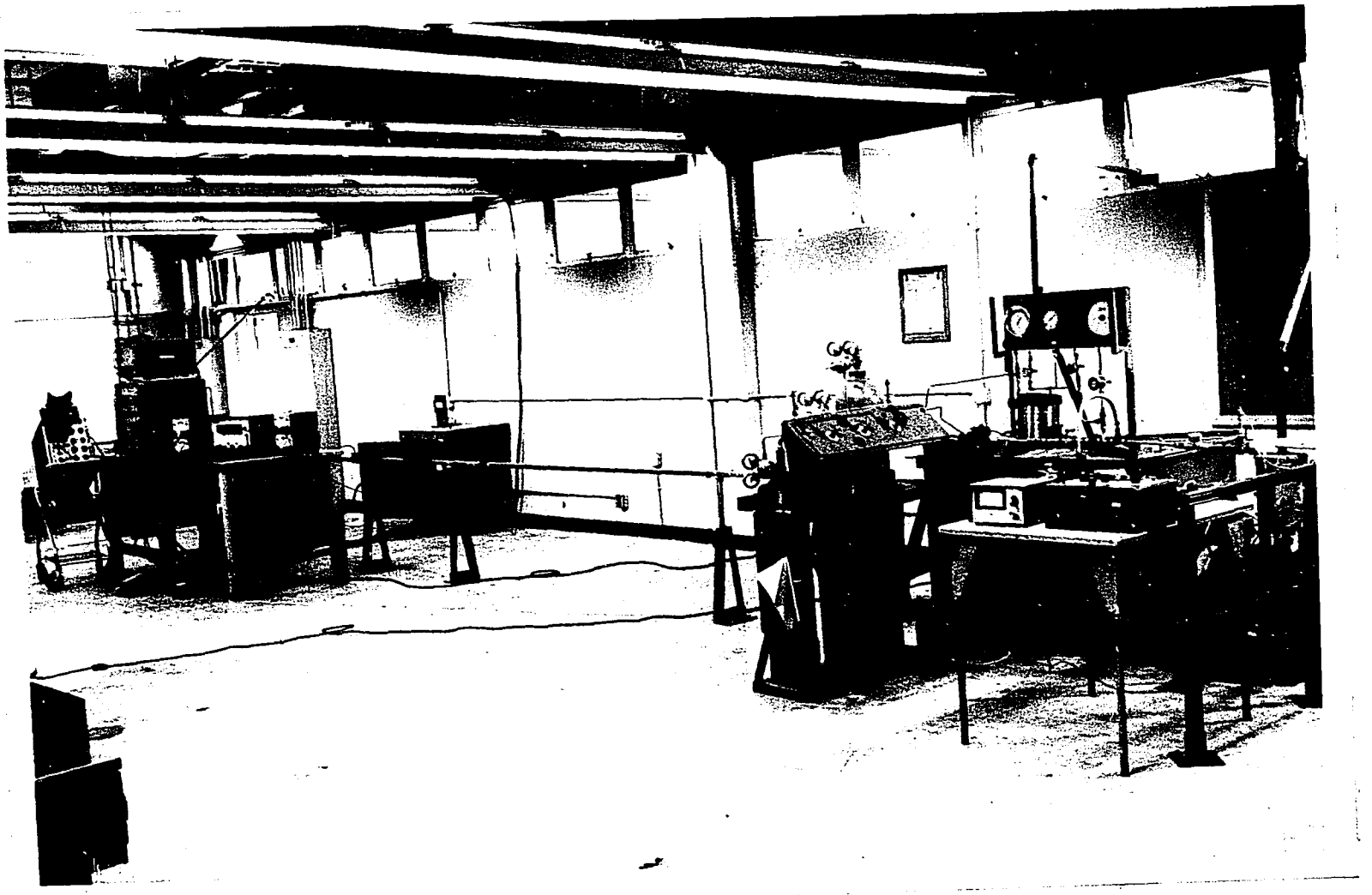

FIGURE 2. EXPERIMENTAL SYSTEM

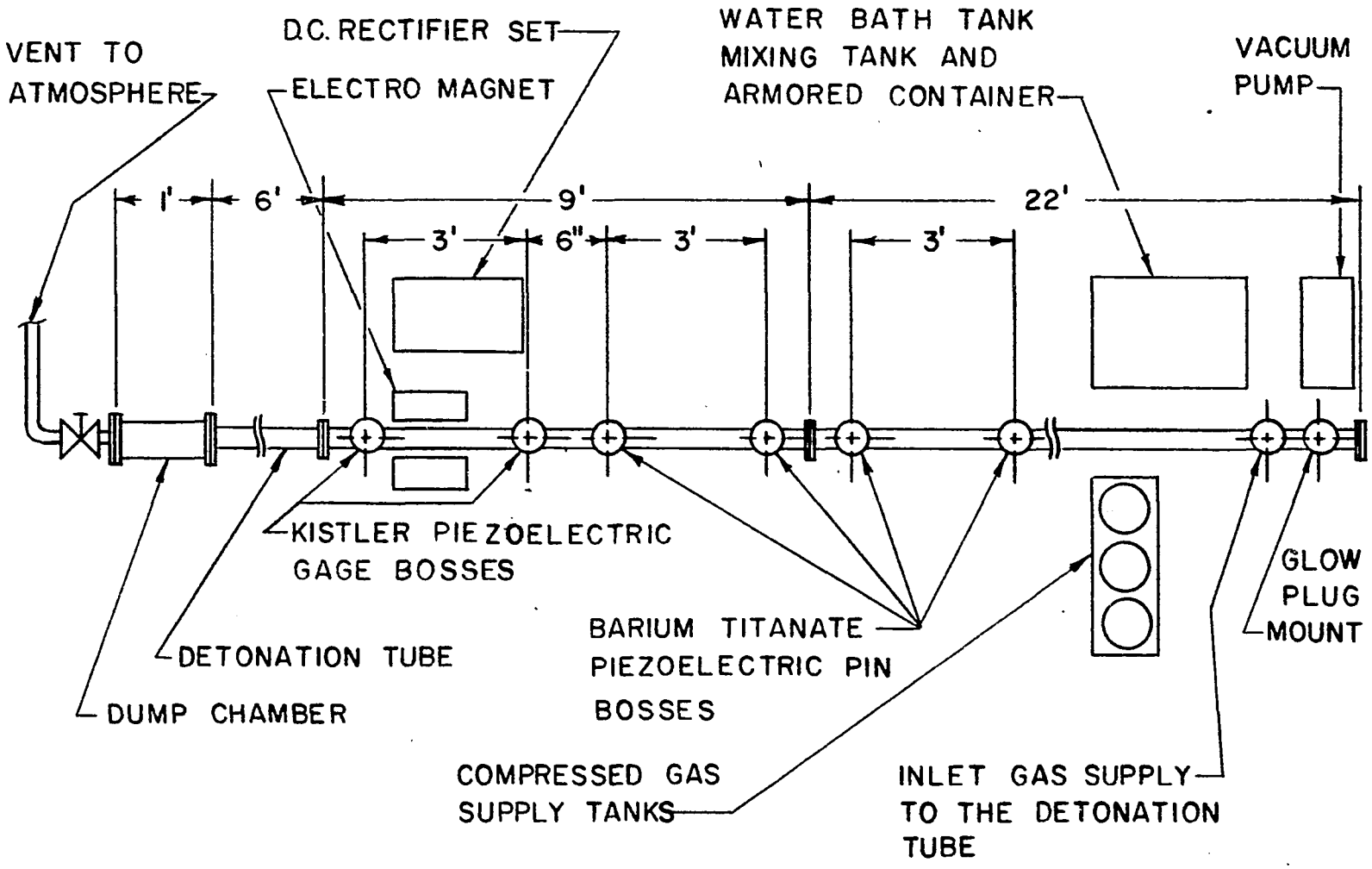

FIGURE 3. SCHEMATIC PLAN VIEW OF DETONATION TUBE SYSTEM

steel prevents the formation of these compounds. In addition the strength of the steel will prevent possible rupture of the system should detonation take place accidentally during either the mixing or transfer processes involved in charging the tube with a detonable mixture.

Additional safety features which were either included in the hardware or used during the operating procedures are as follows:

a) Plexi-glass shields were placed in front of all glass faces of the bourdon type pressure gages. This was done in order to deflect possible glass splinters should the gage be ruptured by an accidental detonation occurring within it.

b) Before ignition of the mixture the tube was isolated from the rest of the system using the following procedure. The connecting valve was closed and then the lines between the tube and the tanks of gas were purged with nitrogen. These lines were then evacuated by means of the vacuum pump and finally recharged with nitrogen. Then all of the valves connecting the pressure gages to the plumbing were closed. The isolation of the tube by means of the valves and the inert gas was in order to confine the detonation process to it alone and thereby prevent the system from rupturing either at its weak points (bourdon gages) or at points in which there are large concentrations of gases at high initial pressures (mixing tank and commercial gas cylinders).

c) A commercially available acetylene pressure regulator was used on the discharge side of the acetylene tank so that the maximum discharge pressure was limited to 30 psig because of the previously mentioned unstable condition of the gas above this pressure.

d) The mixing and water bath tanks were encased in an armored container in order to catch possible flying fragments of metal should the mixing tank be ruptured due to accidental detonation within it.

e) All valves and plumbing were high pressure (rating 3000 psi) in order to prevent their rupturing if subjected to detonation pressures.

Acetylene and oxygen were selected as the gases for the detonable mixture because of their following desirable features.

i) Both gases are easily obtainable in commercial cylinders with suitable pressure regulators for regulating discharge pressures.

ii) There is considerable information available, both experimental and theoretical, on the detonation characteristics of oxyacetylene mixtures.

iii) The oxyacetylene mixture is easily detonable and because of the rapid chemical reactions in the combustion zone a high wave propagation velocity is produced.

iv) For an unseeded mixture high values of electrical conductivity are produced in oxyacetylene detonation waves.

The method of measuring the desired wave characteristics was selected to be by means of electronic instrumentation. Optical methods were ruled out both for the reasons outlined in Chapter 5, under recommendations, and because of the ease with which electronic instruments may be read and their readings interpreted. Also the electronic measurements of velocity and pressure are more accurate than the optical procedures. No consideration was given to mechanical instrumentation for the obvious reason that their inertia would not allow them to follow the high speed events taking place in the detonation phenomena.

All of the instruments in the system were calibrated against suitable standards and found to fall within their normal expected range of accuracy. It was felt that extreme accuracy was not required because of the fact that the main purpose of these tests was to record changes in wave characteristics.

Mixing System and Its Associated Instrumentation

The mixing system consists of the following components:

a) The compressed gas supply cylinders and their pressure regulators.

b) The armored container, water bath and mixing tanks.

c) The vacuum pump.

d) The connecting plumbing between the preceding three system components.

e) The system instrumentation.

The mixing system is shown in Figure 2 at the extreme right hand side of the photograph. Location of the main components of the system with respect to the photo are shown schematically in Figure 3.

The preceding components will be discussed in relation to the following procedures of mixing a detonable mixture in the mixing tank and then charging the detonation tube with the resultant mixture. The normal procedure for obtaining a combustible mixture was by using the mixing tank; however, the system was designed so that the mixing process could also be carried out in the detonation tube. Since only the normal mixing procedure was used in this study, it alone will be discussed.

The function of the plumbing system, shown schematically in Figure 4, is fivefold as follows:

a) It provides means for transferring the fuel and oxidizer to the mixing tank.

b) It provides means for transferring the combustible mixture to the detonation tube.

c) It provides means for evacuating the system components either individually or simultaneously.

d) It provides means for purging (with N_2) and/or venting the system components either individually or simultaneously.

e) It provides means for connecting the pressure measuring instruments to the system.

The mixing procedure involved the following steps. First, the mixing tank and the plumbing connecting it to the compressed gas supply tanks were evacuated. Then the tank was charged first with acetylene and then with oxygen. The pressure of the gas was recorded, when equilibrium had been attained, after each step in the charging procedure. In this way the partial pressures of the components making up the combustible mixture were determined. Since the gases at the temperatures and pressures of this study act very nearly as ideal gases, then the partial pressures of the gases are directly proportional to their amounts in the mixture. The mixture composition is therefore determined through the recorded partial pressures.

The pressure of the gases in the mixing tank was measured with a test gage of the bourdon type manufactured by the Karoll-Warner Corp. The gage had a full scale range of 0 to 60 psig.

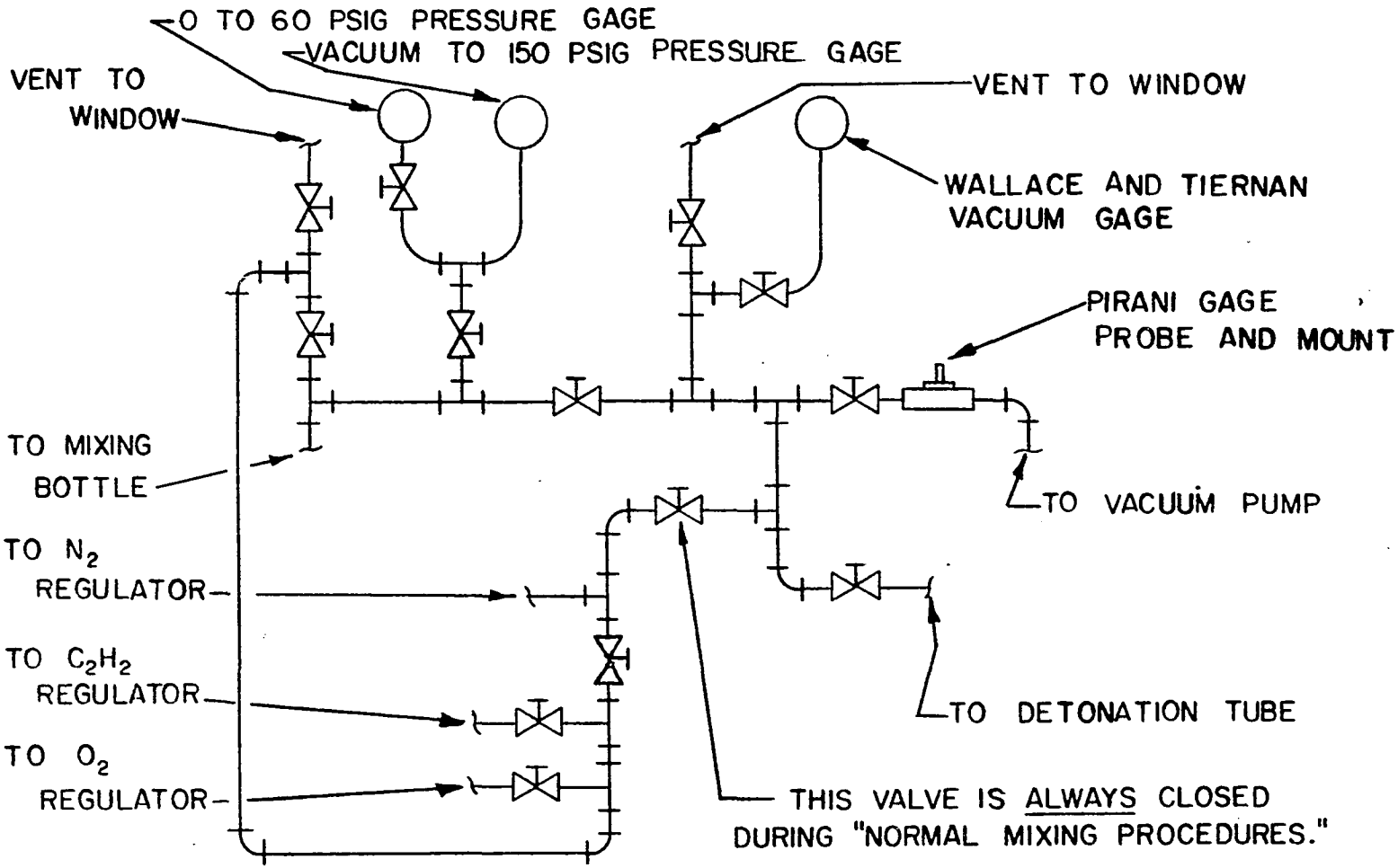

FIGURE 4. SCHEMATIC DIAGRAM OF MIXING SYSTEM PLUMBING

The mixing tank is a commercial CO_2 cylinder with a diffuser section connected to its inlet. The diffuser was made out of a cylindrical piece of pipe. The end of the pipe which was not to be connected to the cylinder inlet was plugged and then holes were drilled at various points through its surface. It was then mounted axially inside the cylinder. The function of the diffuser was to promote proper mixing of the fuel and oxidizer during the charging procedure so that a homogeneous mixture would be rapidly obtained.

The mixing tank was mounted horizontally inside of the water bath tank. The reason for horizontal mounting was in order to try to minimize any possible stratification of the two gases between the time of completion of the mixing procedure and that of charging the detonation tube. This is critical in order to assure that a homogeneous mixture be maintained in the tank and hence that a mixture of known composition be delivered to the detonation tube.

The purpose of the water bath was to help promote equilibrium by heat transfer between the water and the gas after each step in the charging procedure. Heat transfer was promoted by circulating water past the mixing tank surfaces by means of an electrically driven stirrer. The equilibrium temperature of the mixture was assumed to be that of the water. This temperature was recorded by means of an iron constantan thermocouple which was connected to a Leeds and Northrup potentiometer.

After the mixing procedure the lines connecting the mixing tank and the compressed gas supply tanks were purged with N_2 and left vented to the atmosphere.

The charging of the detonation tube involved the following steps.

First, the tube and the lines connecting it to the mixing tank were evacuated. A combustible mixture from the mixing tank was then introduced into the tube through a spring loaded metering valve until the desired initial pressure was attained. The tube was then isolated from the rest of the system by the previously mentioned safety procedure.

Initial pressures of up to 800 mm of Hg(15.5 psia) were recorded by means of a Wallace and Tiernan diaphragm type vacuum gage. For pressures above 800 mm a test gage of the bourdon type was used.

The vacuum pump was a single stage mechanical pump manufactured by the Kinney Corp. Its manufacturer rated capability was 50 microns absolute pressure. This vacuum was deemed sufficiently low for these studies and therefore a diffusion pump was not included in the system.

The pump vacuum was determined by means of a pirani gage and probe system.

Tube, Tube Supports, Instrument Bosses and Ignition System

The tube, tube supports, instrument bosses and the ignition system are visible in Figure 2. The tube and instrument bosses are also shown schematically in Figure 3.

The tube is made up of three sections of square tubing and a cylindrical dump chamber. Each of these was bolted to its adjacent section by means of flanges. The connections were sealed by introducing commercially available O-Rings between the mating flanges. The ignition end of the tube was closed by means of a flange plate while at the other end a vent line and discharge valve were attached to the dump chamber.

The square tube sections were made out of commercially available non-magnetic stainless steel (type 304) tubing. The nominal cross-sectional dimensions of the tube are 1" outside dimension with a 0.123" wall thickness. Non-magnetic steel was chosen in order to minimize flux leakage across the magnet's gap and thereby assure a transverse magnet field. The mechanical strength of this tubing was determined to be adequate for withstanding the dynamic pressures generated by the detonation processes in this study.

The dump chamber was made out of commercially available type 304 stainless steel tubing with nominal dimensions of 3" O.D. and 0.375" wall thickness. The function of the dump chamber was to attenuate reflected shocks from the end of the tube and thereby prevent retriggering of the measuring instrumentation circuits. From examination of the recorded photographic results (Appendix C) the chamber apparently functioned properly at initial pressures of 550 mm (10.6 psia) and 800 mm of Hg (15.5 psia) but not at 15 psig (29.7 psia). At initial pressures of 15 psig it was not possible to set the oscilloscope triggering circuit so as to prevent multiple triggering of the sweep.

The vent line allowed the tube to be purged of burnt gases, after detonation had taken place, in preparation for its recharging with a fresh combustible mixture. Purging of the tube before its evacuation with the vacuum pump was deemed necessary in order to minimize the contamination of the pump oil by impurities, such as carbon particles, formed by the combustion process.

Considerable amounts of soot were formed and deposited inside the tube during the test runs. The density of the deposits increased

towards the end of the tube to which the dump chamber was attached. This can be explained in two ways. First, the following gases behind the detonation front would have a tendency to carry the particles along with them. Second, during the previously mentioned purging of the tube the nitrogen flow would also sweep the particles towards the dump chamber.

Because of these soot deposits the tube was disassembled and cleaned periodically. Cleaning was accomplished by using a plumbers snake to run acetone soaked rags through each section.

The tube supports were designed to allow for proper alignment of the tube sections as well as to hold the tube in a fixed position. Both vertical and horizontal adjustments were available at the supports to allow for tube alignment. Also a clamping arrangement at the supports prevented movement of the tube. Supports were spaced so that there was no sagging of the tube. There are two reasons for preventing tube sag. The first reason is to prevent the mechanical stresses to which the tube would be subjected. Second because of the way propagation velocity was to be measured any sag between the probes would introduce an error in these results.

The instrument bosses were designed to accommodate the instrument probes and their adapters and also so that they could be mounted on the tube with the surface of the boss, adapter probe assembly flush with the inside surface of the tube. This mating of the assembly surface with the inside surface of the tube prevents perturbations of the detonation wave due to its encountering an irregularity in the flow channel cross-sectional area. The assemblies and their method of mounting on the tube are shown in Figures 7, 8, 9 and 10.

Bosses for mounting of an ignition system glow plug and for connecting the plumbing from the mixing system were also attached to the tube.

All of the bosses were made of type 304 stainless steel bar stock and were attached to the tube by means of 3M-Type 2158B/A epoxy.

The ignition system was made up of a glow plug and its 1-1/2 volt battery power source, ignition switch, ignition leads, and a 6 volt relay system with a foot switch for actuating it. The ignition system operation involved the depression of the foot switch in order to actuate the relay system. The relay system closed the ignition switch and thereby provided the required 1-1/2 volt power source to the glow plug.

The ignition system leads were approximately 40 feet long. This allowed for the remote firing of the system (for safety reasons) and it also allowed the placement of the foot switch and relay system near the oscilloscope and its camera. The camera shutter and the ignition system could therefore be operated by a single individual. This facilitated the taking of data.

The Electromagnet and Rectifier Set

The electromagnet and D.C. rectifier set are visible in Figure 5. Their relationship to the other components making up the overall system is shown photographically in Figure 2 and schematically in Figure 3. Also visible in Figure 5 are the following:

a) The tube and its supports.

b) The dump chamber and its vent line.

c) The measuring instrumentation.

d) The ignition relay and its actuating foot switch.

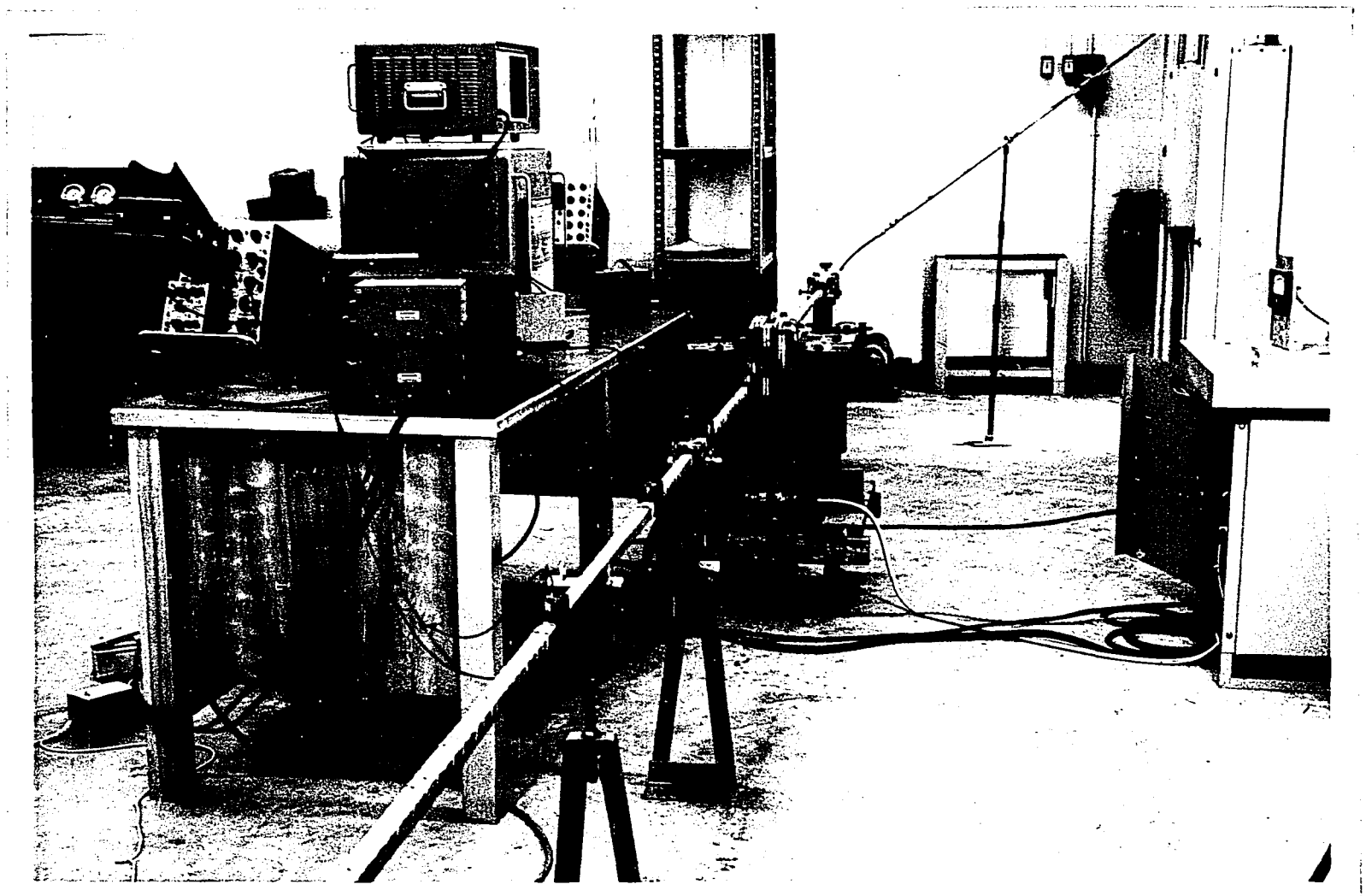

FIGURE 5. THE MEASURING INSTRUMENTATION, ELECTROMAGNET AND RECTIFIER SET

Both the rectifier and the transformer from which the electromagnet was fabricated were purchased from state surplus.

The rectifier set is a navy surplus unit which was originally used for anti-corrosion purposes aboard ship. The set has a maximum rated D.C. output of 1.95 KVA at 130 amps for a 115/440 volt single phase A.C. input. Power supply for the rectifier was obtained from an overhead bus bar system, which runs through the lab.

The transformer had a rating of 50 KVA, single phase, 60 cycle and 2400 volt to 120/240 volts. The electromagnet was fabricated in the following way.

a) The coil-transformer core assembly was removed from its casing and a 1" gap was milled into the upper horizontal leg of the core.

b) Six pole coils with a total of 183 turns were wound and then mounted on the two pole pieces formed by the preceding milling operation. These auxiliary coils were connected in series with the original secondary coils of the transformer and the resultant total of 223 turns was connected to the rectifier output.

The magnetization curve for the electromagnet is shown in Figure 17, Appendix B. The magnetic field strengths for the various rectifier inputs to the magnet were obtained using a gauss meter with its associated search coil. Rectifier outputs or magnet inputs were read by means of a 50 mv ammeter which was connected across a 350 amp shunt.

The Measuring Instrumentation, Probes and Probe Adapters

The measuring instrumentation is shown photographically at the lefthand sides of both Figures 2 and 5. Its circuitry is shown

schematically in Figure 6. The instrumentation consists of the following:

a) Three electronic counters and their associated amplifiers, piezo-electric probes, probe adapters and connecting cables.

b) A tektronix Type 585 oscilloscope.

c) A model 196A Hewlett-Packard (Polaroid Land) Camera, with its adapter for photographing the scope screen.

Upon ignition of the mixture, with its resultant generation of a detonation wave which propagates past the exposed surfaces of the pressure transducers, the following sequence of events occur in the instrumentation circuitry:

i) The individual counter start and stop circuits are triggered by the wave as it passes each successive pair of transducers.

ii) The wave upon passing barium titanate pin No. 4 (Refer to Fig. 6) not only triggers the stop circuit of its counter but also triggers (or starts) the time delay circuit of the oscilloscope. The function of the time delay circuit is to delay the start of the horizontal sweep, of the electron beam, across the scope screen for a time interval which is determined by the setting of the circuit. This setting was made so that the sweep would start just before the wave passes Kistler gage No. 2.

iii) The wave, upon passing Kistler gage No. 2, triggers the stop circuit of its counter and also deflects the electron beam of the scope vertically resulting in the pressure traces which are recorded in Appendix C.

The triggering of the circuits and the vertical deflection of the electron beam are caused by voltage signals which are produced by

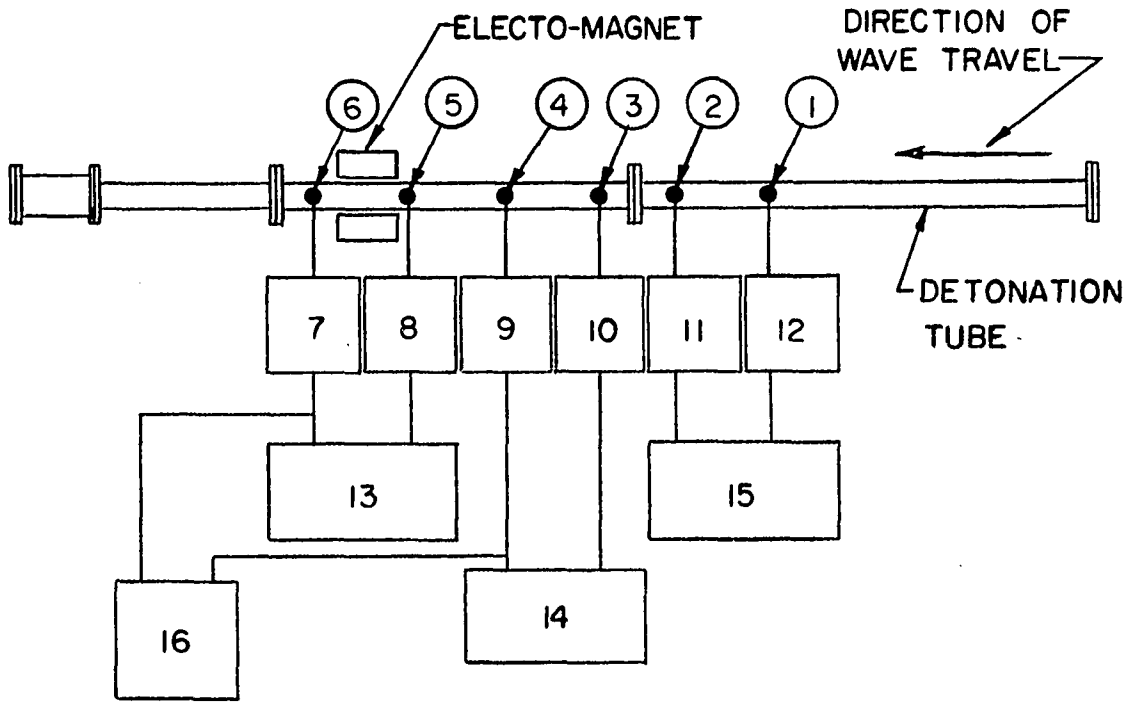

1	BARIUM TITANATE PIEZOELECTRIC PIN No. 1
2	" " " " " 2
3	" " " " " 3
4	" " " " " 4
5	KISTLER PIEZOELECTRIC GAGE No. 1
6	" " " " 2
7	" CHARGE AMPLIFIER
8	" " "
9	HEWLETT-PACKARD AMPLIFIER
10	" " "
11	" " "
12	" " "
13	" " ELECTRONIC COUNTER 2
14	" " " " 1
15	BECKMAN ELECTRONIC COUNTER
16	TEKTRONIX OSCILLOSCOPE

FIGURE 6.

SCHEMATIC OF MEASURING INSTRUMENTATION CIRCUIT

the mechanical deformation of the piezo-electric crystals, within the pressure probes. Amplifiers must be used in the system both because of the small amplitude of these voltages and the high impedance of the transducer. The amplified signals are used to both trigger the circuits and to obtain a pressure record of the passing wave system by means of the display component which in this case is the oscilloscope.

Two types of commercially available piezo-electric pressure probes were used in the study. These two probes were manufactured by the Kistler Instrument Corp. and by Channel Industries, Ltd. The Kistler probe uses a naturally occurring quartz crystal to produce the piezo-electric effect while the pin type probe of Channel Industries uses a manufactured ceramic crystal (barium titanate).

The Kistler gage was selected to produce the voltage pulse for display on the oscilloscope screen both because of the availability of its matching charge amplifier and the fact that it is thermally stable. Acceleration effects were minimized or eliminated both through the selection of a type 603A gage and by the design of the gage adapter. Thermal drift was eliminated by applying a thin (0.010 inch) ablative coating of silastic rubber (Dow Corning RTV 860) to the exposed surface of the gage.

The 603A gage has two crystals one of which is exposed to both pressure and acceleration* while the second is exposed to only acceleration. The second crystal acts as an acceleration compensator. Its signal is subtracted from that of the first crystal so that a net

---

*Acceleration refers to unwanted mechanical vibrations, for which, a pressure gage reading is not desired.

signal due to pressure variations alone is obtained from the gage.

The Kistler gage, adapter, boss assembly is shown schematically in Figure 7 and photographically in Figure 8. As was recommended in References 45 and 46 the gage is mounted in an adapter of large mass (large inertia) which in turn is shock mounted in the boss by means of O-Rings. Both the inertia of the adapter and its shock mounting will tend to eliminate acceleration effects.

Because of their relative inexpensiveness the barium titanate probes were chosen to trigger the first two counters in the circuit. The pins were protected against thermal depolarization by applying an 0.010 inch silastic rubber ablative coating to their surfaces.

The pin, adapter, boss assembly is shown schematically in Figure 10 and photographically in Figure 9. Both the pin and its adapter are shock mounted, the former in a RTV 860 silastic rubber and the latter with O-Rings. Shock mounting was used in order to prevent possible upstream vibrations from triggering the counters prematurely.

The functions of the amplifier are to both amplify the signal output from the piezo-electric transducer and to provide impedance matching between the transducer and its display component. Impedance matching requires that the high impedance (up to 10^{14} ohms) signal from the transducer be converted to a low impedance input to the display components (counters and oscilloscope).

Kistler Model 504 charge amplifiers, with matching low impedance shielded cables, were used for amplification of the signal from the Kistler gages.

Hewlett-Packard Model 450A amplifiers were used for amplification

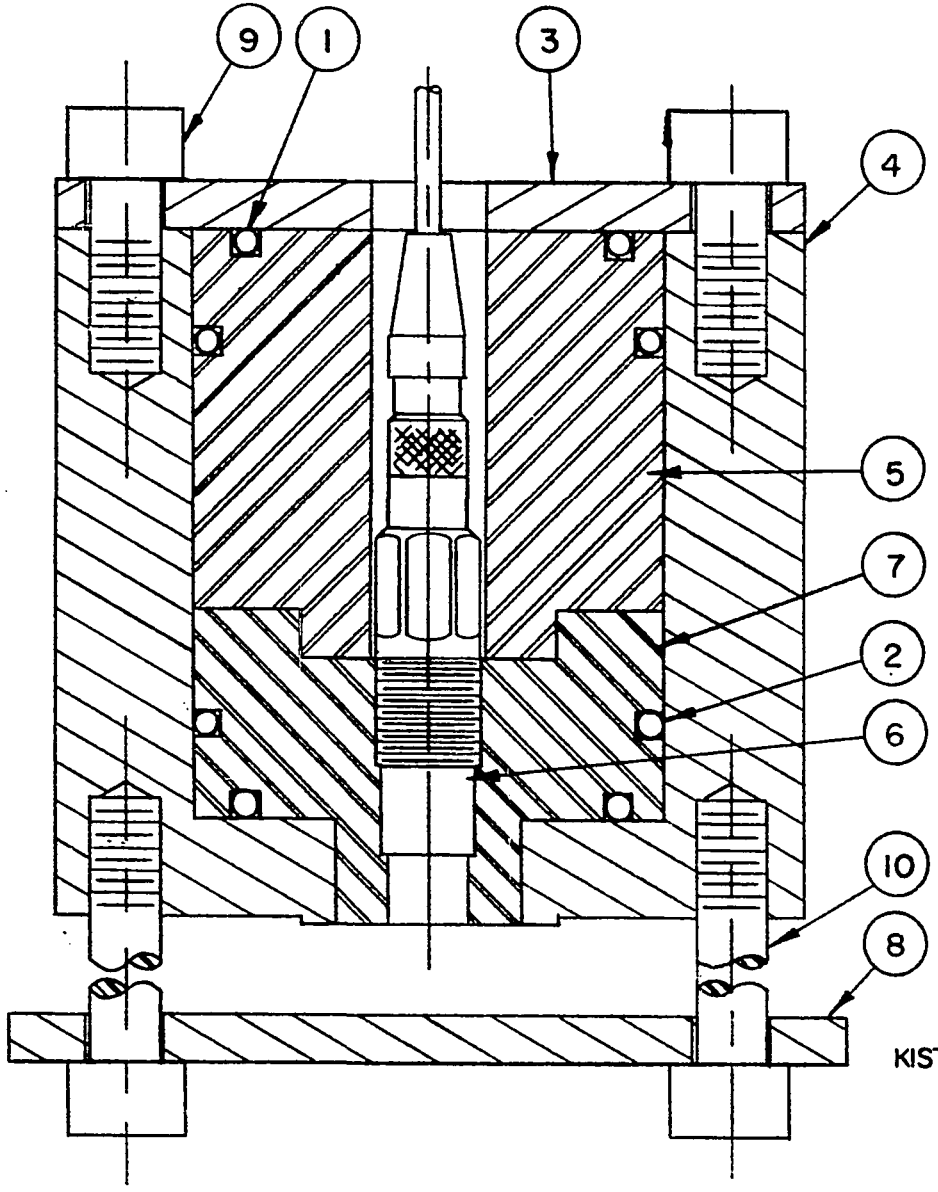

NO.	NAME	QUAN REQ'D	MATERIAL
1	PARKER 211, O-RING	2	
2	PARKER 214, O-RING	2	
3	COVER PLATE	1	NON-MAGNETIC STAINLESS
4	HOUSING	1	NON-MAGNETIC STAINLESS
5	INSTRUMENT MOUNT	1	BRASS
6	KISTLER GAGE AND ADAPTOR CONNECTOR	1	
7	GAGE MOUNT	1	BRASS
8	STRAP	1	NON-MAGNETIC STAINLESS
9	10-32 ALLEN SCREW	6	
10	10-32 ALLEN SCREW	2	

FIGURE 7.
KISTLER PIEZOELECTRIC BOSS ASSEMBLY
NOT TO SCALE

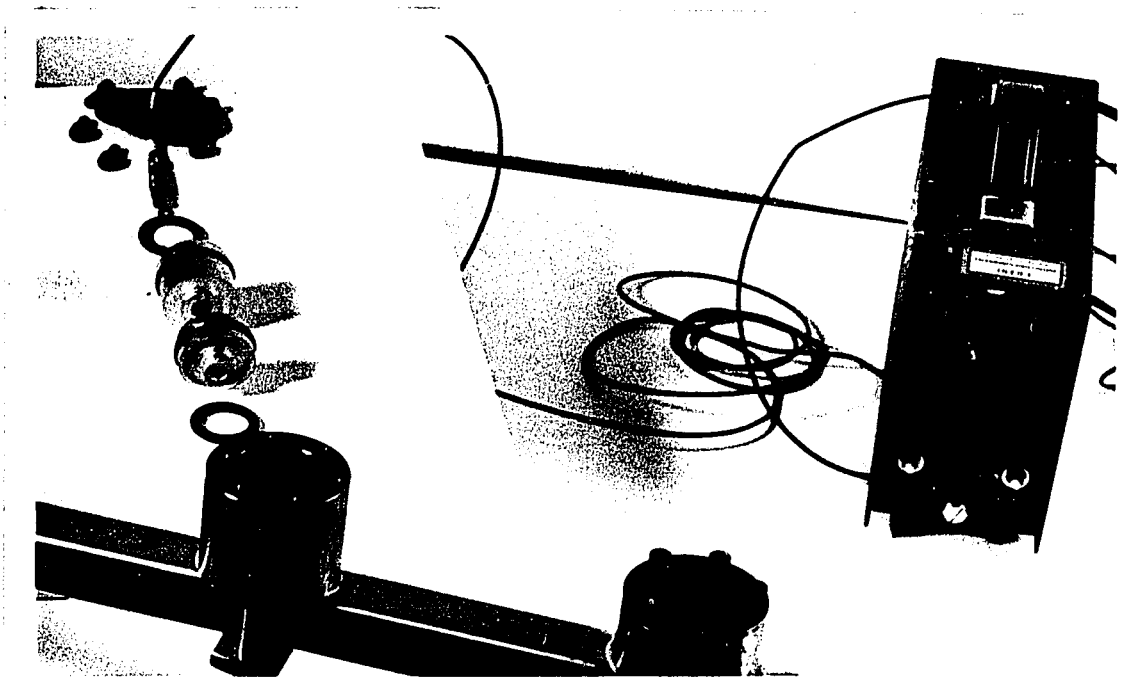

FIGURE 8. KISTLER PIEZOELECTRIC BOSS ASSEMBLY

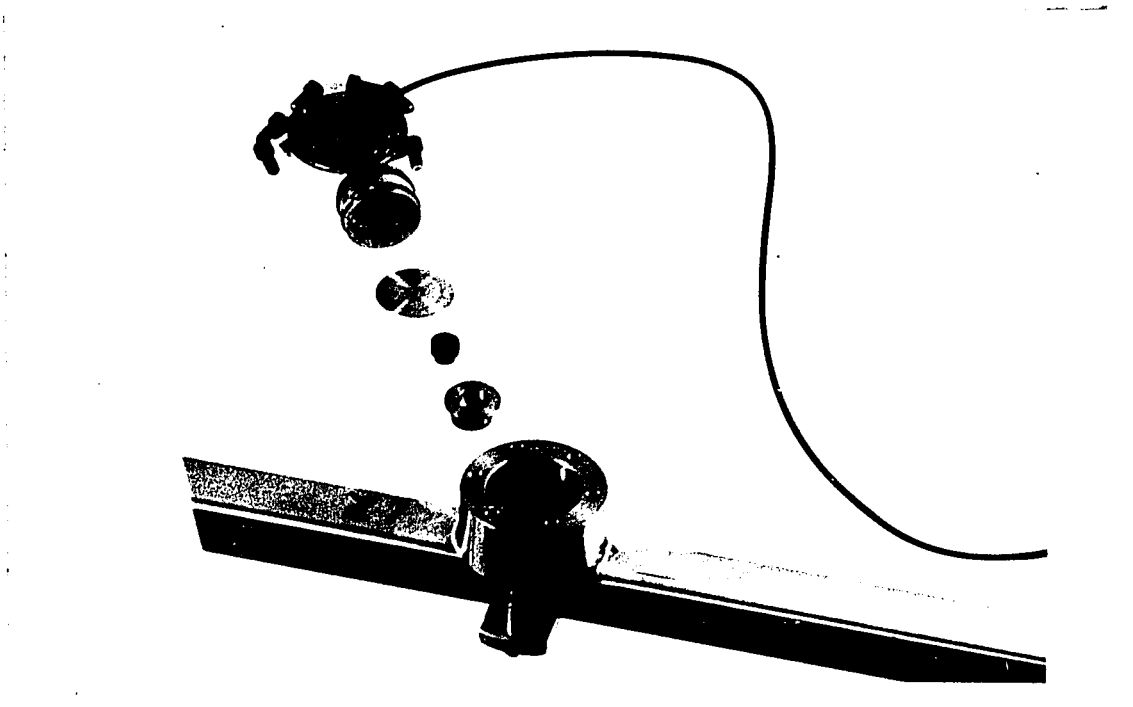

FIGURE 9. PIEZOELECTRIC PIN TRANSDUCER BOSS ASSEMBLY

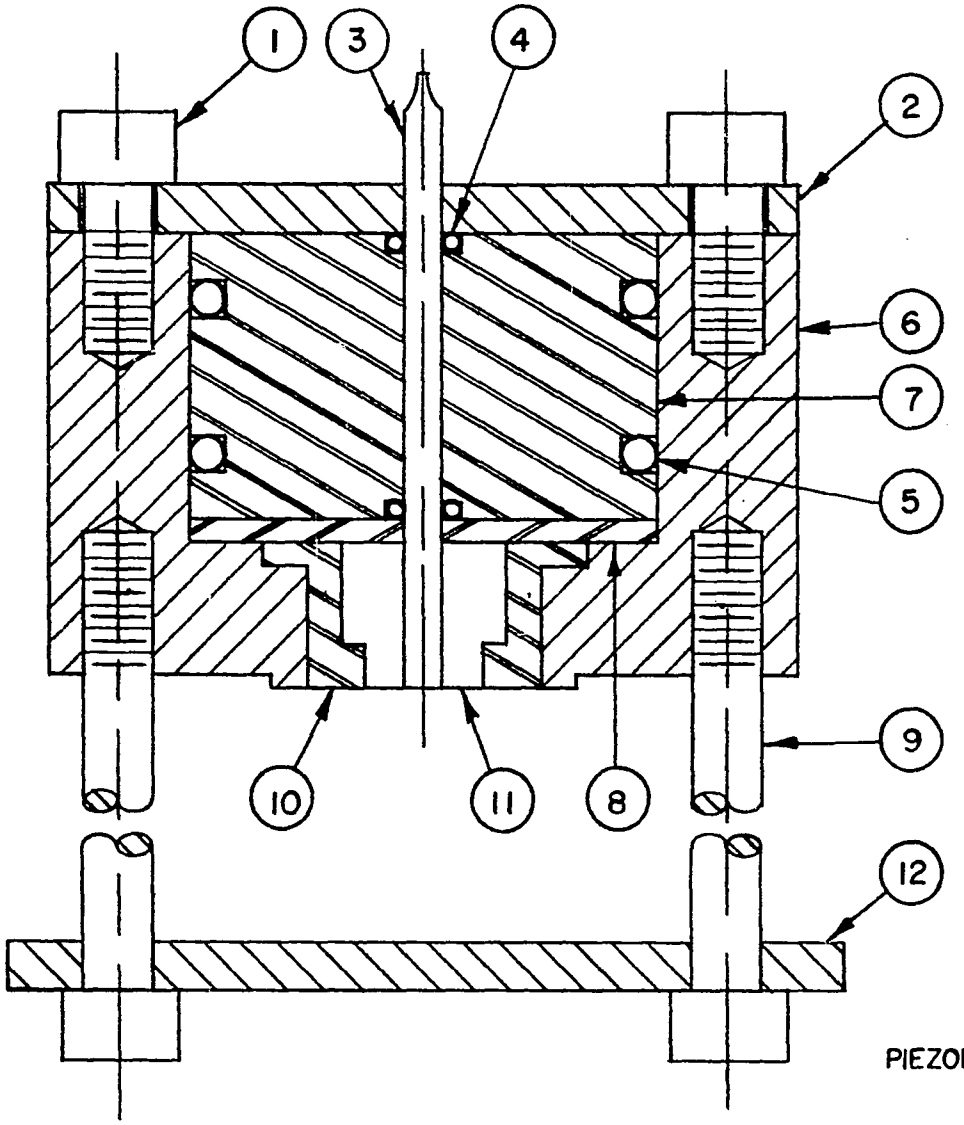

NO.	NAME	QUAN REQ'D	MATERIAL
1	10-32 ALLEN SCREW	6	
2	COVER PLATE	1	STAINLESS
3	PIN TRANSDUCER	1	
4	PARKER 5, O-RING	2	
5	PARKER 121, O-RING	2	
6	HOUSING	1	STAINLESS
7	TRANSDUCER BODY ISOLATOR	1	BRASS
8	WASHER	1	BRASS
9	10-32 ALLEN SCREW	2	
10	TRANSDUCER HEAD ISOLATOR	1	BRASS
11	SILASTIC RUBBER FILLER		
12	STRAP	1	STAINLESS

FIGURE 10.
PIEZOELECTRIC PIN TRANSDUCER BOSS ASSEMBLY
NOT TO SCALE

of the signals from the barium titanate pins. The pins and amplifier were connected by means of low impedance shielded cables which were obtained from the manufacturer (Channel Industries of Santa Barbara) of the pins.

For a given run, the accuracy of the measurement of both the speed of a steady state wave and of any possible variation in its speed due to the presence of a transverse magnetic field is governed by the accuracy of the Hewlett-Packard counter No. 1 (Refer to Fig. 6). Because of system circuitry (Figure 6) the preceding two quantities are measured in the following ways:

a) Steady state propagation by comparing readings of the Beckman and Hewlett-Packard No. 1 counters.

b) Possible variations in propagation velocity by comparing readings of the Hewlett-Packard No. 1 and 2 counters.

The accuracies of the counters are governed by the way in which they operate. The counters have incorporated in them oscillators which can generate AC outputs of standard or fixed frequencies. By means of a suitable input trigger voltage, an electronic binary counting circuit is opened, allowing the output of the oscillator to be counted in terms of the number or frequency of alternating pulses that are generated by it. Upon input of a second trigger voltage the counting circuit is closed. By this means the time interval between the two triggering voltages may be determined in terms of the product of the period for and number of pulses from the oscillator. This time interval is displayed in digital form on the counter control panel. Assuming that the trigger voltage pulses are identical and that the threshold

voltages or points on these pulses at which the counting circuit is triggered open and closed are identical then the possible inaccuracy is $\pm$ 1 counts. That is, there is a possibility of either allowing or disallowing a pulse from the oscillator to enter the counting circuit during both its opening and closing processes. Therefore the nominal accuracy of the counter is $\pm$ 1 the frequency or period of the pulse it is counting. In the cases of both the Beckman and the Hewlett-Packard No. 2 counters this is $\pm$ 0.1 μ sec. For the Hewlett-Packard counter No. 1 the nominal accuracy is $\pm$ 1 μ sec. Therefore the maximum possible variation between the individual counter readings would be 2 counts of the Hewlett-Packard No. 1 or 2 μ secs.

For a given run, with no transverse field, differences between the readings of the Hewlett-Packard No. 2 and the Beckman counters may be accounted for in the following ways:

a) The previously described inherent operating inaccuracy could lead to a spread of 0.2 μ secs or 2 counts.

b) The accuracy to which the triggering piezo-electric gages can be placed physically ($\pm$ 0.01 inches) on the tube axis.

c) The possibility exists that the wave front configuration varies slightly over the tube cross-section. Therefore, if all gages are not aligned exactly, then different points on the wave front will actuate them.

d) Because of the manufacturing procedures involved, the tube is probably not of uniform cross-section and surface roughness. This would lead to slight variations in propagation velocity due to the variations in dissipation effects along the tube axis.

e) Deposits of soot or carbon were not uniform along the tube axis. If the deposits were not removed after each run, this would also lead to a variation in the dissipation effect along the tube axis.

The possible reasons for any observed variations of a counter's reading between individual runs for a given set of experimental conditions are as follows:

i) The previously described operating inaccuracy.

ii) The initial pressure of the mixture for the runs was probably not identically the same because of the accuracy to which the pressure measuring gages could be read.

Because of these counter inaccuracies and possible variations in the physical characteristics of the system, it is concluded that possible velocity deficits will only be firmly established by counter reading variations of greater than 2 μ secs.

The traces on the oscilloscope screen were photographed using high speed polaroid film (ASA 3000, Type 47). The procedure used was to open the camera shutter and leave it open during the time the wave was propagating down the tube.

CHAPTER 3

THEORETICAL ANALYSIS

As has been stated previously (Chapter 1) an exact mathematical solution for the structure and characteristics of a fully developed detonation wave appears to be impossible. The mathematical solution for the detonation wave propagating through a transverse magnetic field would be still more difficult.

Because of the difficulties involved in obtaining exact mathematical solutions to the problem of determining wave characteristics and structure only a simplified mathematical analysis will be attempted in which wave structure does not enter. This analysis will yield a means of computing the steady state velocity and the properties at the rarefaction-detonation wave interface for a wave which is propagating in the absence of magnetic fields. These are the only wave characteristics that are of interest in this study.

Also a simplified one dimensional discontinuous model for a wave which is propagating through a transverse magnetic field will be used in an attempt to devise a means for predicting the order of magnitude of possible perturbations to the wave system. As was explained in Chapter 1 it is anticipated that these perturbations will be both variations in the static pressure profile and a slowing down of the propagating wave.

One-Dimensional Steady State Gaseous Detonation

The following simplified one dimensional analysis for determining significant characteristics of a steady state detonation wave has been abstracted (with some modifications by this author) partially from Reference 7 and partially from Reference 8. The results will give expressions for calculating the steady state velocity and the thermodynamic equilibrium properties (temperature, pressure and density) at the rarefaction-detonation wave interface for a wave which is propagating in the absence of electromagnetic fields.

The model used for the wave is illustrated in Figure 11. It is assumed to be planar (one dimensional) and propagates with a constant velocity D' to the left into the unburned mixture. The properties of

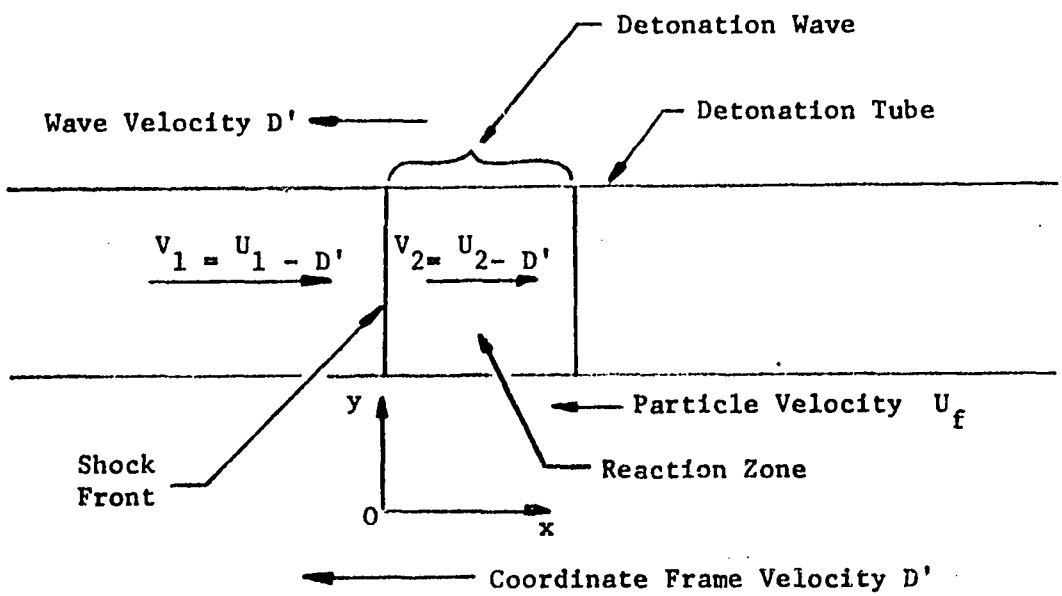

Figure 11. Schematic of a Plane Gaseous Detonation Wave Propagating in a Tube of Constant Cross-Sectional Area.

the unburned mixture are designated by the subscript 1 and those for the fluid behind the shock front by the subscript 2. V and U are, respectively, the relative velocity of the gases with respect to the wave velocity D' and the absolute velocity of the gases with respect to an inertial coordinate frame of reference. The coordinate frame of reference selected for the governing equations is shown in Figure 11 and is one which moves along with the steady state wave. In other words, the coordinate frame of reference will be one which is moving with respect to a stationary observer at a steady velocity (inertial system or a non-accelerating coordinate frame of reference) D' to the left. The resulting fluid velocities in the governing equations will therefore be the relative velocities (V) with respect to the propagating wave.

The following assumptions will be made in the analysis:

i) Relativistic effects are negligible and therefore classical laws and concepts may be used.

ii) The fluid is Newtonian, continuous, homogeneous, and isotropic.

iii) The flow is laminar.

iv) There is negligible coupling between the transport phenomena.

v) Thermodynamic equilibrium is attained at all points in the system.

vi) The wave is planar and parallel to the y-z coordinate plane. Therefore all property variations and gas flows will be one dimensional and in the x coordinate direction.

vii) Body forces are negligible.

viii) There are no electromagnetic effects.

ix) An over-all chemical reaction from reactants to products is considered rather than individual coexistent reactions.

x) The wave is steady state.

xi) Constant or average values for the specific heat and transport coefficients may be used. This assumption is rather strong, but is made for mathematical simplicity.

xii) The chemical reaction goes to completion at the rarefaction-detonation wave interface.

Using the preceding assumptions and approximations, the governing differential equations (which apply on either side of the shock front) reduce to the following forms:

Conservation of Mass:

$$\frac{d}{dx}(\rho V) = 0 \tag{3.1}$$

Conservation of Momentum:

$$\rho V \frac{dV}{dx} = -\frac{dp}{dx} + \frac{4}{3}\frac{d}{dx}\left(\mu \frac{dV}{dx}\right) \tag{3.2}$$

Conservation of Energy:

$$\rho V \frac{d}{dx}\left(\frac{1}{2}V^2 + c_p T - q\varepsilon_p\right) = \frac{d}{dx}\left(\lambda \frac{dT}{dx}\right) + \frac{4}{3}\frac{d}{dx}\left(\mu V \frac{dV}{dx}\right) \tag{3.3}$$

where q is the standard heat of reaction per unit mass of reaction product formed and where ε_p is defined below.

Conservation of Species:

$$\rho V \frac{dY_p}{dx} - \frac{d}{dx}\left(\rho D \frac{dY_p}{dx}\right) = \omega \tag{3.4}$$

The reaction rate equation:

$$\frac{d}{dx}(\rho V \varepsilon_p) = \omega \tag{3.5}$$

where: $$\varepsilon_p = Y_p\left(1 + \frac{V_p}{V}\right) \tag{3.6}$$

V_p is the diffusion velocity of the reaction products and ε_p is the fraction of the total mass flow which is due to the reaction products. The boundary conditions for the problem are as follows:

at $x = +\infty$

$$T = T_f,\ p = p_f,\ \rho = \rho_f,\ V = V_f,\ Y_p = 1,\ \varepsilon_p = 1 \tag{3.7}$$

at $x = -\infty$

$$T = T_1,\ p = p_1,\ \rho = \rho_1,\ V = V_1,\ Y_p = 0,\ \varepsilon_p = 0 \tag{3.8}$$

at $x = \pm\infty$ the following derivatives approach zero asymptotically

$$\frac{dp}{dx},\ \frac{d\rho}{dx},\ \frac{dT}{dx},\ \frac{dY_p}{dx},\ \frac{d\varepsilon_p}{dx} \tag{3.9}$$

Integrating Eq. (3.1) from $x = 0^+$ to $x = +\infty$ and then applying B.C.'s Eq. (3.7) and Eq. (3.8) results in:

$$\rho_1 V_1 = \rho_f V_f = \rho V = m = \text{constant} \tag{3.10}$$

Substituting Eq. (3.5) into Eq. (3.4) and then integrating from $x = 0^+$ to $x = +\infty$ results in:

$$\frac{\rho D}{m}\frac{dY_p}{dx} - Y_p + \varepsilon_p = d \tag{3.11}$$

Applying either Eqs. (3.7) and (3.9) or Eqs. (3.8) and (3.9) to Eq. (3.11) results in $d = 0$ (3.12)

Substitution of Eq. (3.12) into Eq. (3.11) results in:

$$\frac{\rho D}{m}\frac{dY_p}{dx} - Y_p + \varepsilon_p = 0 \tag{3.13}$$

Integrating Eq. (3.2) from $x = 0^+$ to $x = +\infty$ and then applying either B.C.'s Eqs. (3.7) and (3.9) or Eqs. (3.8) and (3.9) results in:

$$p + mV - \frac{4}{3}\mu\frac{dV}{dx} = p_f + mV_f = p_1 + mV_1 \tag{3.14}$$

Integrating Eq. (3.3) from $x = 0^+$ to $x = +\infty$ and then applying B.C.'s either Eqs. (3.7) and (3.9) or Eqs. (3.8) and (3.9) results in:

$$\begin{aligned}\frac{1}{2}mV^2 + mc_pT - mq\varepsilon_p - \lambda\frac{dT}{dx} - \frac{4}{3}\mu V\frac{dV}{dx} \\ = \frac{1}{2}mV_f^2 + mc_pT_f - mq \\ = \frac{1}{2}mV_1^2 + mc_pT_1\end{aligned} \tag{3.15}$$

The solution of equations (3.10), (3.13), (3.14) and (3.15), has been discussed by a number of authors. The following procedure is that suggested by von Karman.

Rearranging terms in (3.5) results in:

$$dx = \frac{m}{w}\,d\varepsilon_p \tag{3.16}$$

Substitute Eq. (3.16) into Eqs. (3.13), (3.14) and (3.15) in order to eliminate x as the independent variable. This results in:

from Eq. (3.13)

$$\frac{\rho w D}{m^2}\frac{dY_p}{d\varepsilon_p} - Y_p + \varepsilon_p = 0 \tag{3.17}$$

from Eq. (3.14)

$$p + mV - \frac{4}{3}\frac{w\mu}{m}\frac{dV}{d\varepsilon_p} = p_f + mV_f = p_i + mV_i \tag{3.18}$$

from Eq. (3.15)

$$\begin{aligned}\frac{1}{2}mV^2 + mc_pT - mq\varepsilon_p - \frac{\lambda w}{m}\frac{dT}{d\varepsilon_p} - \frac{4}{3}\frac{\mu w}{m}V\frac{dV}{d\varepsilon_p} \\ = \frac{1}{2}mV_f^2 + mc_pT_f - mq \\ = \frac{1}{2}mV_i^2 + mc_pT_i\end{aligned} \tag{3.19}$$

Defining a characteristic thermodynamic time τ_{th} as being proportional to the ratio of the mean free path (ℓ) to the mean molecular velocity $(\bar{V})$ and then using the results of kinetic theory $(\mu \propto \rho \bar{V} \ell$ and $\bar{V} \propto \sqrt{T} \propto \sqrt{\frac{p}{\rho}}$) the following is obtained:

$$\tau_{th} \equiv \frac{\mu}{p} \tag{3.20}$$

Defining a characteristic chemical time τ_{ch} as being proportional to the average times between molecular collisions which lead to chemical

reactions results in:

$$\tau_{ch} \equiv \frac{\rho}{\omega} \tag{3.21}$$

Then

$$\alpha = \frac{\tau_{th}}{\tau_{ch}} = \frac{\mu \omega}{P \rho} \tag{3.22}$$

Introducing the following dimensionless groups.

$$\text{Mach Number} = M = \frac{V}{\sqrt{\frac{\gamma P}{\rho}}} = \frac{\text{Inertial Force}}{\text{Elastic Force}} \tag{3.23}$$

$$\text{Prandtl Number} = Pr = \frac{\mu c_p}{\lambda} = \frac{\text{Momentum Diffusivity}}{\text{Thermal Diffusivity}} \tag{3.24}$$

$$\text{Schmidt Number} = Sc = \frac{\mu}{\rho D} = \frac{\text{Momentum Diffusivity}}{\text{Mass Diffusivity}} \tag{3.25}$$

Substituting the dimensionless groups Eqs. (3.22) through (3.25) into equations (3.17), (3.18) and (3.19) results in:

from Eq. (3.17)

$$\frac{1}{\gamma Sc} \frac{\alpha}{M^2} \frac{dY_p}{d\varepsilon_p} - Y_p + \varepsilon_p = 0 \tag{3.26}$$

from Eq. (3.18)

$$p\left(1 + \gamma M^2 - \frac{4}{3} \frac{\alpha}{V} \frac{dV}{d\varepsilon_p}\right) = p_f + mV_f = p_1 + mV_1 = a_D \tag{3.27}$$

from Eq. (3.19)

$$c_p T\left(1+\frac{\gamma-1}{2}M^2-\frac{q}{c_p T}\varepsilon_p-\frac{\alpha}{\gamma P_r M}\frac{1}{T}\frac{dT}{d\varepsilon_p}-\frac{4}{3}\frac{\gamma-1}{\gamma}\frac{\alpha}{V}\frac{dV}{d\varepsilon_p}\right)$$

$$=\frac{1}{2}V_f^2+c_p T_f-q=b_D \tag{3.28}$$

where a_D and b_D are constants

In obtaining Eq. (3.28) the following ideal gas relationships were also used:

$$\frac{p}{\rho}=RT \tag{3.29}$$

$$\frac{\gamma-1}{\gamma}=\frac{R}{c_p} \tag{3.30}$$

The hypothesis is now made that detonation involves relatively slow chemical reactions. This would mean W the rate of creation of products, would be relatively slow and by definition (Eq. 3.21) the characteristic chemical time would be large in comparison with the characteristic thermal time. Then for relatively slow chemical reactions, from Eq. (3.22):

$$\alpha \ll 1 \tag{3.31}$$

It should be noted that because of the observed velocities for the propagating detonation wave the relative velocity (V) of the fluid through which it is propagating should be large. Therefore M^2 should be significant for the fluid.

Then using Eq. (3.31) in Eqs. (3.26), (3.27) and (3.28) results in:

from Eq. (3.26)

$$Y_p = \varepsilon_p \tag{3.32}$$

from Eq. (3.27)

$$p + \gamma p M^2 = p + \rho V^2 = a_D \tag{3.33}$$

from Eq. (3.28)

$$c_p T + \frac{1}{2} V^2 - q \varepsilon_p = b_D \tag{3.34}$$

Equations (3.32), (3.33) and (3.34) indicate that for the system in which M^2 is significant and in which chemical times are long in comparison with thermodynamic times ($\alpha << 1$) the effects of the transport phenomenon (heat conduction, viscosity and mass diffusion) may be neglected in computing the wave propagation velocity. In other words for the system in which $\alpha << 1$ and $M^2 \approx 1$ the wave structure does not enter into the computation of the propagation velocity and therefore a purely hydrodynamic treatment may be used in computing it.

Equations (3.10), (3.32), (3.33) and (3.34) are the usual starting point for a quantitative treatment of detonation.[7] These equations could also have been obtained by using a purely hydrodynamic treatment as is outlined in Reference 8.

The relative velocity (V_2) of the burnt gas behind the shock

front may be determined as a function of the mass fraction of the reaction product ($Y_P = \varepsilon_P = Y_{P,2}$) by using Eq. (3.29) when solving Eqs. (3.10), (3.33) and (3.34) for V. The result of this solution is:

$$V_2 = \frac{\gamma}{\gamma+1}\frac{a_D}{m}\left[1 \pm \sqrt{1 - \frac{2(\gamma^2-1)}{\gamma^2}\frac{m^2}{a_D}(b_D + q Y_{P,2})}\right] \quad (3.35)$$

Since V_2 must be real then the second term under the radical sign must be either equal to or less than one. Also by definition $Y_{P,2}$ must be positive and have a maximum value of one which corresponds to completion of the reaction.

Rearranging Eq. (3.35) in order to solve for $Y_{P,2}$ in terms of V_2 and then differentiating $Y_{P,2}$ with respect to V_2 results in:

$$\frac{dY_{P,2}}{dV_2} = \frac{1}{q}\left[\frac{\gamma}{\gamma-1}\frac{a_D}{m} - \left(\frac{\gamma+1}{\gamma-1}\right)V_2\right] \quad (3.36)$$

But for a maximum value of $Y_{P,2}$ (that is $Y_{P,2} = Y_{P,f} = 1$) $V_2 = V_f$: Therefore setting Eq. (3.36) equal zero in order to maximize $Y_{P,2}$ and then solving for V_2 or V_f results in:

$$V_f = \frac{\gamma}{\gamma+1}\frac{a_D}{m} \quad (3.37)$$

but from Eq. (3.33)

$$p + \rho V^2 = p_f + \rho_f V_f^2 = a_D \quad (3.38)$$

Substituting Eqs. (3.38) and (3.10) into Eq. (3.37) results in:

$$V_f = -\sqrt{\gamma \frac{p_f}{\rho_f}} = -\sqrt{\gamma R T_f} \tag{3.39}$$

Then for $Y_{P,f} = 1$ (or completion of reaction) the relative velocity of the fluid with respect to the propagating wave is the sonic velocity in the burnt gases. The negative sign indicates (by reference to the chosen coordinate system) that the fluid is moving in the same direction or following the propagating detonation wave. This is necessary in order to satisfy conservation of mass.

A schematic plot of equation (3.35) is shown in Figure 12. The upper branch of the curve corresponds to $Y_{P,2} < 1$ and the positive sign in front of the radical, while the lower branch corresponds to $Y_{P,2} < 1$ and the negative sign in front of the radical. Therefore by comparison of Eq. (3.35) with Eq. (3.37) it can be seen that the upper branch corresponds to supersonic ($V_2 > V_f$) and the lower branch to subsonic ($V_2 < V_f$) velocities.

Referring to Figure 12 a qualitative description of the variation of the relative velocity for the fluid in the wave is as follows:

a) The unreacted mixture ($Y_P = 0$) in passing through the shock wave at the detonation front is changed discontinuously from state A to state G' or is changed from a supersonic to a subsonic velocity.

b) Then the reacting gas, with increasing $Y_{P,2}$, increases its velocity continuously along the lower branch from G' to J.

The situation in which the relative velocity of the flowing gas decreases continuously with increasing $Y_{P,2}$ from A to J, along the upper

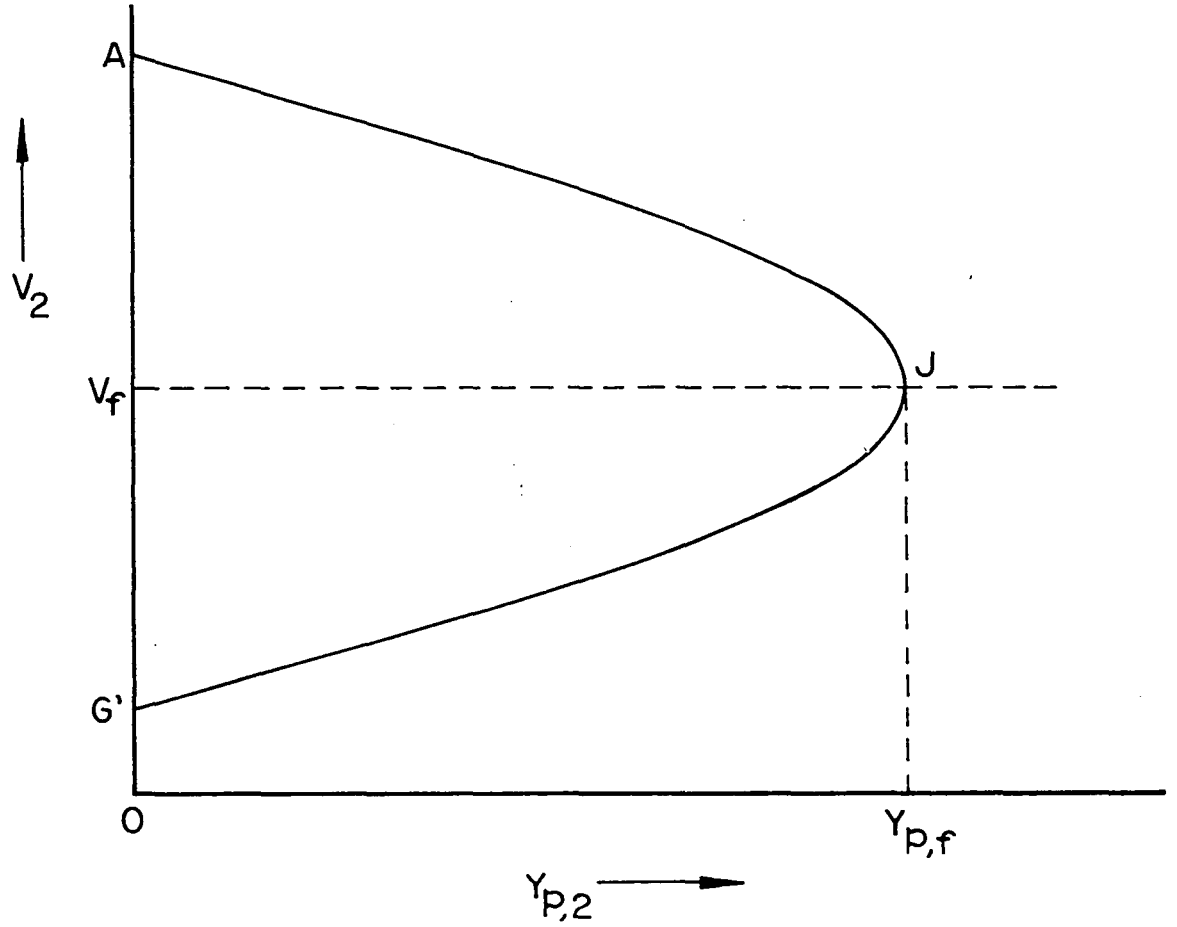

FIGURE 12. A SCHEMATIC PLOT SHOWING THE VARIATION OF V_2 WITH $Y_{P,2}$ (REFERENCE 7.)

branch, has not been observed for a steady-state detonation wave.

Chapman-Jouguet State for the Steady State Detonation Wave

Following is a development in which arguments are made to the effect that the absolute velocity (D') of the propagating steady state detonation wave corresponds to an end state which is specified by point J in Figure 12. This end state is referred to as the Chapman-Jouguet point and the corresponding propagation velocity is called the Chapman-Jouguet velocity.

Applying Equations (3.10), (3.33) and (3.34) across the detonation wave front to some arbitrary point 2 in the reaction zone results in:

from Eq. (3.10)

$$\rho_1 V_1 = \rho_2 V_2 \tag{3.40}$$

from Eq. (3.33)

$$p_1 + \rho_1 V_1^2 = p_2 + \rho_2 V_2^2 \tag{3.41}$$

from Eq. (3.34)

$$c_p T_1 + \frac{1}{2} V_1^2 = c_p T_2 + \frac{1}{2} V_2^2 - q\, Y_{P,2} \tag{3.42}$$

Rearranging terms in Eq. (3.42) and then substitution of Eq. (3.41) results in:

$$-q\, Y_{P,2} + c_p (T_2 - T_1) = \frac{1}{2}\left\{ V_1^2 - \left[\frac{p_1 - p_2}{\rho_2} + \frac{\rho_1}{\rho_2} V_1^2 \right] \right\} \tag{3.43}$$

Substitute Eq. (3.40) into Eq. (3.41) and then rearrange terms to get:

$$p_1 - p_2 = V_1^2 \left[\frac{\rho_1^2}{\rho_2} - \rho_1 \right]$$

and

$$V_1^2 = (p_1 - p_2) \left[\frac{\rho_2}{\rho_1^2 - \rho_1 \rho_2} \right] \tag{3.44}$$

Substitute Eq. (3.44) into Eq. (3.43) and then rearrange terms to get:

$$-q Y_{P,2} + c_p (T_2 - T_1) = \frac{1}{2} (p_2 - p_1) \left(\frac{1}{\rho_2} - \frac{1}{\rho_1} \right) \tag{3.45}$$

Substitution of Eq. (3.29) into Eq. (3.45) and rearrangement of terms results in:

$$q Y_{P,2} = \frac{c_p}{R} \left(\frac{p_2}{\rho_2} - \frac{p_1}{\rho_1} \right) - \frac{1}{2} \left(\frac{p_2}{\rho_2} - \frac{p_1}{\rho_1} \right) + \frac{1}{2} \left(\frac{p_1}{\rho_2} - \frac{p_2}{\rho_1} \right) \tag{3.46}$$

Substitution of Eq. (3.30) into Eq. (3.46) and rearrangement of terms results in:

$$q Y_{P,2} = \frac{\gamma + 1}{2(\gamma - 1)} \left(\frac{p_2}{\rho_2} - \frac{p_1}{\rho_1} \right) + \frac{1}{2} \left(\frac{p_1}{\rho_2} - \frac{p_2}{\rho_1} \right) \tag{3.47}$$

From Eq. (3.44) upon rearrangement of terms the following may be obtained:

$$V_1 = \frac{1}{\rho_1}\sqrt{\frac{p_1 - p_2}{\frac{1}{\rho_2} - \frac{1}{\rho_1}}} = v_1\sqrt{\frac{p_1 - p_2}{v_2 - v_1}} \tag{3.48}$$

also $U_1 = 0$, since the confined gas ahead of the propagating wave is stagnant, and therefore:

$$V_1 = -D' = v_1\sqrt{\frac{p_1 - p_2}{v_2 - v_1}} \tag{3.49}$$

Equation (3.47) represents a family of hyperbolas in the p, $\frac{1}{\rho}$ plane as a function of the chemical energy release parameter $qY_{P,2}$. For fixed or constant initial conditions $(p_1, \frac{1}{\rho_1})$ and a given energy release all possible end states $(p_2, \frac{1}{\rho_2})$ lie along the given hyperbola specified by equation (3.47). These hyperbolas are referred to as Hugoniot curves. For $Y_{P,2} = 0$ the Hugoniot curve corresponds to a shock wave propagating through an unreacting mixture and therefore this curve corresponds to the detonation wave front. For $Y_{P,2} = Y_{P,f} = 1$ the Hugoniot curve corresponds to the plane in the propagating detonation wave at which reaction has been completed and therefore corresponds to the detonation-rarefaction wave interface. This family of hyperbolas is shown schematically in Figure 13. The curves represent planes in

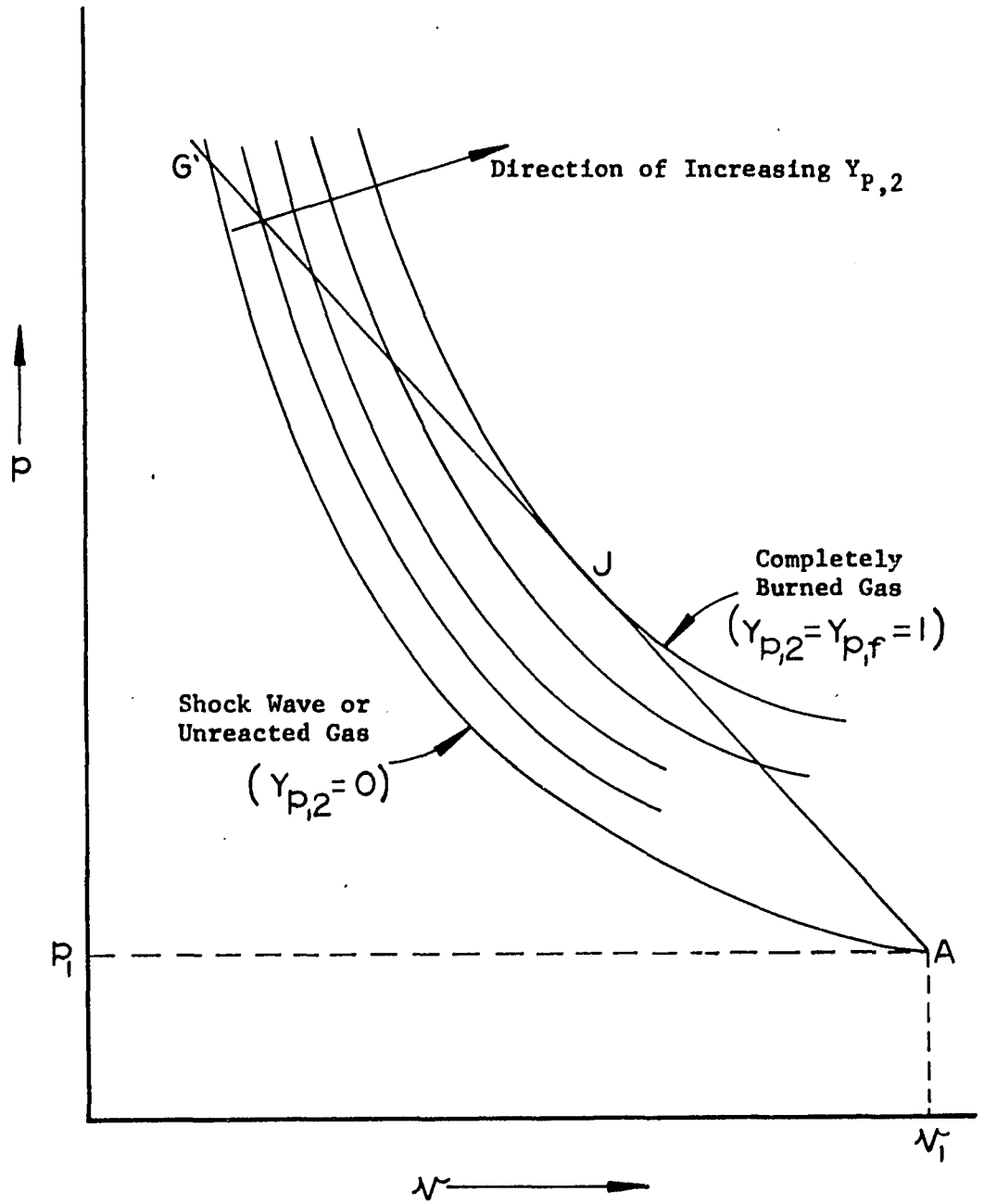

FIGURE 13. SCHEMATIC DIAGRAM SHOWING THE FAMILY OF HUGONIOT CURVES CORRESPONDING TO DIFFERENT VALUES OF THE HEAT RELEASE PARAMETER q $Y_{P,2}$. (REFERENCE 7) .

the steady detonation wave which all propagate at the same absolute velocity D'.

If the reaction zone is assumed to be infinitely thin then the family of hyperbolas given by equation (3.47) is telescoped into a single curve as shown in Figure 14. Therefore the curve in Figure 14 corresponds to that obtained by superimposing the curve $Y_{P,2} = 1$, of Figure 13, on that of $Y_{P,2} = 0$. It can be readily shown by means of equation (3.49) that end states on the curve between G and F ($P_2 > P_1$ and $v_2 > v_1$ or in other words $\frac{P_1 - P_2}{v_2 - v_1} < 0$) lead to imaginary values for the propagation velocity and therefore are not physically possible states. The part of the curve GCJB is the detonation branch while FK is the deflagration branch. No further discussion will be given for the deflagration branch.

Equation (3.47) represents the simultaneous solution to the conservation equations and therefore for a fixed initial state the points on the Hugoniot Curves represent all possible end states which satisfy the conservation equations. However, equation (3.49) shows that since $\frac{P_2 - P_1}{v_2 - v_1}$ is the slope of the straight line between the initial state (P_1, v_1) and the final state (intersection of the Hugoniot Curve at P_2, v_2) then for a given wave speed the maximum number of possible end states is two. These two possible end states are given by the intersection (at points B and C, Figure 14) of the Hugoniot Curve with with a straight line drawn from the initial state at point A. Since the conservation equations did not uniquely specify the end state for

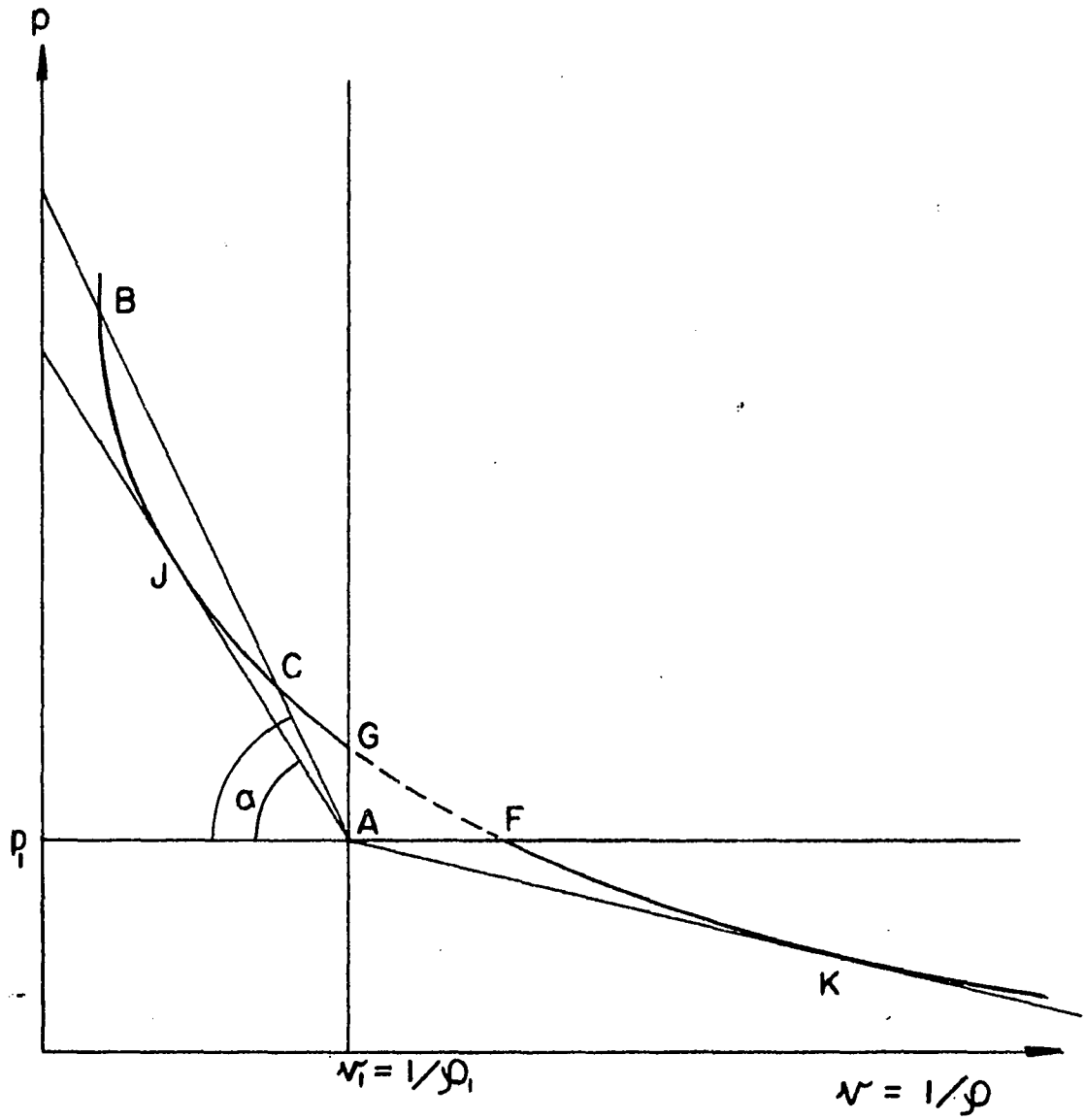

FIGURE 14: HUGONIOT CURVE (REFERENCE 2)

the stable or steady state detonation wave, Chapman hypothesized that the end state would be the point of tangency (point J in Figures 13 and 14) of the Hugoniot Curve for complete reaction ($Y_{P,2} = Y_{P,f} = 1$) and the straight line drawn from the initial state A. Through either equation (3.35) or equation (3.49) this end state uniquely specifies the propagation velocity of a stable detonation wave. Chapman's hypothesis has been extensively verified experimentally to a good approximation and is therefore an accepted empirical fact.[7]

Both physical and thermodynamic arguments have been developed in order to justify Chapman's hypothesis. A brief discussion of some of the arguments will now be given. For a more complete discussion of the proposed arguments consult References 7, 8, 9, and 11.

It can be shown by means of thermodynamic analysis that the propagation speed for the detonation wave for the various regions on the Hugoniot Curve of Figure 14 is as follows:

a) At point J it is sonic with respect to the burnt gases.

b) At points above J towards B it is subsonic with respect to the burnt gases.

c) At points below J towards C it is supersonic with respect to the burnt gases.

The stability arguments are as follows:

i) For points above J the rarefaction wave, which propagates at sonic velocity with respect to the burnt gases, will overtake the detonation wave which is propagating sub-sonically. The rarefaction wave will then weaken the detonation wave (increase the specific volume and decrease the pressure of the flowing gases) until it

propagates sonically with respect to the burnt gas. When this occurs there is no further interaction between the rarefaction and detonation waves and as a result the stable end state (point J in Figures 12, 13, and 14)is attained.

ii) For points below J for which the detonation wave propagates supersonically the rarefaction wave cannot overtake it and therefore the preceding stability argument will not be valid.

For these points two thermo-chemical arguments are given as follows:

a) The chemical reactions are not rapid enough to sustain detonation.

b) The entropy increase from A to B is greater than that from A to C and therefore B is the more thermodynamically probable state. This would mean that the formation of subsonic detonations are thermodynamically more probable than supersonic detonations. The stability argument for subsonic detonations has already been given.

In summary the stable detonation wave propagates at a constant velocity through the unreacted mixture. Its relative velocity of propagation is sonic with respect to the completely reacted gases at the rarefaction-detonation wave interface (Equation (3.39) for $Y_{P,2} = Y_{P,f} = 1$). Therefore its absolute velocity (D') is the sum of the particle velocity (absolute velocity of the following fluid at the rarefaction-detonation wave interface) and the sonic velocity with respect to the completely reacted gases ($Y_{P,2} = Y_{P,f} = 1$ in Figure 13).

Refer to Figure 13 and consider the following two possible continuous reaction paths in getting from the initial state at A to the final state at J. The first path lies along the straight line

from A to J. The second path is from A to G' and then along the straight line from G' to J.

Path A to J corresponds to the upper branch of the curve in Figure 12 and therefore the relative velocity of the burnt gases is always supersonic. This sequence of states would require that as the reaction proceeds the gas is slowed down until it reaches sonic velocity at the final state J. In this sequence of states there is no physical mechanism available for initiating the chemical reaction in the combustion zone. As has been explained previously, the experimentally observed detonation wave has a shock front through which the unreacted mixture is compressed and raised above its ignition temperature causing reaction to take place. No such precompression of the combustion gases exists in the process from A to J and therefore this appears to be a physically impossible sequence of states. Since this indicates that lower points on the Hugoniot Curves are physically unattainable it then substantiates one of the preceding physical stability arguments which was made in order to justify Chapman's hypothesis.

Path G' to J corresponds to the lower branch of the curve in Figure 12 and therefore the relative velocity of the burnt gases is always subsonic. Along this path as the reaction proceeds from $Y_{I,2} = 0$ to $Y_{P,2} = 1$ the burnt gases are accelerated until they attain sonic velocity at the Chapman-Jouguet point (J). Transition from the initial state A to state G' at the detonation front ($Y_{P,2} = 0$) requires a shock wave compression of the unreacted gas. Because this conforms to the observed conditions at the detonation front then the sequence

of states described above seem reasonable for the steady state wave.

State of the Burnt Gas at the Chapman-Jouguet Point

The state of the gas at the Chapman-Jouguet point is specified by the five parameters $Y_{P,f}$, P_f, T_f, ρ_f and D'. $Y_{P,f}$ is assumed to be one and also thermodynamic equilibrium is assumed to be attained. In the following discussion relationships will be developed from which T_f, ρ_f, P_f and D' may be computed using the assumption of the preceding sentence.

This purely theoretical procedure for calculating the four wave parameters P_f, ρ_f, T_f and D' is outlined in References 1 and 2. It is a lengthy and tedious iteration procedure. However, it yields values of D', P_f and T_f that agree closely with their experimentally measured values for detonation occurring in strong or fast reacting mixtures in which the wave appears to approach one dimensionality.

Essentially the iteration procedure involves the following steps:

i) The equilibrium composition of the product gases is computed using the law of mass action and assumed values for P_f and T_f. Knowing the gas composition is necessary in order that values for the gas parameters γ, C_p and R may be computed.

ii) These gas parameters are then substituted into the relationships which follow in order to compute P_f, ρ_f, T_f and D'.

iii) Adjustments to the assumed values of P_f and T_f are made based upon these computed values and then the preceding steps are repeated until convergence or close agreement occurs between the assumed

and computed values.

It should be noted that in order to use the law of mass action it is necessary to know the components making up the product gases. In general, these are not known and would therefore either have to be assumed or determined experimentally. The experimental determination of products of combustion is generally by means of spectroscopic techniques.

The relationships for computing ρ_f, T_f P_f and D' are obtained from the results of the preceding analysis in the following way:
From Eq. (3.45) the Hugoniot equation for the curve on which the Chapman-Jouguet point occurs is:

$$q\,\gamma_{p,f} = q = c_p(T_f - T_1) + \frac{1}{2}(p_1 - p_f)\left(\frac{1}{\rho_f} + \frac{1}{\rho_1}\right) \qquad (3.50)$$

The slope of this curve, in the $P,\frac{1}{\rho}$ plane (Figure 13), at the Chapman-Jouguet point is obtained in the following way:

i) Eqs. (3.29) and (3.30) are substituted into Eq. (3.50).

ii) The resulting equation, from the preceding step, is differentiated with respect to $\frac{1}{\rho_f}$ (Note: q, P_1, ρ_1, C_P are constants). Upon rearrangement of terms the equation resulting from the preceding differentiation becomes:

$$\frac{dp_f}{d\left(\frac{1}{\rho_f}\right)} = \frac{(\gamma+1)p_f + (\gamma-1)p_1}{(\gamma-1)\left(\frac{1}{\rho_1}\right) - (\gamma+1)\left(\frac{1}{\rho_f}\right)} \qquad (3.51)$$

However the slope of the Hugoniot Curve at the Chapman-Jouguet point is also given by:

$$\frac{dp_f}{d\left(\frac{1}{\rho_f}\right)} = \frac{p_f - p_1}{\left(\frac{1}{\rho_f}\right) - \left(\frac{1}{\rho_1}\right)} \tag{3.52}$$

Equate Eqs. (3.51) and (3.52), then cross-multiply and rearrange terms to obtain:

$$\frac{p_f - p_1}{\frac{1}{\rho_f} - \frac{1}{\rho_1}} = -\gamma \rho_f p_f \tag{3.53}$$

Using the ideal gas relationship in Eq. (3.53) and rearranging terms results in:

$$\frac{p_f}{p_1} = \frac{1+\gamma+\sqrt{(1+\gamma)^2 - 4\gamma\left(T_1/T_f\right)}}{2\gamma\left(\frac{T_1}{T_f}\right)} \tag{3.54}$$

Also by rearrangement of terms in Eq. (3.53) the result is:

$$\frac{\rho_f}{\rho_1} = 1 + \frac{1}{\gamma}\left(1 - \frac{p_1}{p_f}\right) \tag{3.55}$$

From Eq. (3.10)

$$V_1 = \frac{\rho_f}{\rho_1} V_f \tag{3.56}$$

Substitute Eq. (3.39) into Eq. (3.56)

$$V_1 = \frac{-\rho_f}{\rho_1} \sqrt{\gamma R T_f} \tag{3.57}$$

But $D' = -V_1$ for a detonation wave propagating into a stagnant mixture and therefore from Eq. (3.57) the propagation velocity of the steady state wave with respect to a stationary observer is:

$$D' = \frac{\rho_f}{\rho_1} \sqrt{\gamma R T_f} = V_f' + U_f \tag{3.58}$$

where: V'_f is the propagation velocity with respect to the burnt gases at the rarefaction-detonation wave interface--this is the sonic velocity with respect to the burnt gases at the interface;

and: U_f is the absolute velocity of the burnt gases at the interface or the particle velocity.

The four parameters D', ρ_f, P_f and T_f may be calculated from equations (3.50), (3.54), (3.55) and (3.58) using the previously described iteration procedure. The results of this type of computation for oxyacetylene mixtures of various initial compositions are summarized in Table I, Appendix B. Since these theoretical computations have proven satisfactory for strong or fast reaction mixtures, then the tabulated results in Table I should be representative of experimental

values. This agreement between the theoretical results in Table I and experimentally measured values has been confirmed.

One Dimensional Detonation Wave Propagating With Respect to a Uniform Transverse Magnetic Field

The following analysis will be used to predict the order of magnitude of the expected changes in the fluid dynamic characteristics for the steady state detonation wave when it propagates through a steady, uniform and transverse magnetic field. The model chosen and the method of computation are such that the calculated results overemphasize these expected changes in wave characteristics. The calculated results are therefore to be considered as first order approximations to the actual changes in characteristics.

A one dimensional analysis involving a considerably simplified mathematical treatment of the actual physical situation is used. In the analysis only the conservation equations of mass and momentum will be considered since the measurements made in this study are not extensive enough to predict energy variations which would be considered in the conservation of energy equation. The elimination of the energy equation also results in the elimination of the conservation of species equation from consideration in the analysis.

The physical model of the propagating wave is chosen to be identical to that for the preceding one dimensional treatment of this chapter. Therefore all of the assumptions used previously, excepting for those of no body forces and no magnetic fields, will also apply to this analysis. As well as the preceding assumptions, some additional

ones are made in order to further simplify the analysis. In general these assumptions will be conservative, or in other words will have a tendency to increase the magnitude of the computed fluid dynamic effects.

The additional assumptions are as follows:

a) The electrical conductivity of the gas has a finite and uniform magnitude across the detonation wave and a zero value in the rarefaction wave. This approximates the conductivity profile reported by Kelly, Toong and Tung[25] at low initial pressures. This assumption will result in a maximum computed choking effect by the detonation wave on the gases following it in the rarefaction wave.

b) The system is considered to be inviscid and adiabatic. This assumption is based on the results of the preceding one dimensional analysis, in which transport properties were eliminated from consideration.

c) The gases inside the detonation wave are assumed to have a uniform velocity equal to that of the particle velocity.

d) Secondary electromagnetic effects such as induced magnetic fields due to flow of electrical particles are negligible.

In the actual physical system there would be a time variation of certain properties due to its propagation from a region of zero into a region of finite magnetic field strength. As a result of the preceding assumptions these transients are neglected in the following analysis as being small in comparison with steady state values of the corresponding variables. Effectively the assumptions have created a quasi-steady state model.

As a result of these assumptions, the flowing fluid inside of

the detonation wave will act as a discontinuity which is propagating at a constant velocity and which has a uniform conductivity. Because of this, if the wave passes through a transverse magnetic field, the Lorentz type body force induced in each layer or plane of the propagating fluid will be the same and therefore each layer will be slowed down (momentum decrease) equally with no resultant compression.

The following gases in the rarefaction wave, which are considered to have zero conductivity, will have no induced Lorentz type body force acting on them and therefore will not slow down due to the presence of the transverse magnetic field. However because of the model chosen for this analysis they will see an impervious body traveling ahead of them which slows down as it passes through the field. This will cause a slowing down and as a result a compression of the gases in the rarefaction wave. The compression of these gases results in a conversion of part of their dynamic to static pressure. Because of this interaction between the fluids in the rarefaction and detonation waves, the fluid in the detonation wave will also be compressed. Of course, the two effects of slowing and compression of the fluids will take place continuously as the wave propagates through the field rather than as two separate steps in an overall process.

Following are developed relationships for predicting the velocity decrement of the gases in the detonation wave and also the static pressure increase for the gases in the rarefaction wave. For this case the shock front and rarefaction-detonation wave interface are treated as boundaries for the system since it is only the fluid between these two planes which is considered to have a finite

conductivity. The coordinate system chosen is that with respect to a stationary observer since it is only the flow relative to the fixed field which induces a magnetomotive force. Therefore all velocities are absolute velocities and not those relative to the propagating wave.

For this case the equations of motion (Conservation of Mass, Conservation of Momentum) reduce to the following forms:

$$\frac{d(\rho U_x)}{dx} = 0 \tag{3.59}$$

$$F_{B_x} = \rho U_x \frac{dU_x}{dx} + \frac{dp}{dx} \tag{3.60}$$

As a further simplifying procedure in the analysis, the previously described slowing down and compression of the flowing fluid is considered as two separate and succeeding steps in the analysis. In the first step only a slowing down of the fluid inside of the detonation wave, due to the action of the body force, is considered and therefore $\frac{dp}{dx} = 0$. It should be noted that because of the preceding assumption, ρ = constant. Then equation (3.60) becomes:

$$\rho U_x \frac{dU_x}{dx} = F_{B_x} \tag{3.61}$$

It should be noted that in Eq. (3.61) F_{Bx} is the x component of the body force per unit volume. The body force is given by:

$$\vec{F}_B = \vec{J} \times \vec{B} \tag{3.62}$$

$\vec{J}$ is the electric current vector and is given by Ohm's Law as follows:

$$\vec{J} = \sigma (\vec{E} + \vec{V} \times \vec{B}) \tag{3.63}$$

Substitute Eq. (3.63) into Eq. (3.62) noting that there is no applied electric field.

$$\vec{F}_B = \sigma (\vec{V} \times \vec{B}) \times \vec{B} \tag{3.64}$$

But

$$\vec{V} = \hat{i} U_x \quad , \quad \vec{B} = \hat{j} B_y \tag{3.65}$$

Substitute Eq. (3.65) into Eq. (3.64) and perform the indicated operations to get:

$$\vec{F}_B = \hat{i} F_{B_x} = -\hat{i} \sigma U_x B_y^2 \tag{3.66}$$

Substitute Eq. (3.66) into Eq. (3.61)

$$-\sigma U_x B_y^2 = \rho U_x \frac{dU_x}{dx} \tag{3.67}$$

From Eq. (3.67), noting that ρ, σ and B_y are assumed to be constants one obtains:

$$\frac{\sigma B_y^2}{\rho} \int_0^L dx = \int_{U_{x_2}}^{U_{x_0}} dU_x \tag{3.68}$$

Integrating Eq. (3.68) over the length of the magnet's gap results in:

$$U_{x_0} - U_{x_L} = \frac{\sigma B_y^2 L}{\rho} \tag{3.69}$$

where L = length of magnet gap

and U_{x_0} = velocity of fluid entering the gap

and U_{x_L} = velocity of fluid leaving the gap.

Therefore Eq. (3.69) gives the velocity decrement for the fluid in the detonation wave in the absence of its interaction with the following fluid in the rarefaction wave. As the second step in the overall process the following fluid at the rarefaction-detonation wave interface must decrease its velocity by an equal amount. This of course results in compression of both the fluid in the detonation and rarefaction waves.

Since the conductivity of the gases in the rarefaction wave were assumed to have zero conductivity then $F_{B_x} = 0$ and Eq. (3.60) becomes

$$\rho U_x \frac{dU_x}{dx} = - \frac{dp}{dx} \tag{3.70}$$

Integration of Eq. (3.59) results in $\rho U_x = \text{constant} = m'$ (3.71)

Substitute Eq. (3.71) into Eq. (3.70) and integrate over the length of the magnet gap to get

$$m'(U_{x_o} - U_{x_L}) = p_L - p_o \tag{3.72}$$

Equation (3.72) gives the static pressure increase for the fluid at the rarefaction-detonation wave interface due to the slowing down of the fluid in the detonation wave. Therefore the values of the properties P and ρ in equations Eq. (3.69) and Eq. (3.72) will be P_f and ρ_f. In equation (3.71) ρ and U_x will be chosen as respectively ρ_f and U_{x_o}.

CHAPTER 4

DISCUSSION OF RESULTS

The tabulated data for this study are given in Appendix B, while the results both tabulated and photographic are given in Appendix C. Only representative photos for each mixture, at a given initial pressure, are included in the report. Additional photos, which were taken under identical experimental conditions, confirm the reproducibility of these photographic records. Also shown in Appendix C are calculations which are made in an attempt to predict the orders of magnitude of the expected decrease in wave velocity and its accompanying dynamic to static pressure conversion, for a wave which propagates through a magnetic field under conditions which are representative of this study.

Also included in Appendix B is information which will be used both for comparative purposes and as a source of data for the calculations. This additional information is as follows:

a) Table I. This table contains calculated equilibrium properties for a one dimensional steady state detonation wave propagating in various oxyacetylene mixtures at the shown initial conditions. These properties were calculated using the one dimensional theory which was outlined in Chapter 3.

b) Figure 15. This figure shows both experimentally measured and calculated values of electrical conductivity for two oxyacetylene mixtures at varying initial pressures.

c) Figure 16. The figure contains experimentally measured propagation velocities, for various oxyacetylene mixtures, which were determined both by J. Breton (Reference 8, Page 532) and by this author. The plotted data of J. Breton was obtained at an initial pressure of one atmosphere and that of this study at an initial pressure of 15.5 psia (800 mm of Hg.)

d) Figure 17. This curve is the experimentally determined magnetization curve for the electromagnet of this study.

Inspection of the tabulated results for an initial pressure of 800 mm of Hg (15.5 psia) shows that the measured values of D' and P_f agree closely with the values in Table I. This agreement between experimental and theoretical values confirms the validity of using one dimensional wave theory. The measured values of D' also agree closely with the previously reported experimental values of J. Breton as is shown by a direct comparison of the plotted data in Figure 16, Appendix B.

Inspection of the tabulated data shows that it is readily reproducible. The slight variations in the counter readings for runs at a given set of experimental conditions may be accounted for both in terms of the inherent inaccuracies of the instruments and the physical characteristics of the system as explained in Chapter 2. Therefore there are no indicated decreases in wave velocity.

The photographic records indicate the following:

i) The general shape of the static pressure curves conform to the one dimensional model of a propagating wave system. The shock at the wave front is indicated by the sharp rise in pressure while the

following rarefaction wave is indicated by the gradual fall off of pressure behind this initial steep pressure gradient.

ii) Superimposed on the general shape of the pressure curve are local fluctuations in pressure.

iii) With the magnet turned on, noticeable local perturbations or pressure variations occur in certain regions on the curves. These indicated perturbations or variations in the static pressure profile are summarized in the tables on pages 130a and 130b. The more noticeable or largest perturbations occur with the 50% C_2H_2, 50% O_2 mixture. For this mixture, at an initial pressure of 15 psig, local variations with amplitudes of up to approximately 0.1 cm (which corresponds to a local pressure variation of 50 psi) are observed. These perturbations to the flow field due to the presence of the magnetic field seem to parallel the results of the shock wave studies of Patrick and Brogan as reported in Chapter 1.

iv) For a given mixture the magnitude of the perturbations increase with increasing initial pressure.

v) For a given initial pressure the magnitude of the perturbations increase with increasing richness of mixture up to the 50% C_2H_2, 50% O_2 mixture and then decreases for the 60% C_2H_2, 40% O_2 mixture.

The possibility that these variations or perturbations to the static pressure profile were due to electronic noise as a result of turning on the magnet can be ruled out for the following reasons:

a) The measured noise levels with the magnet on and Kistler amplifier settings of 500 psia/volt and 200 psia/volt were respectively

0.015 volts and 0.005 volts peak to peak. With a scope amplifier setting of 1 volt/cm (which corresponds to the experimental setting) the corresponding peak to peak deflections on the screen would be respectively 0.015 cm and 0.005 cm. These deflections would not be noticeable on the photographic records. This was confirmed by setting the scope amplifier gain at 1 volt/cm and then turning the magnet on. With this setting the noise was not discernible on the scope screen.

b) The noise was observed to be AC or periodic in nature. Since the observed perturbations are non-periodic then this rules out electronic noise as their source.

With the magnet turned off the electronic noise was still observed to be periodic in nature with peak to peak values of approximately 50% of those when it was on. Therefore for the same reasons outlined in the preceding paragraph, the possibility that the observed local pressure fluctuations, for runs with the magnet off, are due to electronic noise can be ruled out.

The trend of the previously described variations in magnitude for the observed perturbations correlate with the derived expression for the Lorentz type body force. Reference to equation (3.66) in Chapter 3 indicates that the magnitude of any observable MGD Effect due to the induced Lorentz type body force should increase with increasing conductivity, velocity of propagation and magnetic field strength.

The magnetic field strength ($\vec{B}$) was maintained essentially constant for all runs at a maximum value of approximately 12,000 gauss. This value of field strength was governed by the maximum rated current

output for the rectifier set, which is 130 amps. Inspection of the magnetization curve (Figure 17, Appendix B) shows that, at this current, the magnet is approaching saturation and therefore the risk of overloading the rectifier in order to obtain additional field strength is not warranted. Then, for a constant magnetic field strength, the variations in the observed MGD Effect should only be a function of conductivity and propagation velocity.

For a given mixture, the increase in the magnitude of the perturbation with increasing initial pressure correlates with the trend of measured conductivities as was reported in Chapter 1. It may be noted from the tabulated results that the propagation velocity also increases with increasing initial pressure and therefore the variation in perturbations is also attributable to this velocity change. However, these increments in propagation velocity over the pressure ranges of this study are not significant in comparison with the total velocity and therefore the variations in the perturbations should be attributed primarily to the changes in conductivity.

At a given initial pressure, the variation in the observed perturbations with varying mixture ratio may be attributed primarily to the changes in propagation velocity. Measured values of conductivity for a given initial pressure (Figure 15, Appendix B and Figure 2, Reference 33) indicate that, for the mixtures of this study, the variations in conductivity are not as significant as the measured variations in velocity. Therefore the perturbations should be greater for those mixtures having greater propagation velocities. The observed

perturbations agree with this conclusion.

The calculations in Appendix C use the resultant equations from the one dimensional analysis of Chapter 3 and are made for a stochiometric mixture at initial conditions of one atmosphere pressure and a temperature of 73.5°F. The initial conditions and mixture ratio are representative of those in this study. Therefore the orders of magnitude for both the static pressure increase and velocity decrease predicted by the calculations will apply to this study. The results of the calculations, using the measured conductivity due to Kelly, Toong and Tung,[25] indicate that, because of the possible measuring resolution of the instrumentation, there should be no observable change in either the propagation velocity or the static pressure profile.

Also included in Appendix C is a calculation in which an experimentally observed static pressure variation was used to find the possible order of magnitude of the electrical conductivity for the gases of this study. The computed value of conductivity was approximately 2 mhos/cm. This indicated value of conductivity exceeds by far the values measured by Kelly, Toong and Tung.[25]

CHAPTER 5

CONCLUSIONS AND RECOMMENDATIONS

Conclusions

The close agreement between the measured values of this study and those calculated using one dimensional steady state wave theory confirms the validity of using this theory to predict wave parameters for detonation in fast reacting mixtures.

The presence of the transverse magnetic field seems to perturb the flow field of the gases following the propagating detonation wave causing an increase in their static pressure. This increased static pressure would result from a slowing down of the gases causing a conversion of part of their velocity pressure into static pressure.

Comparison of the observed perturbations (in the static pressure profile) with the calculated value Δp (i.e. $p_L - p_o$) in Appendix C seems to indicate that conductivities far in excess of those reported in References 25 and 33 are present in the wave system.

The fact that there were no observed decreases in wave velocity seems to indicate the following:

a) Chemi-kinetic effects are either non-existent or are too small to cause appreciable slowing down of the wave front.

b) The observed hydrodynamic disturbances (perturbation of the static pressure profile) are not strong enough to cause slowing down of the wave front through hydrodynamic coupling. It should be noted

that, since the wave front travels sonically with respect to the burnt gases at the rarefaction-detonation wave interface, then any perturbations inside the rarefaction wave would have to travel supersonically in order to overtake and weaken the wave front. This would mean that the disturbance would have to be a shock wave. The observed disturbances do not appear to be shock waves.

Since the trend in the magnitude of the disturbances correlates with the derived expression for the Lorentz body force, this indicates that the disturbances are due solely to hydrodynamic causes. This confirms the preceding conclusion that chemi-kinetic effects are either negligible or non-existent.

Recommendations

It is recommended that the preceding study be extended in two ways. First, attempts should be made to accentuate the MGD Effect in order to see whether changes in wave velocities can be produced. Second, optical studies should be made in order to observe the indicated perturbations to the flow field. The following paragraphs contain some preliminary discussion of these two proposed studies.

As was explained previously, the MGD Effect may be accentuated by increasing any one or all of the three parameters of conductivity, propagation velocity and magnetic field strength.

The electrical conductivity of the gases in the propagating wave may be increased in the following ways:

a) Increase the initial pressure of the mixture. This presents a structural problem with respect to the containing vessel or

detonation tube and, associated with it, concurrent problems with respect to the propagation velocity and magnetic field. Because of the high dynamic pressures generated (up to approximately 45 times the initial pressure) the tube wall thickness would have to be increased if the initial pressure were to be increased still further. If the gap of the magnet is to remain constant (in this study 1") the result will be a decrease in the cross-sectional area of the flow passage. A decrease in the flow passage area will cause a decrease in propagation velocity due to increased viscous or dissipation effects. Also, if the flow passage is decreased beyond a certain point it will not be possible to generate a steady state wave. If the flow passage is to remain constant, then the gap of the magnet will have to increase with increasing initial pressure. This will lead to problems in maintaining the magnetic field strength due to the increased gap losses. The increased gap losses may be overcome by increasing the current through and/or increasing the number of turns for the magnet's coils. The number of turns is generally limited by spatial considerations while the allowable current through the coils is governed by the temperature that their insulation can withstand.

b) Seed the wave with easily ionizable materials. There are certain technical problems involved in this procedure. The first problem is in devising a means of distribution of the ionizable material throughout the combustible mixture before initiation of detonation takes place. Ideally the seed material should be of uniform size and consistency and should be distributed uniformly throughout the mixture. The second problem is to prevent the seed material from

settling out during the time required between charging of the tube and ignition of the mixture. It should be noted that these two problems do not arise in the MHD generator in which there is a continuous flow of reactants and products of combustion.

c) Subject the wave to a high frequency strong oscillating electric field before it enters the magnet's gap. This procedure would probably not be advisable in these studies because the oscillating electric field would induce a time varying or oscillating magnetic field. Also the acceleration of charged particles due to the changes of direction of the electric field would produce electromagnetic radiation. These oscillating electric and magnetic fields as well as the radiation would probably affect the functioning of the electronic instrumentation.

The wave propagation velocity is dependent upon the type of mixture, the mixture ratio , the initial conditions (temperature and pressure) and the cross-sectional area of the flow passage. In this study the type of mixture was oxyacetylene and the most desirable mixture ratio was 50% C_2H_2, 50% O_2 (this is confirmed by studying Figure 16, Appendix B). Since propagation velocity increases with an increasing rate of chemical reaction then the most desirable types of mixture are those that are fast reacting, which is the case for the oxyacetylene mixture. Propagation velocity decreases with increasing initial temperature and therefore it is desirable to maintain as low an initial temperature as possible. The initial temperature in general is governed by environmental conditions. Propagation velocity as a function of both initial pressure and flow passage areas has already been explained in the preceding paragraphs.

The preceding discussion on magnetic field generation has been with respect to steady state fields, which result from a steady flow of electrical current through the magnet coils. A number of studies[37,43,47] have been conducted in which the magnetic field is generated by dumping a large amount of power, from a capacitor bank, through a coil which is mounted axially on the tube. Since the resulting current from the discharge of the capacitor bank is transient, then both the I^2R losses and the generated field will also be transient.

The major advantage of this method of generating the field is that larger currents may be passed through the coils because of the transient nature of the I^2R losses. This of course results in the possibility of generating larger fields.

The major disadvantages are:

a) Additional costs and space requirements of the capacitor system.

b) The passage of the wave through the coil must be synchronized with the peak value for the generated field.

c) The generated field is non-uniform across the tube cross-section.

d) The generated field has both axial and radial components. The axial components are much larger than the radial or transverse components. Therefore the advantage of generating larger fields is partially canceled out since it is the transverse components of field which cause the MGD Effects of interest in this study.

Information on methods which can be used and characteristics which can be measured using optical techniques are outlined in

References 7, 8, 10, 11.

The optical study will have both advantages and disadvantages when compared to the method of study used in this report. The major advantages and disadvantages will be discussed briefly in the following paragraphs.

First, the major advantages are as follows:

a) The characteristics of the wave system may be studied throughout the flow passage. In this study the characteristics were recorded only at a fixed point at the tube surface.

b) Additional properties such as temperature may be recorded by observing the radiation characteristics of the system and then interpreting these spectroscopically.

The major disadvantages are:

a) The prohibitive cost of the high speed cameras used in certain of the optical studies.

b) Structural problems which are encountered because of the fact that transparent materials such as plexi-glass are much weaker than steels.

c) Because of the space requirements of the transparent tube the magnet's gap must be increased with the resultant problems in generating suitable magnetic fields as was discussed previously.

APPENDIX A

DEFINITION OF SYMBOLS AND SUBSCRIPTS

Definition of Symbols

a_D = constant; defined by Eq. (3.27)

b_D = constant; defined by Eq. (3.28)

$\vec{B}$ = magnetic field strength vector

C_p = specific heat at constant pressure

C_v = specific heat at constant volume

D = mass diffusion coefficient as defined by Fick's Law of Diffusion

D' = steady state propagation velocity of a detonation wave

$\vec{E}$ = electric field strength vector

$\vec{F}_B$ = body force per unit volume

$\vec{F}_L$ = Lorentz Force

$\vec{J}$ = electrical current vector

L = length of the gap of the electromagnet

M = Mach number

m = mass rate of flow as defined by Eq. (3.10)

m' = mass rate of flow as defined by Eq. (3.71)

p = thermodynamic pressure

Pr = Prandtl number

q = standard heat of reaction or the chemical energy release (referenced to a standard reaction temperature) per unit mass of products formed from a unit mass of reactants

q' = magnitude of the charge on an electrically charged particle

R = ideal gas constant

Sc = Schmidt number

T = absolute thermodynamic temperature

U = absolute velocity of the flowing fluid with respect to a stationary observer

V = relative velocity of the flowing fluid with respect to the wave velocity D'

V_f = $-V_f'$ = relative velocity of the flowing fluid at the rarefaction-detonation wave interface

V_p = diffusion velocity of the chemical reaction products

v = specific volume

Y_p = mass fraction of chemical reaction products formed

α = ratio of the characteristic thermal time (τ_{th}) to the characteristic chemical time (τ_{ch})

γ = ratio of the specific heat at constant pressure (C_p) to that at constant volume (C_v)

ε_p = the fraction of the total mass flow which is due to the reaction products.

λ = conductive heat transfer coefficient as defined by Fourier's Law of Conduction

μ = fluid viscosity, coefficient as defined by Newton's equation

ρ = density

σ = electrical conductivity

τ_{ch} = characteristic chemical time as defined by Eq. (3.21)

τ_{th} = characteristic thermal time as defined by Eq. (3.20)

ω = rate of creation of products, due to a chemical reaction, as defined by Eq. (3.5)

Definition of Subscripts

1 - refers to the unreacted gases ahead of the detonation wave front

2 - refers to the gases behind the detonation wave front (i.e. behind the shock wave at the leading edge of the detonation wave)

f - refers to the gases at and behind rarefaction-detonation wave interface

L - represents the fluid properties as the wave leaves the gap of the electromagnet

0 - represents the fluid properties as the wave enters the gap of the electromagnet

P - refers to the products of the chemical reaction

x_L - x coordinate at the exit to the electromagnet's gap

x_0 - x coordinate at the entrance to the electromagent's gap

APPENDIX B

DATA AND SUPPORTING INFORMATION

Data Sheet

Atmospheric Pressure: 761 mm

Mixture Composition: 30% C_2H_2, 70% O_2

Run No.	Initial Pressure of Mixture	Counter Reading (μ sec)			Thermo-couple Potentio-meter Reading (mv)	Oscilloscope Settings		Kistler Ampli-fier Setting ($\frac{psi}{volt}$)	Recti-fier Current Output (amps)	Comments
		Beckman	H.P. #1	H.P. #2		Sweep ($\frac{\mu sec}{cm}$)	Gain ($\frac{volts}{cm}$)			
1	15 psig	363.1	363	363.6	1.27	20	1	500	---	Magnet Off
2	15 psig	363.4	363	363.8	1.27	20	1	500	129	Magnet On
3	15 psig	363.2	363	363.8	1.27	20	1	500	129	Magnet On
4	800 mm	368.2	368	369.9	1.3	20	1	200	---	Magnet Off
5	800 mm	368.5	368	369	1.3	20	1	200	---	Magnet Off
6	800 mm	368	367	368.4	1.3	20	1	200	130	Magnet On
7	800 mm	368.1	368	368.4	1.3	20	1	200	129	Magnet On
8	550 mm	374	374	374.3	1.3	20	1	200	---	Magnet Off
9	550 mm	373.8	373	373.7	1.3	20	1	200	127	Magnet On

Data Sheet

Atmospheric Pressure: 761 mm

Mixture Composition: 40% C_2H_2, 60% O_2

Run No.	Initial Pressure of Mixture	Counter Reading (μ sec)			Thermo-couple Potentio-meter Reading (mv)	Oscilloscope Settings		Kistler Ampli-fier Setting ($\frac{psi}{volt}$)	Recti-fier Current Output (amps)	Comments
		Beckman	H.P. #1	H.P. #2		Sweep ($\frac{\mu sec}{cm}$)	Gain ($\frac{volts}{cm}$)			
1	15 psig	327.5	327	327.9	1.27	20	1	500	---	Magnet Off
2	15 psig	327	327	327.9	1.27	20	1	500	---	Magnet Off
3	15 psig	327.3	327	328.1	1.27	20	1	500	130	Magnet On
4	800 mm	333.1	333	333.4	1.32	20	1	200	---	Magnet Off
5	800 mm	333.7	332	333.1	1.32	20	1	200	---	Magnet Off
6	800 mm	333.2	332	333.1	1.32	20	1	200	130	Magnet On
7	800 mm	333.6	332	333.3	1.32	20	1	200	130	Magnet On
8	800 mm	333	331	332.9	1.32	20	1	200	---	Magnet Off
9	550 mm	335.8	335	336.1	1.32	20	1	200	---	Magnet Off
10	550 mm	335	335	336.3	1.32	20	1	200	129	Magnet On

Data Sheet

Atmospheric Pressure: 761 mm

Mixture Composition: 50% C_2H_2, 50% O_2

Run No.	Initial Pressure of Mixture	Counter Reading (μ sec)			Thermo-couple Potentio-meter Reading (mv)	Oscilloscope Settings		Kistler Ampli-fier Setting $\left(\frac{psi}{volt}\right)$	Recti-fier Current Output (amps)	Comments
		Beckman	H.P. #1	H.P. #2		Sweep $\left(\frac{\mu sec}{cm}\right)$	Gain $\left(\frac{volts}{cm}\right)$			
1	15 psig	312	311	312	1.27	20	1	500	---	Magnet Off
2	15 psig	311.8	311	312.6	1.27	20	1	500	134	Magnet On
3	15 psig	312	312	312.7	1.27	20	1	500	133	Magnet On
4	800 mm	316.1	315	315	1.12	20	1	200	---	Magnet Off
5	800 mm	316.8	316	315.7	1.12	20	1	200	135	Magnet On
6	800 mm	316.9	316	315.7	1.12	20	1	200	---	Magnet Off
7	800 mm	316.4	316	315.8	1.12	20	1	200	132.5	Magnet On
8	800 mm	316.3	316	316	1.12	20	1	200	133	Magnet On
9	550 mm	318	318	318.3	1.12	20	1	200	---	Magnet Off
10	550 mm	318	317	317.5	1.12	20	1	200	---	Magnet Off
11	550 mm	318.7	318	317.4	1.12	20	1	200	135	Magnet On
12	550 mm	318.8	318	317.3	1.12	20	1	200	135	Magnet On

Data Sheet

Atmospheric Pressure: 762 mm

Mixture Composition: 60% C_2H_2, 40% O_2

Run No.	Initial Pressure of Mixture	Counter Reading (μ sec)			Thermo-couple Potentio-meter Reading (mv)	Oscilloscope Settings		Kistler Ampli-fier Setting $\left(\frac{psi}{volt}\right)$	Recti-fier Current Output (amps)	Comments
		Beckman	H.P. #1	H.P. #2		Sweep $\left(\frac{\mu sec}{cm}\right)$	Gain $\left(\frac{volts}{cm}\right)$			
1	15 psig	364	363	363.9	1.27	20	1	500	---	Magnet Off
2	15 psig	363.8	364	364.6	1.27	20	1	500	127	Magnet On
3	15 psig	364.2	364	364	1.27	20	1	500	127	Magnet On
4	800 mm	366.6	366	366.3	1.22	20	1	200	---	Magnet Off
5	800 mm	366.7	367	366.7	1.22	20	1	200	132	Magnet On
6	800 mm	367.6	367	366.6	1.22	20	1	200	---	Magnet Off
7	800 mm	366.9	366	366.2	1.22	20	1	200	132	Magnet On
8	550 mm	369.8	371	369.1	1.22	20	1	200	---	Magnet Off
9	550 mm	370.3	370	369.8	1.22	20	1	200	132	Magnet On
10	550 mm	370.1	371	369.5	1.22	20	1	200	---	Magnet Off
11	550 mm	369.9	371	369.6	1.22	20	1	200	131	Magnet On

Table I

Calculated Equilibrium Properties at the Chapman-Jouguet Point for Detonation in Oxyacetylene Mixtures[11,33]

(P_1 = 1 atmosphere, T_1 = 23°C = 73.5°F)

Initial Composition of the Mixture		Calculated C.-J. Pressure Ratio: P_f/P_1 (Atmospheres)	Calculated C.-J. Temperature (°K)	Calculated C.-J. Prop. Velocity (meters/sec)	Calculated C.-J. Electrical Conductivity (10^{-4} mhos/cm)
% C_2H_2	% O_2				
25	75	29.5	4,075	2,332	5.8
28.6	71.4	33.8	4,212	2,426	---
30	70	34.7	4,240	-----	8.43
40	60	41.0	4,460	-----	12.4
45	55	41.3	4,480	-----	8.65
49.9	50.1	43.5	4,478	2,944	2.98
53	47	40.6	4,275	2,750	9.5
70	30	30.4	3,722	2,441	1.61

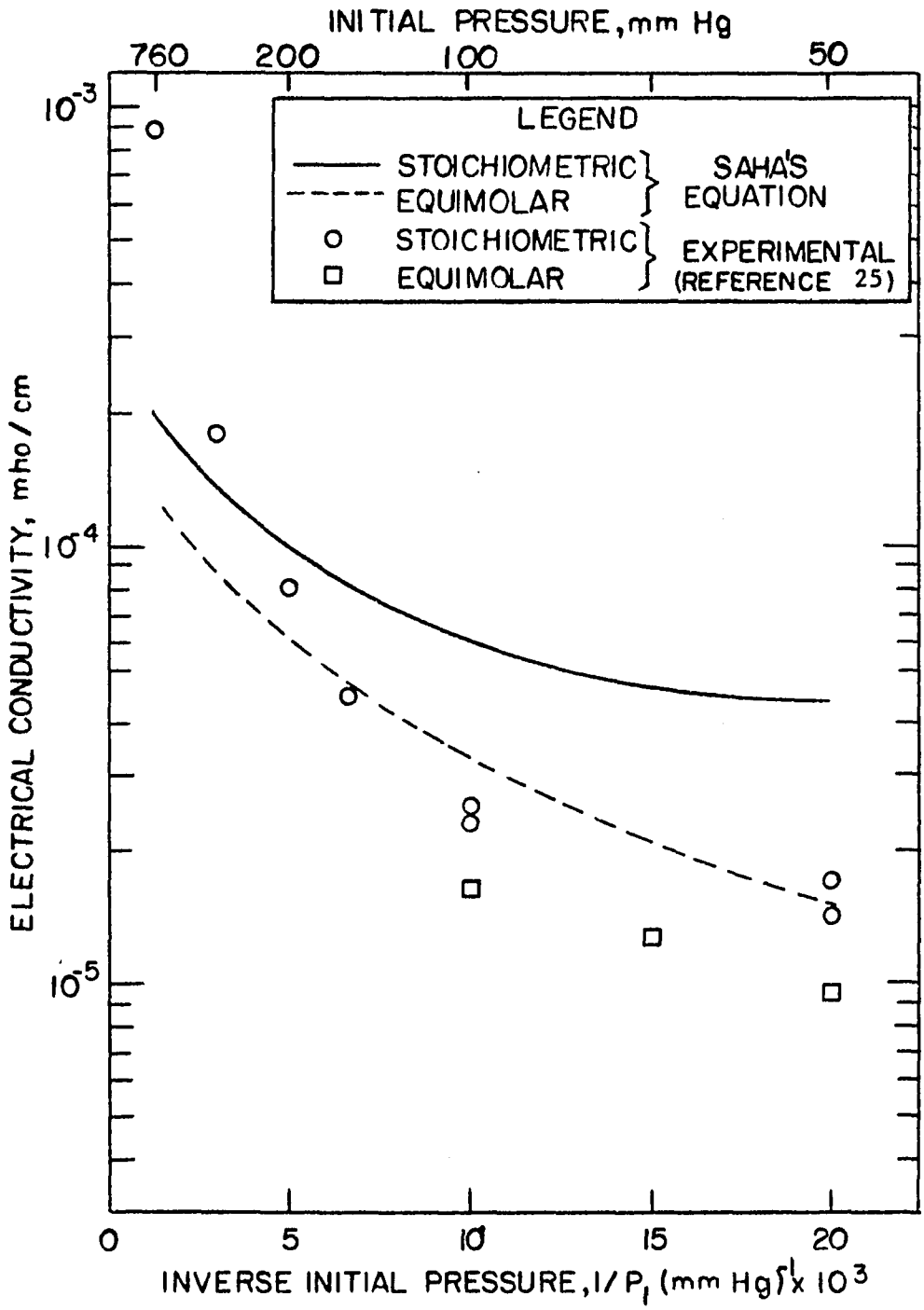

FIGURE 15. THERMAL OR EQUILIBRIUM CONDUCTIVITY VERSUS INVERSE INITIAL PRESSURE FOR STOCHIOMETRIC AND EQUIMOLAR C_2H_2 - O_2 DETONATIONS. (REFERENCE 25)

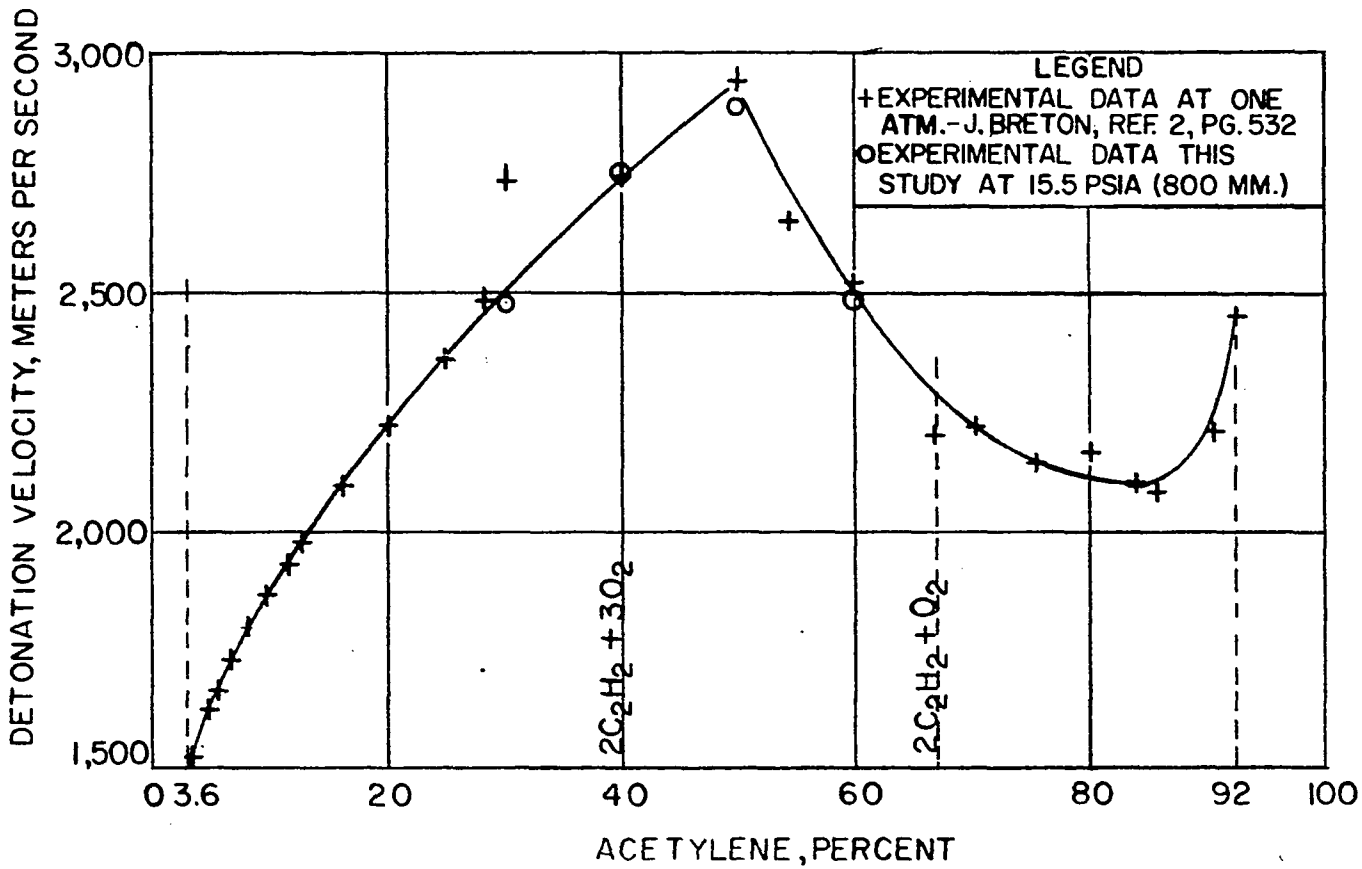

FIGURE 16. DETONATION VELOCITIES OF C_2H_2 - O_2 MIXTURES. (REFERENCE 8)

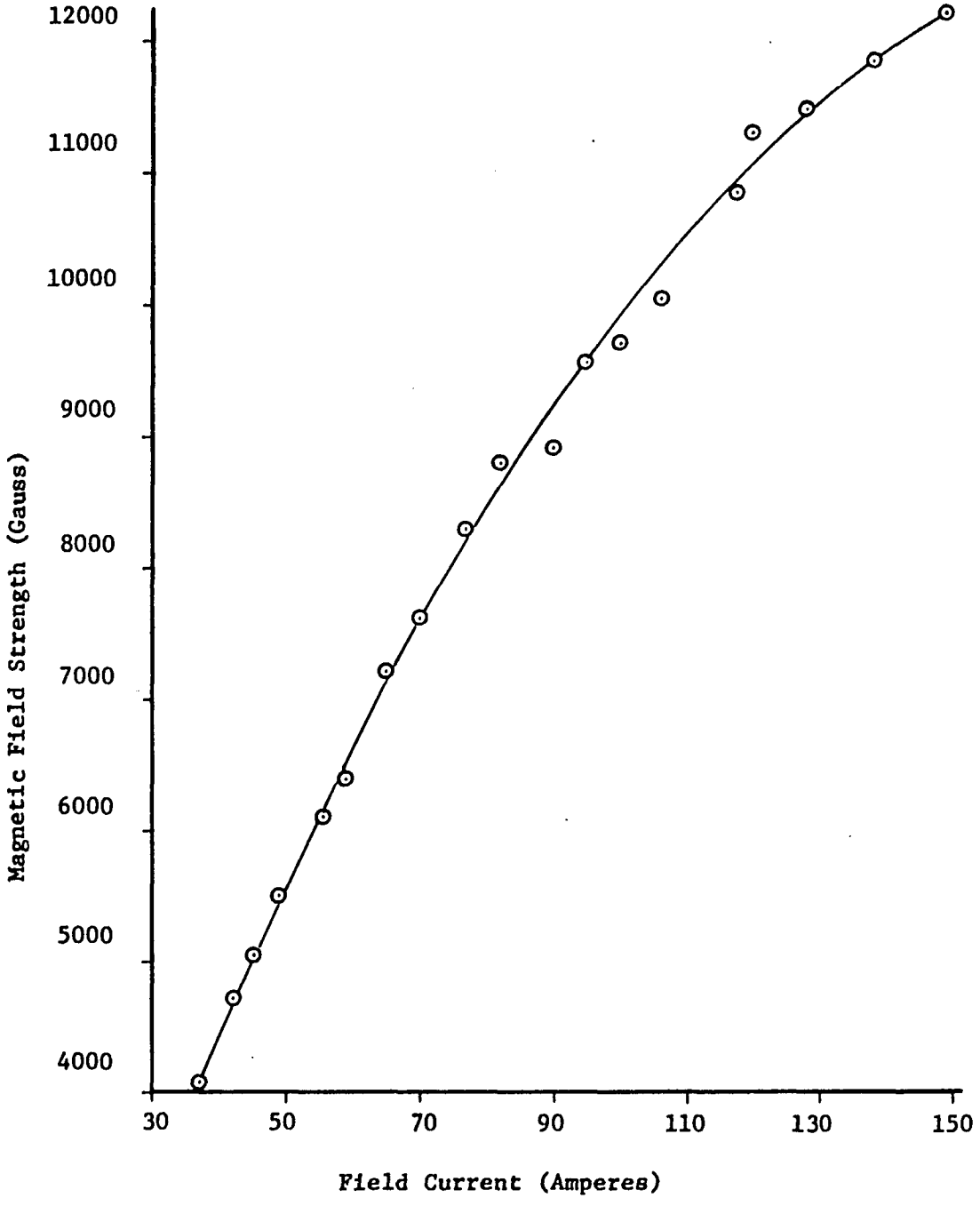

FIGURE 17. MAGNETIZATION CURVE FOR THE ELECTROMAGNET.

APPENDIX C

RESULTS AND CALCULATIONS

Results

Mixture Composition: 30% C_2H_2, 70% O_2

Run No.	Press. of Unreacted Mixture p_1 (psia)	Temp. Unreacted Mixture T_1 (°F)	Magnetic Field Strength (Gauss)	Average Propagation Velocity D'		Pressure Reacted Mixture p_f (psia)	Observed Velocity Deficit	Perturbations to Rarefaction Wave Static Press. Profile Occur at: (Measured from Wave Front in cm)
				$\frac{\text{feet}}{\text{sec}}$	$\frac{\text{meters}}{\text{sec}}$			
1	29.7	77	----			1,030		
2	29.7	77	11,550			1,030		2.4 to end of curve
3	29.7	77	11,550	8,260	2,520	1,030	none	2.4 to end of curve
4	15.5	78	----			510		
5	15.5	78	----			510		
6	15.5	78	11,600			510		0.2 to end of curve
7	15.5	78	11,550	8,150	2,480	510	none	0.2 to end of curve
8	10.6	78	----			350		
9	10.6	78	11,450	8,020	2,450	350	none	2.6 to end of curve

Results

Mixture Composition: 40% C_2H_2, 60% O_2

Run No.	Press. of Unreacted Mixture p_1 (psia)	Temp. Unreacted Mixture T_1 (°F)	Magnetic Field Strength (Gauss)	Average Propagation Velocity D'		Pressure Reacted Mixture p_f (psia)	Observed Velocity Deficit	Perturbations to Rarefaction Wave Static Press. Profile Occur at: (Measured from Wave Front in cm)
				$\frac{\text{feet}}{\text{sec}}$	$\frac{\text{meters}}{\text{sec}}$			
1	29.7	77	----			1,240		
2	29.7	77	----			1,240		
3	29.7	77	11,600	9,170	2,790	1,240	none	0.9 to end of curve
4	15.5	79	----			620		
5	15.5	79	----			620		
6	15.5	79	11,600			620		1.3 to end of curve
7	15.5	79	11,600			620		1.3 to end of curve
8	15.5	79	----	9,010	2,750	620	none	
9	10.6	79	----			420		
10	10.6	79	11,550	8,960	2,730	420	none	2.5 to end of curve

Results

Mixture Composition: 50% C_2H_2, 50% O_2

Run No.	Press. of Unreacted Mixture p_1 (psia)	Temp. Unreacted Mixture T_1 (°F)	Magnetic Field Strength (Gauss)	Average Propagation Velocity D'		Pressure Reacted Mixture p_f (psia)	Observed Velocity Deficit	Perturbations to Rarefaction Wave Static Press. Profile Occur at: (Measured from Wave Front in cm)
				$\frac{\text{feet}}{\text{sec}}$	$\frac{\text{meters}}{\text{sec}}$			
1	29.7	77	----			1,390		
2	29.7	77	11,750			1,390		0.3 to end of curve
3	29.7	77	11,720	9,620	2,930	1,390	none	0.3 to end of curve
4	15.5	72	----			665		
5	15.5	72	11,800			665		2.4 to end of curve
6	15.5	72	----			665		
7	15.5	72	11,710			665		1.4 to end of curve
8	15.5	72	11,720	9,490	2,890	665	none	1.4 to end of curve
9	10.6	72	----			460		
10	10.6	72	----			460		
11	10.6	72	11,800			460		3.2 to end of curve
12	10.6	72	11,800	9,430	2,870	460	none	3.2 to end of curve

Results

Mixture Composition: 60% C_2H_2, 40% O_2

Run No.	Press. of Unreacted Mixture p_1 (psia)	Temp. Unreacted Mixture T_1 (°F)	Magnetic Field Strength (Gauss)	Average Propagation Velocity D'		Pressure Reacted Mixture p_f (psia)	Observed Velocity Deficit	Perturbations to Rarefaction Wave Static Press. Profile Occur at: (Measured from Wave Front in cm)
				feet/sec	meters/sec			
1	29.7	77	----			970		
2	29.7	77	11,450			970		0.6 to end of curve
3	29.7	77	11,450	8,240	2,510	970	none	0.6 to end of curve
4	15.5	75	----			485		
5	15.5	75	11,700			485		1.4 to end of curve
6	15.5	75	----			485		
7	15.5	75	11,700	8,180	2,490	485	none	1.4 to end of curve
8	10.6	75	----			350		
9	10.6	75	11,700			350		1.8 to end of curve
10	10.6	75	----			350		
11	10.6	75	11,650	8,110	2,470	350	none	1.8 to end of curve

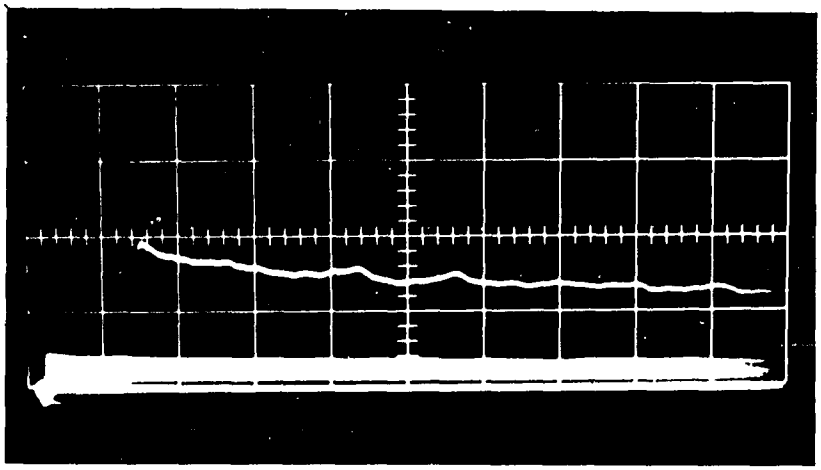

FIGURE 18. PRESSURE TRACES OF 30% C_2H_2 - 70% O_2 DETONATION AT 29.7 PSIA INITIAL PRESSURE AND MAGNET OFF

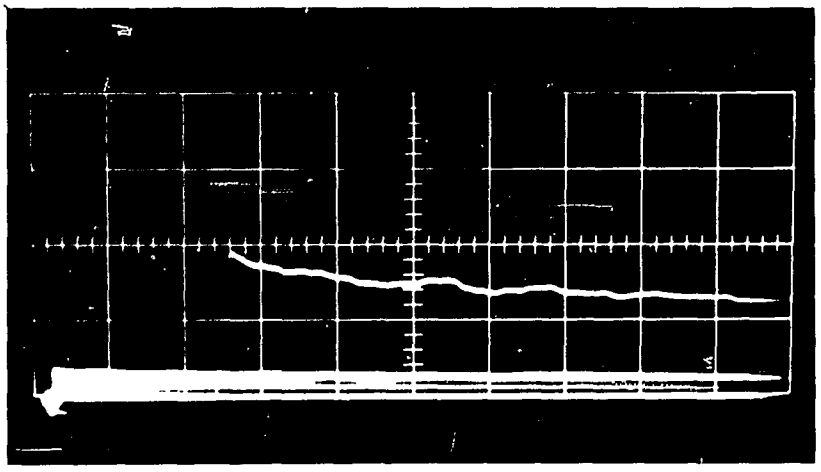

FIGURE 19. PRESSURE TRACES OF 30% C_2H_2 - 70% O_2 DETONATION AT 29.7 PSIA INITIAL PRESSURE AND MAGNET ON

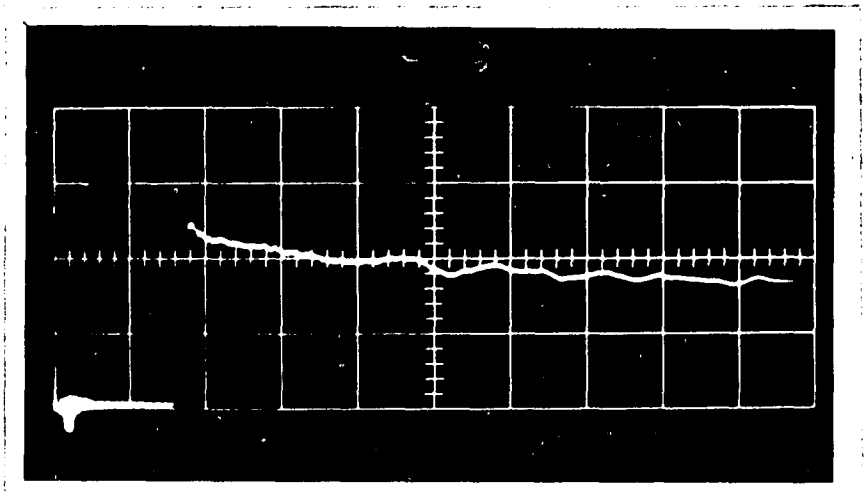

FIGURE 20. PRESSURE TRACES OF 30% C_2H_2 - 70% O_2 DETONATION AT 15.5 PSIA INITIAL PRESSURE AND MAGNET OFF

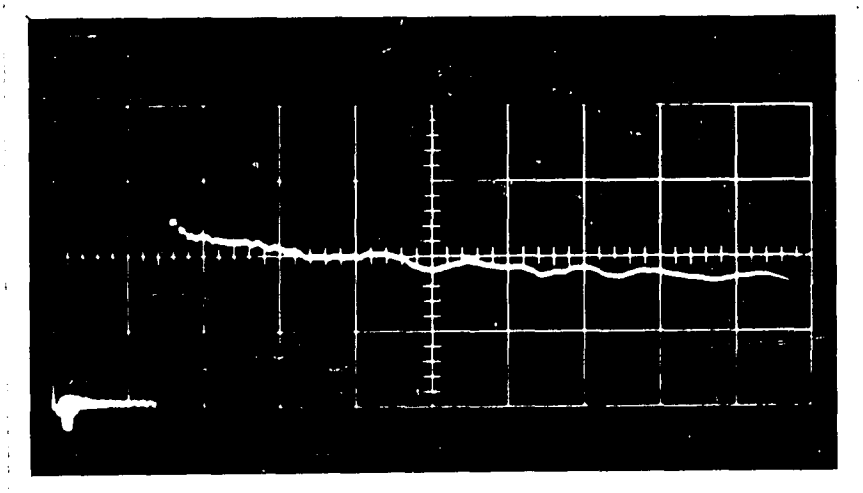

FIGURE 21. PRESSURE TRACES OF 30% C_2H_2 - 70% O_2 DETONATION AT 15.5 PSIA INITIAL PRESSURE AND MAGNET ON

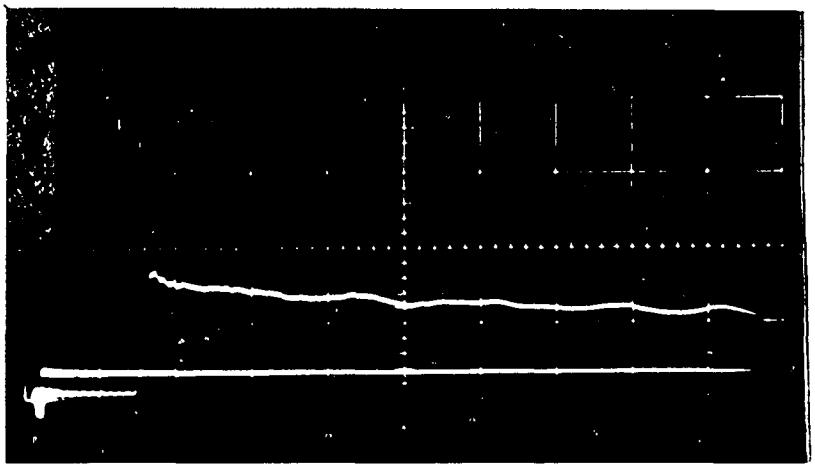

FIGURE 22. PRESSURE TRACES OF 30% C_2H_2 - 70% O_2 DETONATION AT 10.6 PSIA INITIAL PRESSURE AND MAGNET OFF

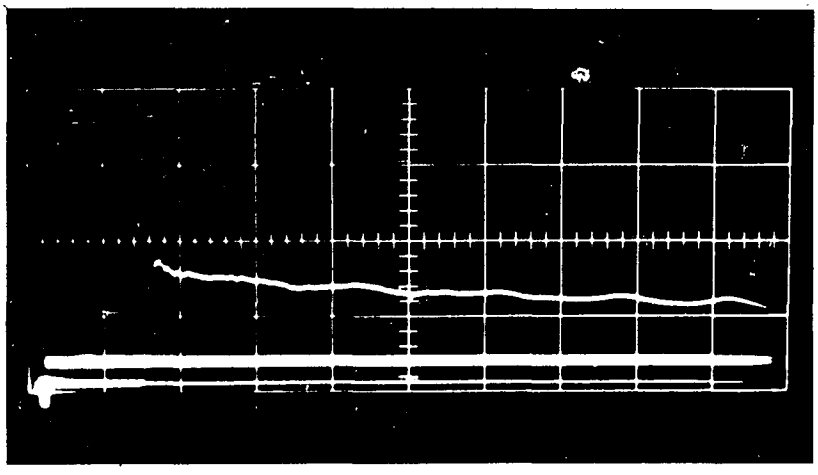

FIGURE 23. PRESSURE TRACES OF 30% C_2H_2 - 70% O_2 DETONATION AT 10.6 PSIA INITIAL PRESSURE AND MAGNET ON

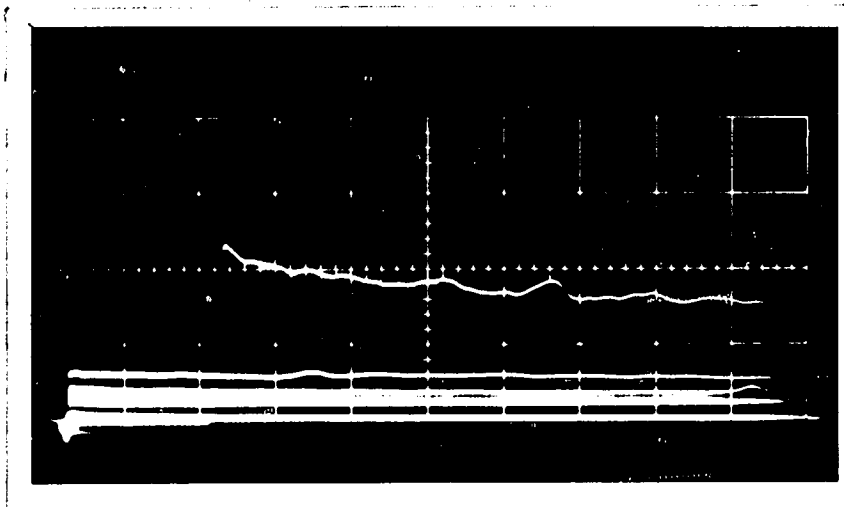

FIGURE 24. PRESSURE TRACES OF 40% C_2H_2 - 60% O_2 DETONATION AT 29.7 PSIA INITIAL PRESSURE AND MAGNET OFF

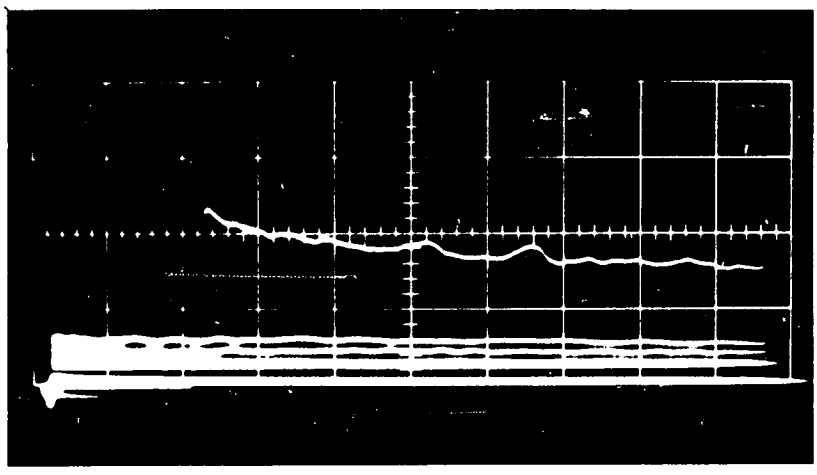

FIGURE 25. PRESSURE TRACES OF 40% C_2H_2 - 60% O_2 DETONATION AT 29.7 PSIA INITIAL PRESSURE AND MAGNET ON

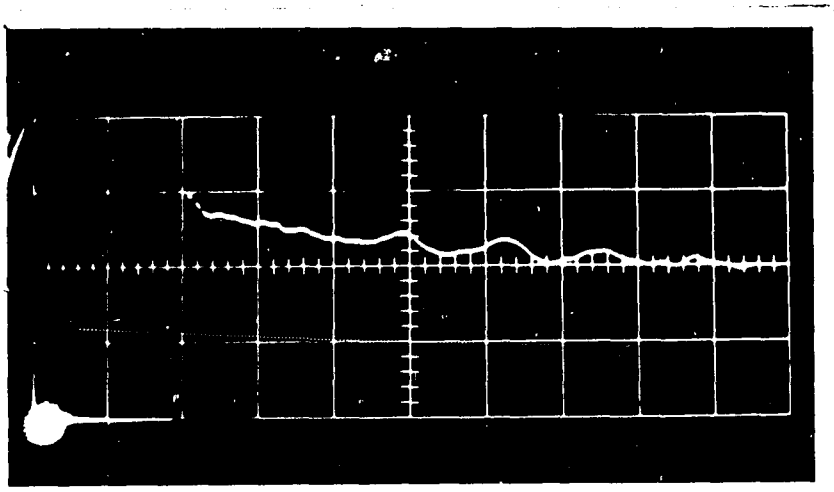

FIGURE 26. PRESSURE TRACES OF 40% C_2H_2 - 60% O_2 DETONATION AT 15.5 PSIA INITIAL PRESSURE AND MAGNET OFF

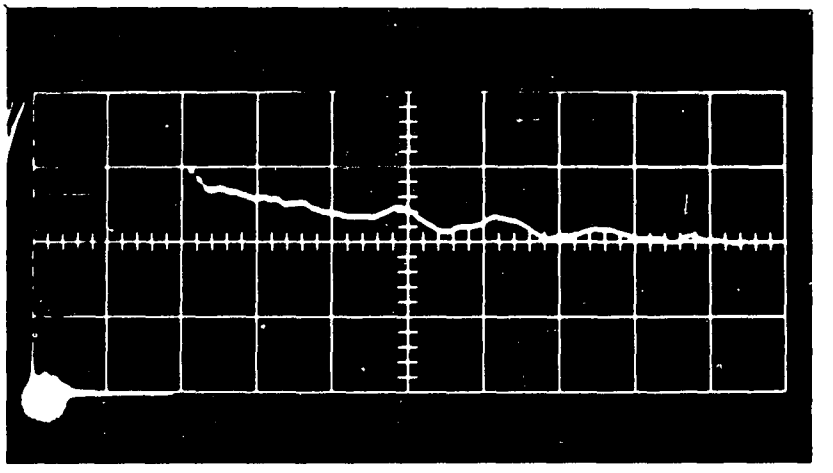

FIGURE 27. PRESSURE TRACES OF 40% C_2H_2 - 60% O_2 DETONATION AT 15.5 PSIA INITIAL PRESSURE AND MAGNET ON

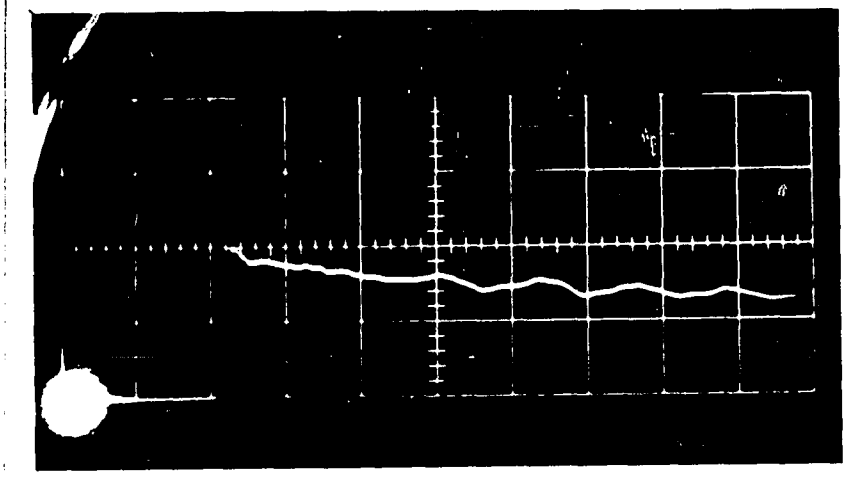

FIGURE 28. PRESSURE TRACES OF 40% C_2H_2 - 60% O_2 DETONATION AT 10.6 PSIA INITIAL PRESSURE AND MAGNET OFF

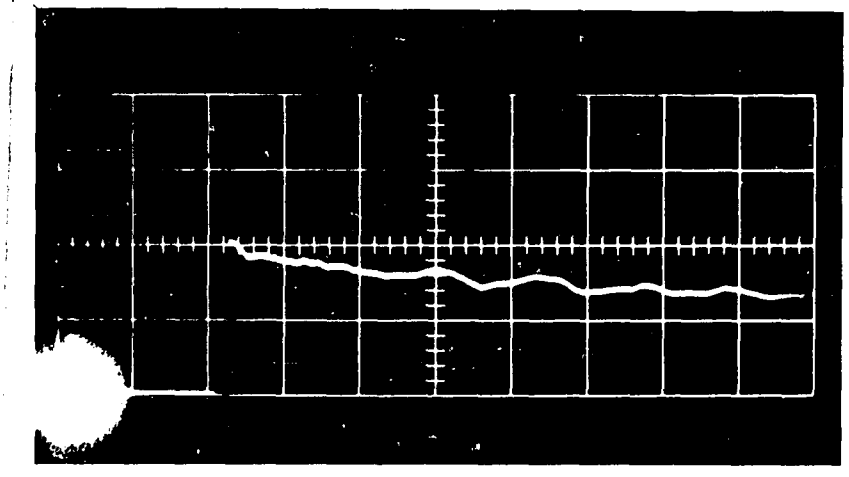

FIGURE 29. PRESSURE TRACES OF 40% C_2H_2 - 60% O_2 DETONATION AT 10.6 PSIA INITIAL PRESSURE AND MAGNET ON

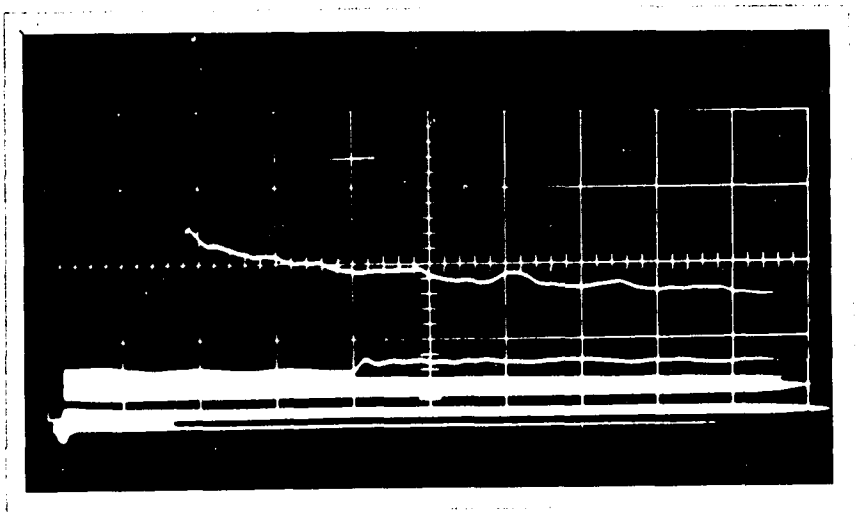

FIGURE 30. PRESSURE TRACES OF 50% C_2H_2 - 50% O_2 DETONATION AT 29.7 PSIA INITIAL PRESSURE AND MAGNET OFF

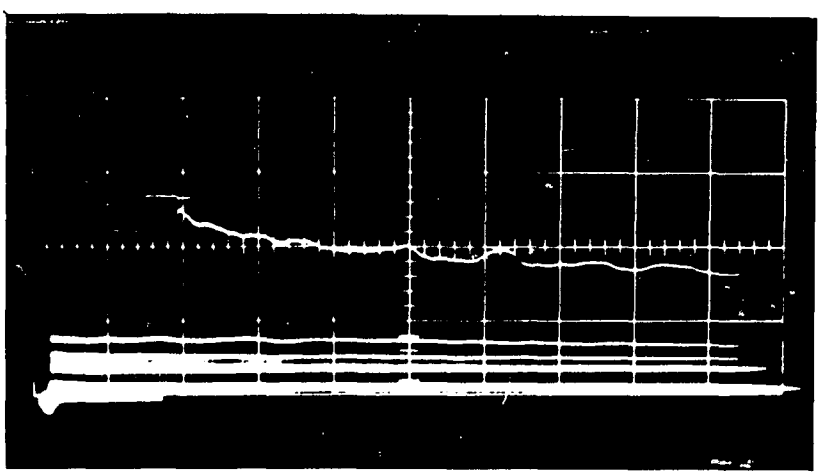

FIGURE 31. PRESSURE TRACES OF 50% C_2H_2 - 50% O_2 DETONATION AT 29.7 PSIA INITIAL PRESSURE AND MAGNET ON

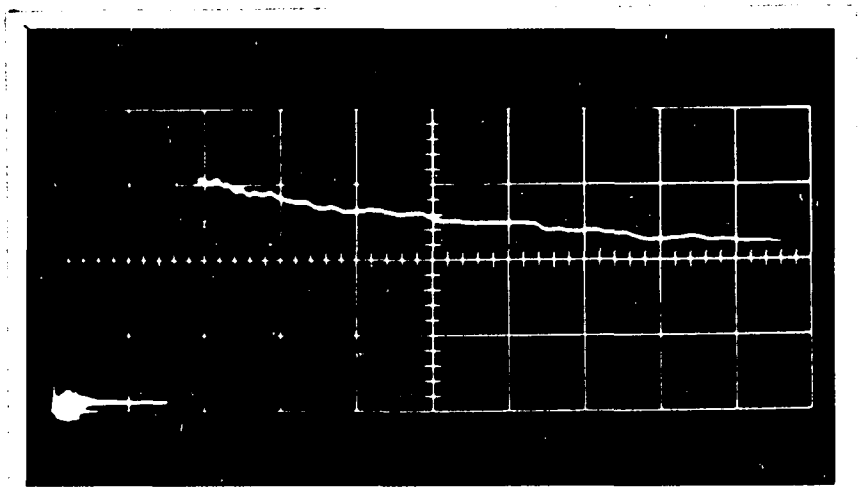

FIGURE 32. PRESSURE TRACES OF 50% C_2H_2 - 50% O_2 DETONATION AT 15.5 PSIA INITIAL PRESSURE AND MAGNET OFF

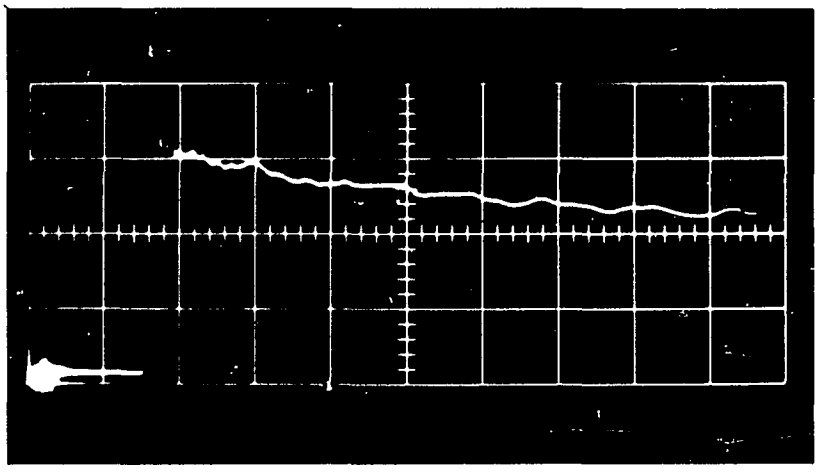

FIGURE 33. PRESSURE TRACES OF 50% C_2H_2 - 50% O_2 DETONATION AT 15.5 PSIA INITIAL PRESSURE AND MAGNET ON

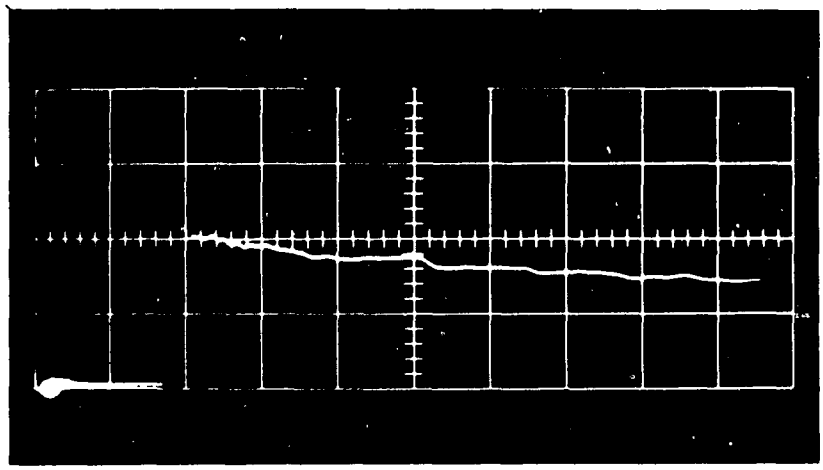

FIGURE 34. PRESSURE TRACES OF 50% C_2H_2 - 50% O_2 DETONATION AT 10.6 PSIA INITIAL PRESSURE AND MAGNET OFF

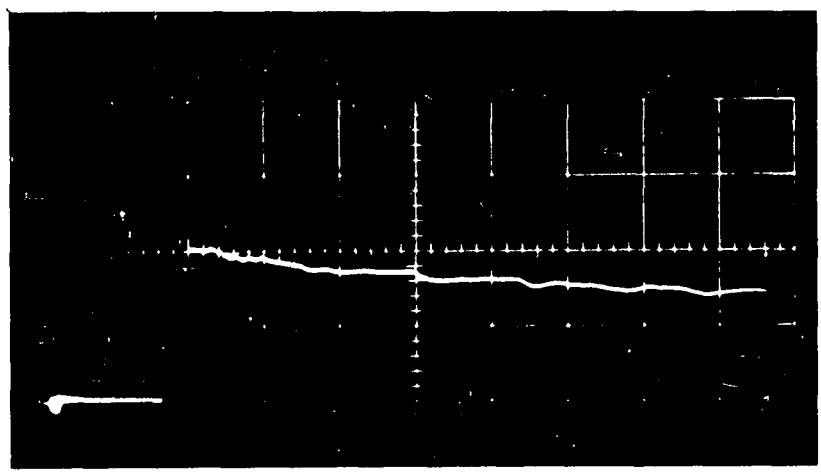

FIGURE 35. PRESSURE TRACES OF 50% C_2H_2 - 50% O_2 DETONATION AT 10.6 PSIA INITIAL PRESSURE AND MAGNET ON

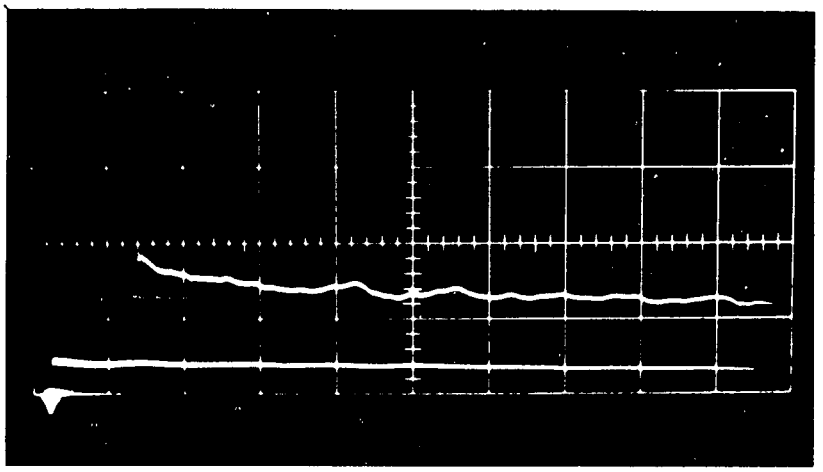

FIGURE 36. PRESSURE TRACES OF 60% C_2H_2 - 40% O_2 DETONATION AT 29.7 PSIA INITIAL PRESSURE AND MAGNET OFF

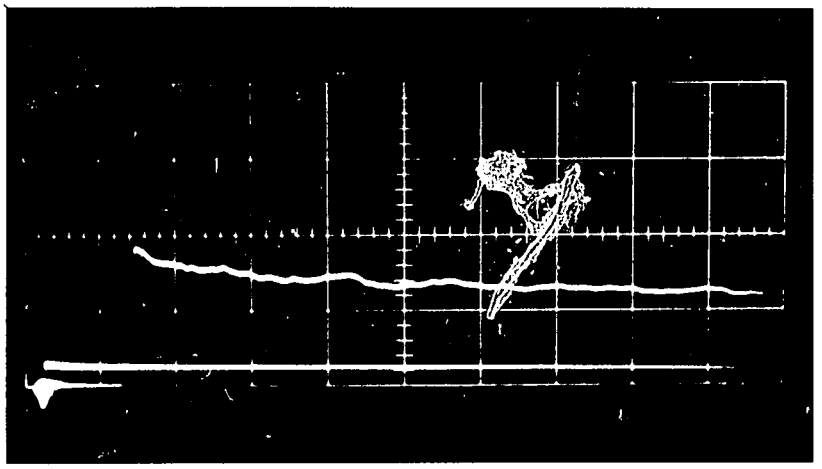

FIGURE 37. PRESSURE TRACES OF 60% C_2H_2 - 40% O_2 DETONATION AT 29.7 PSIA INITIAL PRESSURE AND MAGNET ON

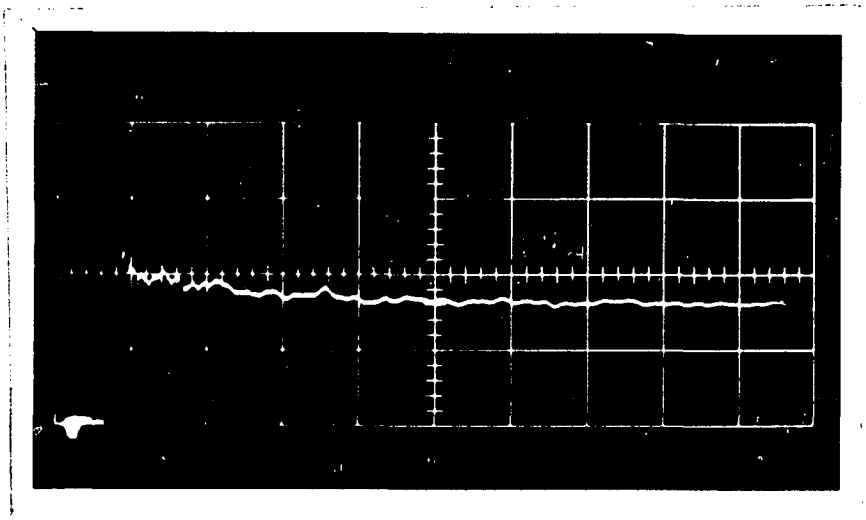

FIGURE 38. PRESSURE TRACES OF 60% C_2H_2 - 40% O_2 DETONATION AT 15.5 PSIA INITIAL PRESSURE AND MAGNET OFF

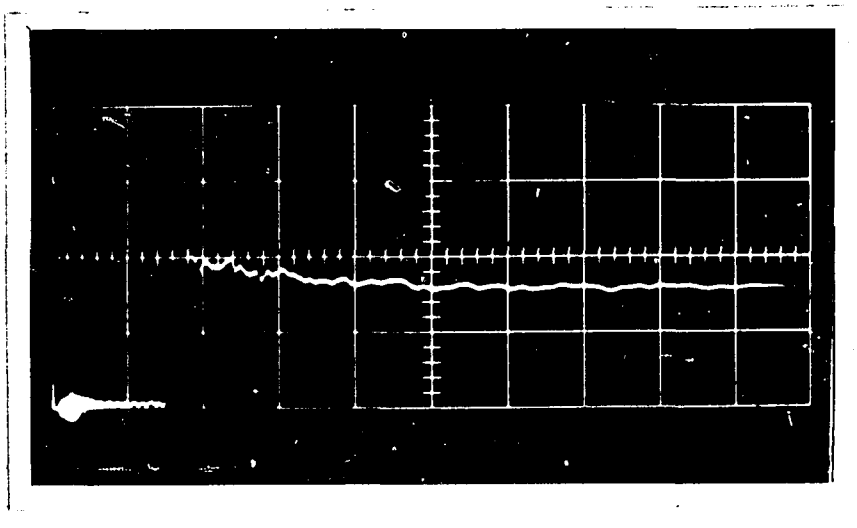

FIGURE 39. PRESSURE TRACES OF 60% C_2H_2 - 40% O_2 DETONATION AT 15.5 PSIA INITIAL PRESSURE AND MAGNET ON

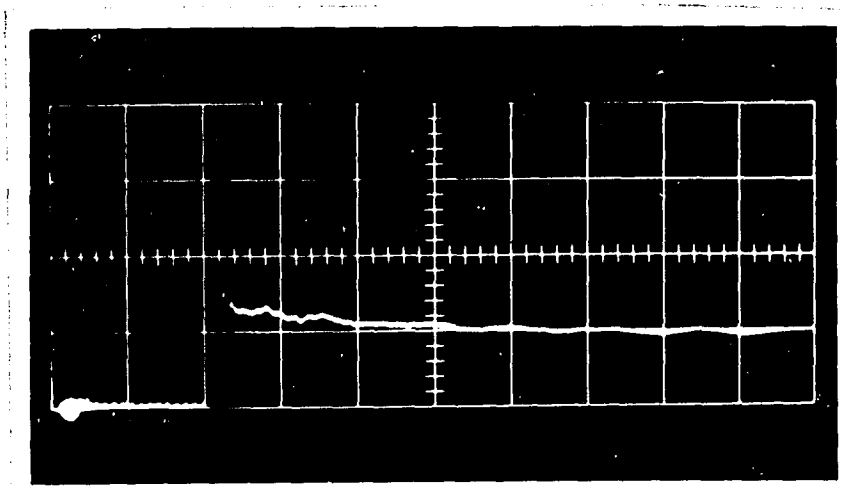

FIGURE 40. PRESSURE TRACES OF 60% C_2H_2 - 40% O_2 DETONATION AT 10.6 PSIA INITIAL PRESSURE AND MAGNET OFF

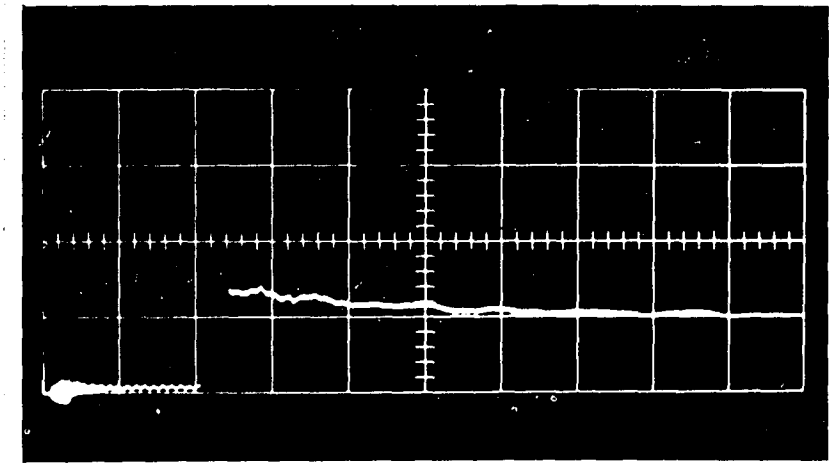

FIGURE 41. PRESSURE TRACES OF 60% C_2H_2 - 40% O_2 DETONATION AT 10.6 PSIA INITIAL PRESSURE AND MAGNET ON

Static Pressure Variations

Variations in the rarefaction wave static pressure profile, which are indicated through a comparison of the figures on pages 119 through 124.

Mixture Composition	Initial Press. (Psia)	Figures Which Are Compared To Obtain The Indicated Press. Variations	Point At Which Variations In Static Press. First Occur (Measured from wave front in cm.)	Magnitude of Static Pressure Variation	Magnitude of Max. Static Press. Variation and Its Point of Occurrence (Measured from wave front in cm.)
30% C_2H_2 70% O_2	29.7	18 & 19	0.6 cm, then variation is continuous for remainder of the trace.	Barely discernible excepting as indicated by the max. variation.	30 psia 2.9, 4.1 cm
30% C_2H_2 70% O_2	15.5	20 & 21	0.2 cm, then variation is continuous for remainder of the trace.	"	20 psia 2.6, 3.4 cm
30% C_2H_2 70% O_2	10.6	22 & 23	2 cm, then variation is continuous for remainder of the trace.	"	15 psia 3.4 cm
40% C_2H_2 60% O_2	29.7	24 & 25	0.9 cm, then variation is continuous for remainder of the trace.	"	40 psia 1.6, 5.1, 6.3 cm
40% C_2H_2 60% O_2	15.5	26 & 27	1.3 cm, then variation is continuous for remainder of the trace.	"	20 psia 2.9 cm
40% C_2H_2 60% O_2	10.6	28 & 29	0.9 cm, then variation is continuous for remainder of the trace.	"	15 psia 0.9, 2.7 cm

Static Pressure Variations

Variations in the rarefaction wave static pressure profile, which are indicated through a comparison of the figures on pages 125 through 130.

Mixture Composition	Initial Press. (psia)	Figures Which Are Compared To Obtain The Indicated Press. Variations	Point At Which Variations In Static Press. First Occur (Measured from wave front in cm.)	Magnitude of Static Pressure Variation	Magnitude of Max. Static Press. Variation and Its Point of Occurrence (Measured from wave front in cm.)
50% C_2H_2 50% O_2	29.7	30 & 31	0.3 cm, then variation is continuous for remainder of the trace.	Barely discernible excepting as indicated by the max. variation.	50 psia 0.9, 1.5, 3.1, 4.3 cm
50% C_2H_2 50% O_2	15.5	32 & 33	1.1 cm, then variation is continuous for remainder of the trace.	"	40 psia 1.3, 3.3, 5.1 cm
50% C_2H_2 50% O_2	10.6	34 & 35	0.5 cm, then variation is continuous for remainder of the trace.	"	15 psia 0.7, 1.3 cm
60% C_2H_2 40% O_2	29.7	36 & 37	0.6 cm, then variation is continuous for remainder of the trace.	"	35 psia 1.2, 1.8, 2.1 cm
60% C_2H_2 40% O_2	15.5	38 & 39	0.4 cm, then variation is continuous for remainder of the trace.	"	20 psia 0.7 cm
60% C_2H_2 40% O_2	10.6	40 & 41	1.8 cm, then variation is continuous for remainder of the trace.	"	15 psia 1.8 cm

Calculations

From Equation (3.55) Chapter 3

$$\frac{\rho_f}{\rho_1} = 1 + \frac{1}{\gamma}\left(1 - \frac{p_1}{p_f}\right) \tag{3.55}$$

From Table VIII page 137, Reference 5 $\gamma = 1.152$ is obtained. This value of γ is the calculated equilibrium value, at one atmosphere, of the reaction products for a stochiometric mixture of oxygen and acetylene. It should be noted that this value of γ, when used in the equations developed for one dimensional steady state detonation, results in the calculated values for the wave parameters listed in Table I. These calculated values agree closely with those obtained experimentally. Therefore this value of γ and the other properties listed in Table I are representative for a stochiometric oxyacetylene mixture.

From Table I, Appendix B:

$$\frac{p_1}{p_f} = \frac{1}{33.8}$$

Substitute γ and $\frac{p_1}{p_f}$ into Eq. (3.55)

$$\frac{\rho_f}{\rho_1} = 1 + \frac{1}{1.152}\left(1 - \frac{1}{33.8}\right)$$

$$= 1 + \frac{1}{1.152}\left(1 - 0.03\right) = 1.84 \tag{i}$$

From Eq. (3.58) Chapter 3

$$D' = V_f' + U_f = \frac{\rho_f}{\rho_1} \sqrt{\gamma R T_f} \tag{3.58}$$

Where from Eq. (3.39) Chapter 3

$$V_f' = \sqrt{\gamma R T_f} \tag{ii}$$

From Table I, Appendix B:

$$D' = 2426\ (3.28) = 7960\ \text{ft/sec}$$

Then from Eqs. (i) and (3.58)

$$\sqrt{\gamma R T_f} = \frac{7960}{1.84} = 4320\ \text{ft/sec} \tag{iii}$$

Substitute Eqs. (ii) and (iii) into Eq. (3.58)

$$U_f = 7960 - 4320 = 3640\ \text{ft/sec} \tag{iv}$$

$$R_1 = \frac{[2.5\ (32)]\ (1544)}{[2.5\ (32) + 26](32)} + \frac{(26)(1544)}{[25(32) + 26](26)}$$

$$= 36.2 + 14.5 = 50.7\ \frac{\text{ft}\ \text{lb}_f}{\text{lb}_m\ ^\circ\text{R}} \tag{v}$$

From Equation (3.29) Chapter 3

$$\rho_1 = \frac{P_1}{R_1 T_1} \tag{3.29}$$

From Table I, Appendix B:

$$p_1 = 14.7 \text{ psia}, \quad T_1 = 533.5°R$$

Then from Eq. (3.29)

$$\rho_1 = \frac{(14.7)(144)}{(50.7)(533.5)} = 0.0785 \ \frac{lb_m}{ft^3} \tag{vi}$$

From Eqs. (i) and (vi)

$$\rho_f = 1.84 \ (0.0785) = 0.144 \ \frac{lb_m}{ft^3} \tag{vii}$$

From Eq. (3.71) Chapter 3

$$\rho U_x = m' = \text{constant} \tag{3.71}$$

Substitute Eqs (iv) and (vii) into Eq. (3.71)

$$m'_f = 0.144 \ (3640) = 522 \ \frac{lb_m}{ft^2 \ sec} \tag{viii}$$

From Eq. (3.69) Chapter 3

$$U_{x_o} - U_{x_L} = \frac{\sigma B_y^2 L}{\rho} \tag{3.69}$$

From the assumptions made in Chapter 3

$$U_{x_o} = U_{f_o} \quad \text{and} \quad U_{x_L} = U_{f_L}$$

and therefore from (iv)

$$U_{x_o} = 3640 \text{ ft/sec} \tag{ix}$$

From Figure 15, Appendix B the measured electrical conductivity is approximately:

$$\sigma \approx 10^{-3} \text{ mhos/cm} \tag{x}$$

From the experimental data and results, representative values for the magnetic field strength and magnet gap are respectively:

$$B_y = 11{,}600 \text{ gauss}, \quad L = \frac{17}{12} \text{ ft} \tag{xi}$$

From Eqs. (vii), (x), (xi) and (3.69)

$$U_{x_o} - U_{x_L} = \frac{\left[10^{-3} \frac{\text{mhos}}{\text{cm}}\right]\left[11{,}600 \text{ gauss}\right]^2\left[\frac{17}{12} \text{ ft}\right]^2\left[\frac{1 \frac{\text{volt-sec}}{\text{meter}}}{10^4 \text{ gauss}}\right]\left[10^2 \frac{\text{cm}}{\text{meter}} \frac{1 \text{ meter}}{3.28 \text{ ft}}\right]^4}{\left[0.144 \frac{\text{lb}_m}{\text{ft}^3}\right]\left[\frac{1}{32.2 \frac{\text{ft.lb}_m}{\text{lb}_f \text{ sec}^2}}\right]\left[\frac{1 \text{ Newton}}{0.2248 \text{ lb}_f}\right]\left[1 \frac{\text{volt-amp sec}}{\text{meter}} \frac{}{\text{Newton}}\right]}$$

$$= 0.082 \text{ ft/sec} \tag{xii}$$

Therefore from Eq. (xii) the slowing down of the fluid is negligible and

$$U_{x_L} \approx U_{x_o} = 3640 \text{ ft/sec}$$

From Eq. (3.72)

$$m' (U_{x_o} - U_{x_L}) = p_L - p_o \qquad (3.72)$$

Substitute Eqs. (viii) and xii) into Eq. (3.72)

$$p_L - p_o = \frac{522(0.082)}{32.2\ (144)} = 0.0093\ \frac{lb_f}{in^2} \qquad (xiii)$$

Therefore from (xiii) the increase in static pressure is negligible.

Following is a calculation which is made in order to find the probable order of magnitude of the electrical conductivity for the gases of this study.

The mixture ratio for the stochiometric mixture in the preceding calculation approximates that of the 30% C_2H_2 - 70% O_2 mixture of this study. Then by a direct proportionality, which is indicated by the substitution of Eq. (3.69) into Eq. (3.72), the following is obtained:

$$\sigma' = \sigma \frac{(p_L - p_o)_{\text{observed}}}{(p_L - p_o)_{\text{calculated}}} \qquad (xiv)$$

where: σ' = the order of magnitude of electrical conductivity which is indicated by the observed results of this study.

and: σ = electrical conductivity from Figure 15.

From the table on page 130a the observed maximum variation in pressure at 15.5 psia and a 30% C_2H_2 - 70% O_2 mixture is approximately 20 psia.

Then using (xiii) in (xiv) results in:

$$\sigma' = \frac{(10^{-3})(20)}{9.3 \times 10^{-3}} = 2 \frac{\text{mhos}}{\text{cm}}$$

SELECTED BIBLIOGRAPHY

1. Berthelot, M. and P. Vieille. Ann. de Chim. et de Phys. (5), V 28:289, 1883.

2. Mallard, E. and H. LeChatelier. "Combustion des Melanges Gaseux Explosifs," Ann. Mines. V 8:274-568, 1883.

3. Chapman, D. L. Philosophical Magazine. (5), V 47:90, 1899.

4. Jouguet, E. J. Math. p. 347, 1905; p. 6, 1906.

5. Bollinger, Loren E. Detonability of Combustible Mixtures. Ohio State University, Rocket Research Laboratory, AD 630641, 1965.

6. Oppenheim, A. K. "Novel Insight into the Structure and Development of Detonation," Astronautica ACTA 11, 1965.

7. Penner, S. S. and B. P. Mullins. Explosions, Detonations, Flammability and Ignition. Pergamon Press, 1959.

8. Lewis, Bernard and Guenther von Elbe. Combustion, Flames and Explosions of Gases. Academic Press, 1961.

9. Zeldovich, Ia B. and A. S. Kompaneets. Theory of Detonation. Academic Press, 1960.

10. Lewis, B., R. N. Pease, H. S. Taylor (Editors). Combustion Processes. Princeton University Press, 1956.

11. Soloukhin, R. I. Shock Waves and Detonations in Gases. Mono Book Corporation, 1966.

12. Denison, Yu N. and Yu K. Troshin. USSR. "Structure of Gaseous Detonation in Tubes," U.S.J.P.R.S. 7224, 1960.

13. Oppenheim, A. K. and J. Rosciszewski. "Determination of the Detonation Wave Structure," Ninth Symposium (International) on Combustion. pp. 424-441. Academic Press, 1963.

14. Fay, J. A. "The Structure of Gaseous Detonation Waves," Eighth Symposium (International) on Combustion. pp. 30-40. Williams and Wilkins, 1962.

15. von Elbe, Guenther. "The Rates of Elementary Reaction," Eighth Symposium (International) on Combustion. pp. 41-43. Williams and Wilkins, 1962.

16. Berets, D. J., E. F. Greene and G. B. Kistiakowsky. Gaseous Detonations II, Initiation by Shock Waves. Harvard University, 1949.

17. Kirkwood, J. G. and W. W. Wood. "Structure of a Steady-State Plane Detonation Wave with Finite Reaction Rate," J. of Chem. Phys., 22, 1915, 1954.

18. Evans, M. W., F. I. Given and W. E. Richeson. "Effects of Attenuating Materials on Detonation Induction Distances in Gases," J. of Applied Phys., 26, 1111, 1955.

19. Oppenheim, A. K. and P. A. Urtiew. On the Genesis of Gaseous Detonation. Dept. of Aeronautical Sciences. Berkeley: University of California, 1967.

20. Laderman, A. K., P. A. Urtiew and A. K. Oppenheim. "Gasdynamic Effects of Shock-Flame Interactions in an Explosive Gas," AIAA Journal, 3, 876, 1965.

21. Urtiew, P. A. and A. K. Oppenheim. Detonative Ignition Induced by Shock Merging. Dept. of Aeronautical Sciences. Berkeley: University of California.

22. Bone, Fraser and Wheeler. "The Phenomenon of Spin in Detonation," Part IV, Phil. Trans. A. 230, 373, 1932.

23. Noddack, W. and E. Grosch. "Measurement of the Detonation Pressures of Initiator - Type Explosives," Explosivstoffe, V. 4, No. 4, 69, 1956.

24. Fong, M. C., L. E. Bollinger and R. Edse. Magnetohydrodynamic Effects on Exothermal Waves. ARL Technical Report 69, AD 269280, 1961.

25. Kelly, J. R., Tau-Yi Toong and Chee-Chen Tung. Chemi-Ionization in Gaseous Detonations. Cambridge, Mass: M.I.T., 1966.

26. Toong, T. Y. Ionization in Gaseous Detonation Waves, Ionization in High Temperature Gases. 1963.

27. Calcote, H. F. "Mechanisms for the Formation of Ions in Flames," Combustion and Flames, Vol. 1, p. 385, 1957.

28. Shuler, K. E. and J. Weber. "A Microwave Investigation of the Ionization of Hydrogen-Oxygen and Acetylene-Oxygen Flames," J. of Chemical Physics, Vol. 22, p. 491, 1954.

29. Calcote, H. F. and I. R. King. "Studies of Ionization in Flames by Means of Langmuir Probes," Fifth International Symposium on Combustion. Reinhold Publishing Corp., 1955.

30. Petschek, H. E., P. H. Rose, H. S. Glick, A. Kane, and A. Kantrowitz, "Spectroscopic Studies of Highly Ionized Argon Produced by Shock Waves," J. of Applied Physics, Vol. 26, p. 83, 1955.

31. Lin, Shao-Chin, E. L. Resler and A. Kantrowitz. "Electrical Conductivity of Highly Ionized Argon Produced by Shock Waves," J. of Applied Physics, Vol. 26, p. 95, 1955.

32. Saha, M. Proc. Roy. Soc. (London) 99A, 135, 1921.

33. Edwards, D. H. and T. R. Lawrence. "Ionization Measurements in Detonation Waves," Annals of Physics, 1957.

34. Laderman, A. J., G. J. Hect, R. A. Stern, and A. K. Oppenheim. "Flame Ionization During the Development of Detonation," Eighth Symposium (International) on Combustion. Baltimore: Williams and Wilkins.

35. Cambel, Ali Bulent. Plasma Physics and Magnetofluidmechanics. McGraw-Hill, 1963.

36. Resler, E. L. and W. R. Sears. "The Prospects for Magneto-Aerodynamics," J. of Aero. Sciences, 25, 235, 1958.

37. Patrick, R. M. and T. R. Brogan. "One-Dimensional Flow of an Ionized Gas Through a Magnetic Field," J. of Fluid Mechanics, Vol. 5, p. 289, 1959.

38. deLeeuw, J. H. The Interaction of a Plane Strong Shock Wave with A Steady Magnetic Field. University of Toronto, UTIA Report No. 49, 1958.

39. Gross, R. A., W. Chinitz and T. J. Rivlin. "Magnetohydrodynamic Effects on Exothermal Waves," J. of Aero/Space Sciences, p. 283, April, 1960.

40. Gross, R. A. "A Note on One-Dimensional Plasma Motion," J. of Aero/Space Sciences, p. 788, Dec., 1958.

41. Helliwell, J. B. "Gas-Ionizing Shock and Combustion Waves in Magnetogasdynamics," J. of Fluid Mechanics, p. 405, April, 1962.

42. Lazish, E. and I. Shekhtman. "Propagation of Detonation Waves in the Presence of a Magnetic Field," Soviet Physics JETP, Vol. 35, Jan., 1959.

43. Dolder, K. and R. Hide. "An Experiment on the Interaction Between a Plane Shock and a Magnetic Field," Nature, Vol. 181, p. 1116, 1958.

44. Handbook of Compressed Gases, Reinhold Publishing Corp., 1966.

45. Amend, W. E., A. J. Laderman and A. K. Oppenheim. Dynamic Performance of Pressure Transducers in Shock and Detonation Tubes. IER Report No. 64-13. Berkeley: University of California, 1964.

46. Harrje, D., V. Agosta, R. Richmond, S. Rogero, R. Wesley and J. Witherspoon. Special Considerations for Combustion Instability Instrumentation and Data Representation. CPIA Publication No. 170. John Hopkins Applied Physics Lab., 1968.

47. Kelly, J. R. and T. Y. Toong. "Detonation Wave in Electromagnetic Field," Eleventh International Symposium on Combustion, Berkeley: University of California, 1966.